

**Methods to Selectively Introduce Radicals into DNA.  
An EPR spectroscopic Study.**

**Dissertation  
zur Erlangung des Doktorgrades  
der Naturwissenschaften**

**vorgelegt beim Fachbereich  
“Chemische und Pharmazeutische Wissenschaften“  
der Johann Wolfgang Goethe - Universität  
in Frankfurt am Main**

**von  
Emiliano Feresin  
aus Aiello del Friuli, Udine (Italien)**

**Frankfurt (2004)  
(DF1)**

**Vom Fachbereich 14 “Chemische und Pharmazeutische Wissenschaften“  
der Johann Wolfgang Goethe - Universität als Dissertation angenommen.**

**Dekan: Prof. Dr. H. Schwalbe**

**Gutachter: Prof. Dr. T. F. Prisner**

**P.D. Dr. O. Schiemann**

**Datum der Disputation: 21. September 2004**

*Fatti non foste a viver come bruti  
ma per seguir virtute e conoscenza*

*(Dante, Divina)*



---

**Table of Contents**
**Symbols and Abbreviations**

<b>Introduction.....</b>	<b>1</b>
Aim of the Thesis.....	1
Scientific Contributions.....	3
<b>Chapter 1. DNA and Electron Transfer.....</b>	<b>5</b>
1.1 The DNA Double Helix: Structure and Function.....	5
1.2 Electron Transfer Processes in DNA.....	8
1.2.1 Unselective high-energy ionization of DNA detected by EPR.....	9
1.2.2 Selective radical formation in DNA by photoinduced Electron Transfer.....	11
1.2.3 Mechanistic picture for hole transfer in DNA.....	16
1.2.3a Superexchange.....	17
1.2.3b Hopping mechanism between guanines.....	19
1.2.3c Hopping mechanism between adenines.....	20
1.2.3d Polaron assisted mechanism.....	21
1.2.3e Proton coupled electron transfer.....	21
1.2.4 Excess Electron Transfer in DNA.....	22
1.2.5 Biradicals in DNA? Possible correlation between charge transfer rate and exchange coupling.....	23
1.3 References.....	25
<b>Chapter 2. EPR Theory and Model Spectra.....</b>	<b>31</b>
2.1 Introduction.....	31
2.2 Spin and Zeeman interaction.....	32
2.3 Static Spin Hamiltonian and its Components.....	36
2.3.1 The g tensor.....	37
2.3.2 The hyperfine tensor.....	39

---

	2.4 Spectral Analysis of Isotropic Hyperfine Patterns.....	42
	2.4.1 $\pi$ -type organic radicals: spin density and spin polarization .....	42
	2.4.2 <i>Tert</i> -butyl radical: hyperconjugation.....	44
	2.4.3 The thymyl radical.....	48
	2.5 Relaxation Phenomena.....	50
	2.6 Cw X-Band EPR Spectrometer.....	54
	2.7 References.....	55
<b>Chapter</b>	<b>3. EPR Spectroscopic Study of Novel Aromatic Nitroxides as Potential DNA Intercalators .....</b>	<b>57</b>
	3.1 Materials and Methods.....	58
	3.1.1 Sample preparation.....	58
	3.1.2 Simulation and fit program.....	58
	3.2 Results and Discussion.....	59
	3.2.1 EPR spectroscopy and simulations of the experimental spectra.....	59
	3.2.2 DFT calculations.....	62
	3.3 Conclusions.....	65
	3.4 References.....	65
<b>Chapter</b>	<b>4. EPR Detection of Selectively Generated Guanine Radicals in DNA.....</b>	<b>67</b>
	4.1 Materials and Methods.....	67
	4.1.1 Sample preparation and irradiation.....	67
	4.1.2 The flash quench-technique.....	68
	4.2 Results and Conclusions.....	69
	4.3 References.....	71
<b>Chapter</b>	<b>5. The 4'-Pivaloyl Substituted Thymidine as Precursor for the Thymyl Radical.....</b>	<b>73</b>
	5.1 Materials and Methods.....	74

5.1.1	Sample preparation.....	74
5.1.2	Generation of radicals by UV Irradiation.....	76
5.1.3	Photolysis of the pivaloyl group and radical formation..	76
5.1.4	Component differentiation of composite EPR spectra...	78
5.2	Results.....	79
5.2.1	Sample dissolved in CH <sub>3</sub> CN.....	79
5.2.2	Sample dissolved in H <sub>2</sub> O and in D <sub>2</sub> O.....	82
5.2.3	Simulations and computer reconstructions.....	85
5.2.4	Double strand DNA modified with the nucleotide derivative of <b>1</b> .....	88
5.3	Discussion and Conclusions.....	89
5.3.1	Components and radical structures.....	89
5.3.2	Mechanism of radical formation.....	92
5.3.3	Discussion about the modified double strand DNA.....	94
5.4	References.....	95
<b>Chapter 6</b>	<b>A New Modified Thymidine as Precursor for a Thymine Based Radical and as Electron Injector into DNA.....</b>	<b>99</b>
6.1	Materials and Methods.....	100
6.1.1	Sample preparation.....	100
6.1.2	Generation of radicals by UV Irradiation.....	100
6.2	Results.....	100
6.2.1	Sample dissolved in H <sub>2</sub> O and D <sub>2</sub> O.....	100
6.2.2	Sample dissolved in CH <sub>3</sub> CN.....	103
6.2.3	Simulations and computer reconstruction of experimental spectra.....	106
6.3	Discussion and Conclusions.....	109
6.4	References.....	113
	<b>Summary and Outlook.....</b>	<b>115</b>

*Table of Contents*

---

<b>Zusammenfassung und Ausblick.....</b>	121
<b>Appendix A.....</b>	127
<b>Appendix B.....</b>	131
<b>Lebenslauf.....</b>	133
<b>Acknowledgements</b>	



## **SYMBOLS AND ABBREVIATIONS**

A	Adenine
$a_{\text{iso}}$	isotropic hyperfine coupling
a.u.	arbitrary units
C	Cytosine
CT	Charge Transfer
cw	continuous wave
DFT	Density Functional Theory
DNA	DeoxyriboNucleic Acid
DPPH	( $\alpha, \alpha'$ )-diphenyl- $\beta$ -picrylhydrazyl
ENDOR	Electron Nuclear Double Resonance
EPR	Electron Paramagnetic Resonance
ESEEM	Electron Spin-Echo Envelope Modulation spectroscopy
ET	Electron Transfer
Fig.	Figure
$g_e$	Free electron $g$ -factor
$g_N$	Nuclear $g$ -factor
G	Gauss
G	Guanine
hf	hyperfine
HPLC	High Performance Liquid Chromatography
I	Inosine
$I$	Intensity
Lw	linewidth
m.f.	molecular formula
mw	microwave
NHE	Nerst Hydrogen Electrode
PELDOR	Pulsed Electron Double Resonance
RT	Room Temperature (25 °C)
T	Thymine
UV	Ultra Violet
vis	visible



## **INTRODUCTION**

The  $\pi$ -stack base pairs of B-form DNA provide a unique medium for the investigation of charge transfer (CT) processes. Hole transfer (HT) has been extensively studied on very well defined donor (D)-DNA-Acceptor (Ac) systems. In most of these systems the transfer is initiated by photochemical methods and investigated by several techniques, such as optical and EPR spectroscopy. By now, a lot of questions about this phenomenon have been worked out and a detailed picture has been emerged including important aspects such as mechanisms, charge transfer rates  $k_{CT}$ , distance dependence and DNA sequence dependence. On the other hand still little is known about excess electron transfer (EET) in DNA. In order to further investigate EET processes, specifically designed D-DNA-Ac systems are needed, which must be fully characterized on the basis of the radicals formed and the mechanisms involved.

A challenging study in DNA, which up to date has not yet been performed, is to correlate the charge transfer rates  $k_{CT}$  to the spin-spin exchange coupling constant  $J$  between two unpaired electrons, which, as well as  $k_{CT}$ , depends on the mediation properties of the bridge connecting the two radical centers.

### **AIM OF THE THESIS**

The aim of this thesis is to study the properties and the applicability of four different methods suitable to selectively introduce radicals into DNA by means of Electron Paramagnetic Resonance.

The investigation focuses on the selectivity of the methods in order to understand if and how it can be possible to generate biradicals in DNA in specific positions. These studies are the essential starting point within a project having as long term goal to measure the exchange coupling constant  $J$  in biradical DNA and to correlate it with the charge transfer rate constant  $k_{CT}$ .

In particular, for two thymidine derivatives which have been specifically designed to be used as charge transfer injectors to photoinduce HT and EET in DNA, the question, which radicals are formed and which are the mechanisms involved after UV irradiation is addressed, to get new insights on the initiation processes of CT in DNA.

*Outline.* The first method studied suitable to introduce radicals into DNA involves the use of stable nitroxides as intercalators between DNA base pairs. To investigate J coupling in biradical DNA generated with stable intercalated aromatic nitroxides it is necessary that the interacting spins are well inside the DNA base stack. For that reason intercalation ought to happen with the N-O group between the bases or, if this does not occur, the spin density has to be delocalised into the intercalating part of the nitroxide. In chapter 3 the spin density distribution of these potential intercalators is studied by simulation of the hyperfine patterns of the nitroxides EPR spectra, and the applicability of these systems is discussed.

The following methods studied are suitable to photoinduce the generation of transient radicals within DNA via UV light excitation.

In particular in chapter 4 the analysis of transient guanine radicals generated in DNA utilizing a Ruthenium intercalator and the Flash Quench Technique is presented and the selectivity involved in the radical formation is addressed.

In chapter 5 and 6 the photoinduced processes that occur after UV irradiation of two thymidine derivatives are investigated. The two modified thymidines are currently used as charge injectors into DNA.

Many systems that enable injection of a single electron/hole in DNA by means of photochemical methods have been produced during the last decade of studies on CT in DNA (see section 1.2.2). Nevertheless the mechanisms involved and the radicals formed are not yet fully understood. Herein EPR spectroscopy has been applied for the first time to give new insight on the radicals formed after photoexcitation of two different pivaloyl substituted thymidine derivatives and on the mechanisms that govern their generation. The EPR spectra will be detected on UV irradiated frozen solutions and will be compared with the data obtained from the studies on radiation damage in DNA (see section 1.2.1).

In chapter 5 the first EPR characterization of the photoinduced processes occurring after UV irradiation of a nucleoside modified with the photocleavable pivaloyl group in the 4' sugar position is discussed. DNA duplexes modified with this group have been widely used by Giese and co-workers to inject one hole in DNA and study the HT process (see also section 1.2.2).

In chapter 6 the characterization of the photoinduced processes occurring after UV irradiation of a similar derivative of thymidine, which has been specifically designed to

---

inject one excess electron into the DNA upon irradiation, is studied for the first time with EPR. The analysis is done in an analogous way as done in the previous chapter.

## SCIENTIFIC CONTRIBUTIONS

This work has provided the following scientific contributions:

### List of publications:

- 1) Beyer, M.; Fritscher, J.; **Feresin, E.**; Schiemann, O.; *Synthesis of Novel Aromatic Nitroxides as Potential DNA Intercalators. An EPR spectroscopical and DFT computational Study.* Journal of Organic Chemistry **2003**, 68, 2209-2215.
- 2) Schiemann, O.; **Feresin, E.**; Carl, T.; Giese, B.; *4'-Pivaloyl Substituted Thymidine as a Precursor for the Thymyl Radical: An EPR Spectroscopic Study.* ChemPhysChem **2004**, 5, 270-274.
- 3) Giese, B.; Carl, B.; Carl, T.; Carell, T.; Behrens, C.; Hennecke, U.; Schiemann, O.; **Feresin, E.**; *Excess Electron Transport through DNA: A Single Electron Repairs more than One UV-Induced Lesion.* Angewandte Chemie **2004**, 43, 1884-1887 (cover picture).

Posters (the presenting author is given in bold):

- 1) Schiemann, O.; **Feresin, E.**; Turro, N. J.; Barton, J. K.; *EPR detection of selectively generated guanine radicals in DNA.* GDCh-Jahrestagung Chemie, Würzburg, Germany, September **2001**.
- 2) **Feresin, E.**; Giese, B.; Schiemann, O.; *EPR Studies on Transient DNA Radicals from 4'-Pivaloyl substituted Thymidine.* EPR Tutorial, Bremen, Germany, September **2002**. (3<sup>rd</sup> prize award)

- 3) **Feresin, E.**; Giese, B.; Schiemann, O.; *EPR Studies on Transient DNA Radicals from 4'-Pivaloyl substituted Thymidine*. Modern EPR Spectroscopy Euro-Summer School, Retie, Belgium, December **2002**.
  
- 4) **Bode, B.**; Fritscher, J.; Beyer, M.; Feresin, E.; Schiemann, O.; *Aromatic Nitroxides-Potential Intercalators for Ribonucleic Acids*. Conference on RNA-Structure, Function and Ligand Interaction, Frankfurt, Germany, October **2003**.
  
- 5) **Schiemann, O.**; Giese, B.; Feresin, E.; *Pivaloyl Substituted Thymidines as Initiators for Electron Transfer in DNA. An EPR spectroscopic study*. Southeast Regional Meeting of the American Chemical Society, Atlanta, USA, November **2003**.

# 1. DNA AND ELECTRON TRANSFER

## 1.1 THE DNA DOUBLE HELIX: STRUCTURE AND FUNCTION

The discovery of a new organic phosphate compound in cells rich in nuclear substance clocked the birth of a new era in biology. It was 1869, and Friedrich Miescher named this compound nuclein<sup>[1]</sup>, which was subsequently shown to consist of deoxyribonucleic acid (DNA) and protein<sup>[2]</sup>. Analysis of isolated DNA showed it to contain four kinds of building blocks, called nucleotides. A nucleotide is characterized by its base, which can be a purine, namely adenine (A) or guanine (G), or a pyrimidine, namely thymine (T) or cytosine (C). The structures of DNA nucleotides are depicted in Fig. 1.1.

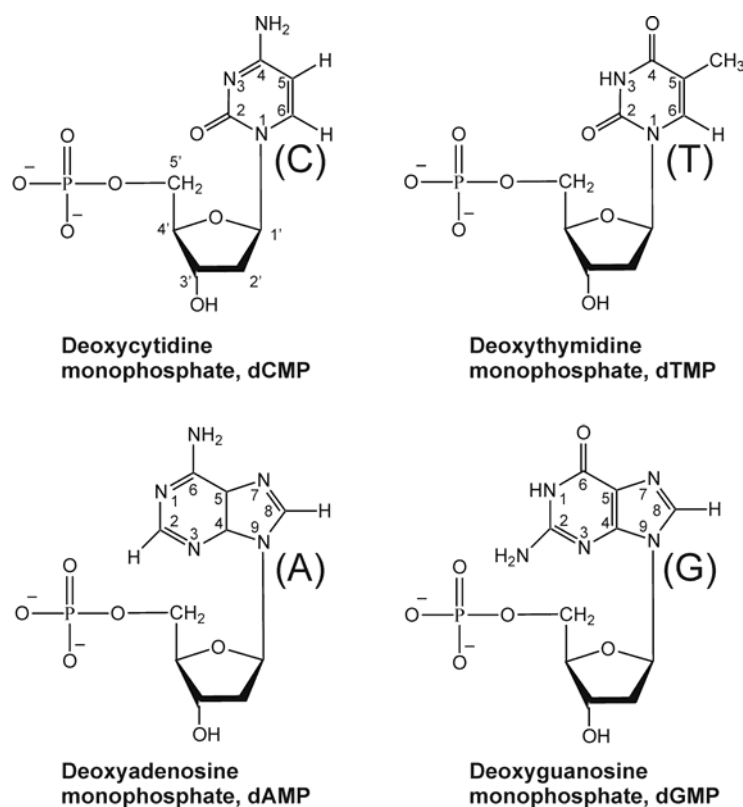


**Figure 1.1** Structures of nucleotides of DNA. Every base is linked by an N-glycosidic bond to a 5-carbon cyclic sugar (the combination of base and sugar is called nucleoside). A phosphate group is esterified to the hydroxyl on carbon 5' of the sugar.

Since DNA is composed of only four nucleotides, while proteins are composed of twenty different amino acids, in the first half of the 19<sup>th</sup> century the genetic role was still attributed to the proteins. It was in 1944 that the first important evidence that DNA is the genetic substance was reported: Avery et al. showed that the purified DNA from one strain of *Pneumococcus* carried a genetic message that could be assimilated and expressed by cells of another strain.<sup>[3]</sup> But it certainly was the discovery by Watson and Crick, in 1953, of the *double helical (duplex)* structure of DNA (see Fig. 1.2) that put a milestone in the understanding of this molecule.<sup>[4]</sup> In their paper<sup>[4]</sup> they postulated that “This structure has two helical chains each coiled round the same axis...” and that “it is found that only specific pairs of bases can bond together... adenine A (purine) with thymine T (pyrimidine), and guanine G (purine) with cytosine C (pyrimidine)”. A model of the Watson-Crick duplex is depicted in Fig. 1.2.

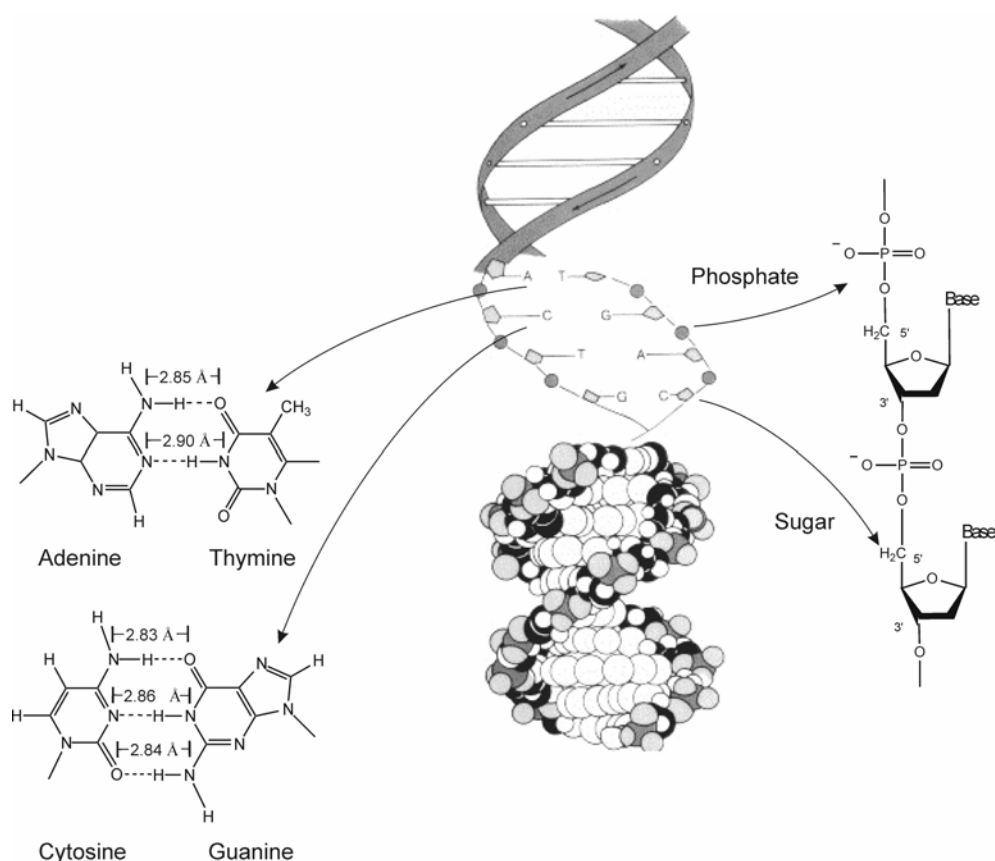


**Figure 1.2** Watson and Crick's double helical model of DNA. The hydrophobic core of the hydrogen-bonded AT/GC base pairs (magnified on the left) is surrounded by the hydrophilic sugar-phosphate backbone (magnified on the right).



The DNA structure postulated by Watson and Crick is the most common conformation of duplex DNA *in vivo* and in solution, and it is called B-DNA. In B-DNA the base pairs form a one-dimensional  $\pi$ -stacked array with an average distance between the planes of two neighboring base pairs of 0.34 nm. The long axis of each base pair is rotated approximately  $36^\circ$  with respect to its neighbor. As a result, the right-handed double helix makes a turn every 10 bases, thus every 3.4 nm. The intertwined strands make two grooves of different widths, named major and minor groove, which may facilitate binding of specific proteins (Fig. 1.3).

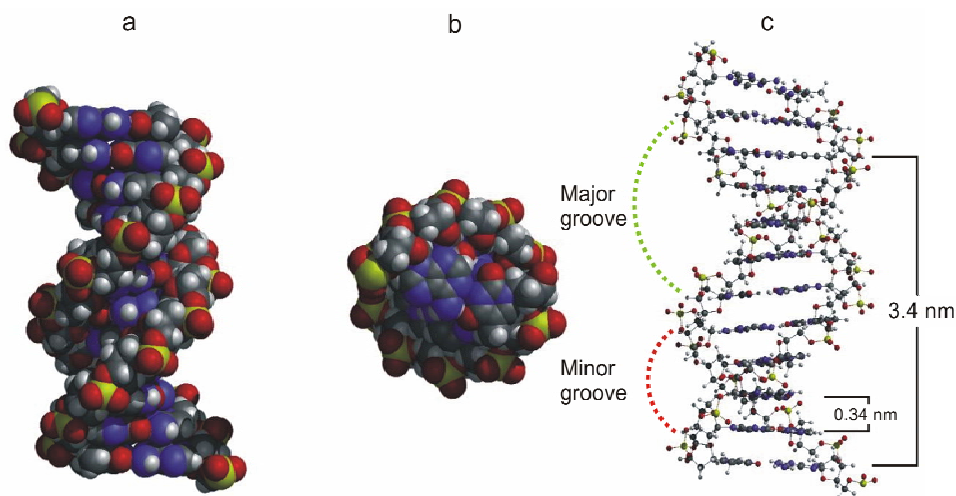


**Figure 1.3** Molecular models of DNA. a) B-form of the DNA, side view. b) B-form of the DNA, top view. c) B-form of the DNA where the characteristic distances and grooves are indicated. (Adapted from [http://wps.prenhall.com/wps/media/objects/FG27\\_05.JPG](http://wps.prenhall.com/wps/media/objects/FG27_05.JPG))

The stability of the duplex helix depends on: the hydrogen bonds between the base pairs (there are 2 H-bonds in AT and 3 in GC) and the base  $\pi$ -stacking. Moreover, hydrophobic interactions, van der Waals forces, and neutralizations of the electrostatic repulsive forces of the phosphate groups by cations do stabilize the helix as well.<sup>[5]</sup>

As it was already postulated by Watson and Crick, the structure of DNA is strictly related to its function. The linear array of four nucleotides, arranged in a definite order allows the molecule to encode an essentially endless and diverse amount of information. The duplex structure maintains two copies of the information at all times. Complementary pairing of the nucleotide constituents of one strand to those of the second strand provides the basis for the two major functions of DNA. First, DNA contains the code for all the cell's

proteins; second DNA serves as a template for its own replication prior to cell division, in order to maintain the genetic code over many generations of cells (for reviews see Kornberg et al. <sup>[5]</sup>).

In the last 50 years the knowledge of the functions of DNA and the ability to manipulate it have enormously improved. The innovations are evident everywhere in medicine, phage genetics, crystallography, molecular biology, and even agro-biological sciences. One of the most significant events in biology in the last years has been the publication in *Science* and *Nature*, in February 2001, of the first analysis of the draft human genome sequence.

This thesis will deal with a branch of studies on DNA which have attracted the attention of biophysicists and spectroscopists, namely the DNA mediated charge transfer (CT) processes and the methods suitable to introduce radicals in DNA in specific positions.

## **1.2 ELECTRON TRANSFER PROCESSES IN DNA**

The question of whether and how the  $\pi$ -stacked array of base pairs in B-form DNA might function as a pathway for electron migration was suggested over 40 years ago. <sup>[6, 7]</sup> Since then the charge transfer (CT) properties of DNA have been mainly studied by means of two different experimental approaches. Radiation chemists were able to unravel primary radical formation in DNA and to obtain evidence for charge migration along DNA using high-energy ionizing radiation (the subject is presented in section 1.2.1). Photochemists, on the other hand, used well-defined photo-excitable donor (D)-DNA-acceptor(Ac) systems to inject and study holes (positive charges, Fig. 1.4) and excess electrons (negative charges, Fig. 1.4) in DNA (the subject is presented in section 1.2.2).

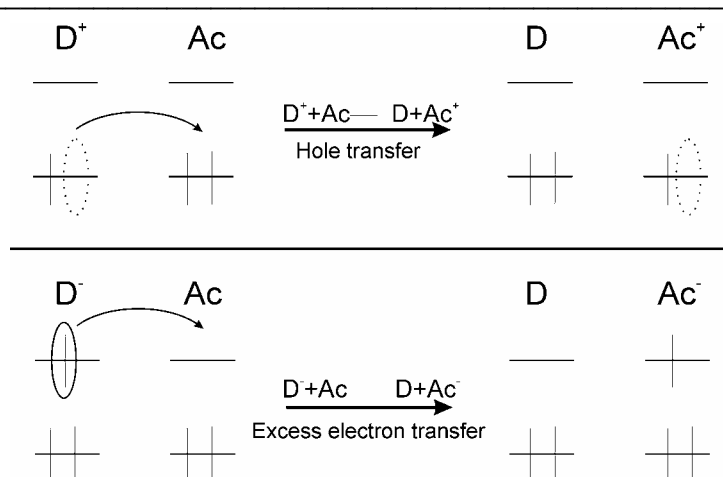


**Figure 1.4** Schematic representation of Hole Transfer (HT) processes and Excess Electron Transfer (EET) process. HT: a positive charge is transferred from the charge donor to the charge acceptor (it is also possible say that an electron is moved from the acceptor to the donor). EET: an electron is transferred from the electron donor to the electron acceptor.

The huge amount of experimental and theoretical attention that the field has attracted in the last ten years was partly stimulated by the question of whether CT in DNA can occur almost distance-independent over long ranges, as in a “molecular wire”.<sup>[8]</sup>

On the other hand the current studies on CT in DNA are of great importance for the knowledge of the primary processes in oxidative DNA damage, which may cause apoptosis, mutations and cancer,<sup>[9-13]</sup> and for the development of novel electrochemical, sensoric and nanoelectronic devices.<sup>[14-17]</sup>

To date, a lot of aspects about HT in DNA have been clarified and a detailed mechanistic picture has emerged, which accounts for distance/base sequence/energy dependence (the subject is presented in section 1.2.3). On the contrary, still less is known about EET. As in the case of the hole-transfer studies, oligonucleotides with known donor-acceptor distances and complementary analytical and spectroscopic techniques are required for a complete understanding of the EET in DNA.

### 1.2.1 Unselective high energy ionization of DNA detected by EPR

Ultraviolet, x-ray, or particle irradiation of living cells is well known to induce mutagenesis since many years.<sup>[18]</sup> Being the DNA the molecular source of genetic

information, long-standing and intense efforts have been made by radiation chemists to unravel primary radical formation in DNA damaged by ionizing radiation. Next to optical spectroscopy, Electron Paramagnetic Resonance (EPR) was frequently used to detect the radicals formed. EPR measurements were mainly done in glassy solutions of irradiated DNA or single nucleosides/nucleotides. The spectra obtained were usually the superposition of multiple components, which led to an initial assumption that the radicals are formed in a random way upon ionizing radiation. Actually high energy radiation unspecifically ionizes DNA components approximately in direct proportion to the number of valence electrons available. On this basis, ca. 45% of the ionizations should occur at the bases (with no specificity among them), and 55% at the sugar-phosphate groups.<sup>[19]</sup> However the EPR spectroscopists (Gräslund, Gregoli, Hüttermann and Sevilla among many others) were able to unravel the multicomponent EPR spectra obtained upon ionizing radiation of DNA thus revealing that the final damage to DNA is not unspecific (Several reviews and articles presented the results of these investigations<sup>[20-27]</sup>). In fact the radical cations are localized only on the guanine bases, leading to a guanine radical cation ( $G^{\bullet+}$ ), while the radical anions are trapped at cytosine ( $C^{\bullet-}$ ) at very low temperatures (4-10 K), and at thymine bases ( $T^{\bullet-}$ ) at 77 K [for a review on the scavenging ability of the DNA bases see Barnes and Bernhard<sup>[28]</sup>]. In the latter case the trapping is made efficient by the subsequent and irreversible protonation at C6 position of the T molecule, which leads to a stable neutral radical,  $TH^{\bullet}$  [see also section 2.4.3].

The low temperature DNA ion radical distribution is a clear indication that hole and excess electron transfer processes occur after the initial unspecific damage induced by ionizing radiation. The radical formation in HT follows the trend for the electrochemical oxidation potentials of the bases.<sup>[29, 30]</sup> On the other hand the generation of radical anions in EET follows the trend for the electrochemical reduction potentials of the bases.<sup>[29]</sup> In the following the order of oxidative and reductive potentials (V vs NHE) obtained by cyclic voltammetry of the bases in acetonitrile<sup>[29]</sup> are reported:

$$\begin{array}{l} \text{Oxidation potentials (V vs NHE):} \\ \quad G < A < C \approx T \\ \quad 1.49 \quad 1.96 \quad 2.14 \quad 2.11 \end{array} \quad (1.1)$$

---


$$\begin{array}{ccccccc} & T & > & C & > & A & > & G \\ \text{Reduction potentials (V vs NHE):} & -2.18 & & -2.35 & & -2.52 & & -2.76 \end{array} \quad (1.2)$$

The values reported<sup>i</sup> are valid for single nucleosides. In DNA the trend is the same but the differences seem to be shallower. From the trend reported in eq. (1.1), the guanine base, with the lowest oxidation potential, is the most easily oxidized.

In the trend reported in eq. (1.2) the values for T and C are similar, thus they are the most easily reduced species. The order of eq. (1.2) is the same for the electron affinities of the nucleobases, as it has been calculated by Voityuk et al.<sup>[31]</sup>

Despite of the remarkable results obtained, the studies on ET processes by means of high-energy irradiation have a major disadvantage: the electron injection and the electron trapping do not occur site-selectively. Therefore Sevilla et al. had to use statistical models, in conjunction with EPR, in their studies of EET on  $\gamma$ -irradiated DNA<sup>[32-34]</sup> (see also section 1.2.4 for current state of the art in EET).

### 1.2.2 Selective radical formation in DNA by Photoinduced Charge Transfer

Most research groups have focused their work on the study of oxidative charge transfer in DNA, where it has been shown that the guanines are the charge carriers<sup>[35]</sup> (see also preceding paragraph). Usually the following experimental strategy has been adopted:

1. Attachment of the charge injection system to DNA.
2. Charge Injection into DNA by photochemical or electrochemical techniques.
3. Trapping and Detection of the charge at the final acceptor after its migration along DNA.

As depicted in the following scheme (Fig. 1.5) for a general photoinduced electron transfer process, in the injection step also the charge recombination process can take place. Moreover for the injection step to be effective it is of crucial importance that the charge injection system has the necessary redox potential to oxidize the next Ac, usually the nearest guanine.

---

<sup>i</sup> The potentials reported have to be considered only as indicative values, because of the irreversibility of the electrode processes in the electrochemical measurements. Other studies showed the same trend but higher values (e.g.  $\approx 1.58$  V for the guanine).<sup>[30]</sup>

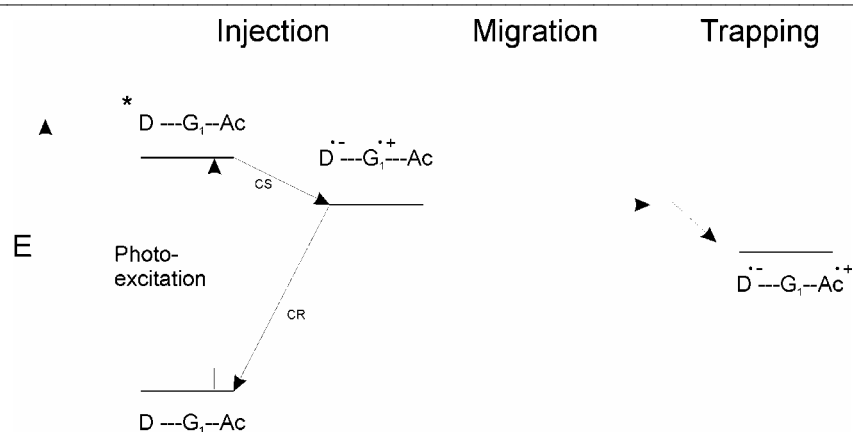


**Figure 1.5** Schematic picture of DNA-mediated photoinduced hole transfer. The hole transfer can stop either at the first guanine or at a distant final Ac. CS is the charge separation process, CR the charge recombination.

The advantage of this approach in comparison with the high energy radiation experiments, is that near UV or visible light can be used to selectively excite the artificial charge donor, leaving the DNA bases undamaged. Among the different experiments that have been carried out to probe the charge transfer properties of DNA, four examples, which are thought to be the most representative, will be described in the following.

One of the approaches utilized by Barton and co-workers involved the use of a DNA intercalating metal complex as charge donor along the DNA chain.<sup>[36-38]</sup> The final charge acceptor could be either another metallointercalator (as in Fig. 1.6) or nucleobases.<sup>[39]</sup>

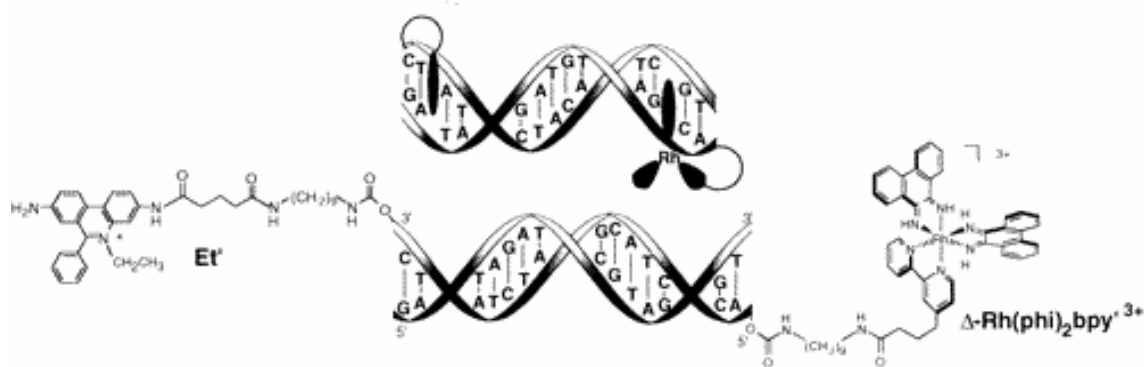


**Figure 1.6** A Rhodium bipirydine<sup>[40]</sup> charge donor and ethidium<sup>[41]</sup> charge acceptor covalently attached to duplex DNA at defined positions (linkers are enlarged here relative to the duplexes for clarity). The photoinduced CT reaction occurs between the intercalated donor and acceptor (top, schematic). The CT reaction was probed by fluorescence quenching (Adapted from <sup>[36]</sup>)

Even though many variations on these systems have been utilized, still ambiguities occurred with respect to the structural perturbations that the intercalating molecule may bring, and the location of the donor and acceptor, leading to uncertainties in the distance separating donors and acceptors.<sup>[42]</sup>

Zewail and co-workers were able to overcome some of the ambiguities, using nucleic acid bases as donor and acceptor.<sup>[43]</sup> A lot of assemblies were studied, one is presented in Fig. 1.7: the modified base 2-Aminopurine (2Ap) is the photoexcitable charge donor while a distant guanine G is the charge acceptor. The charge transfer process was directly detected by means of femtosecond spectroscopy.

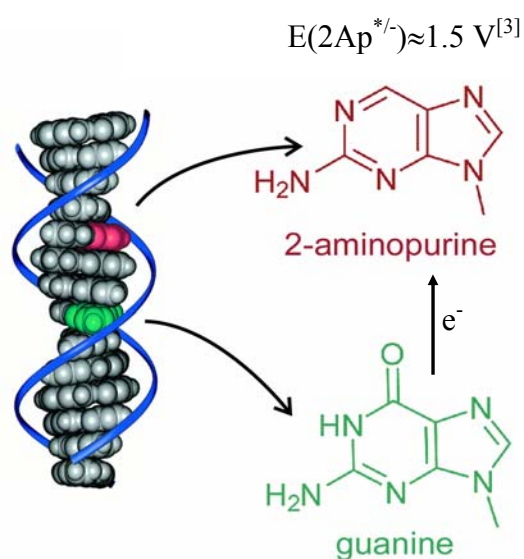


**Figure 1.7** Molecular model schematically illustrating the base pair stack within a DNA-duplex. The sugar phosphate backbone is depicted schematically in blue. (Adapted from <sup>[43]</sup>)

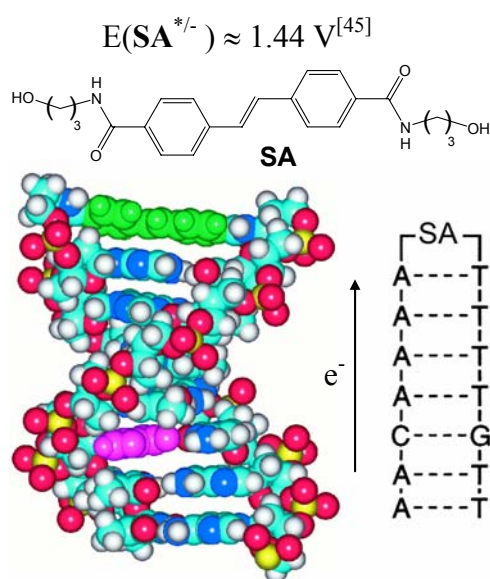


**Figure 1.8** Stilbene hairpin linker (SA, top panel) attached to DNA (lower panel). (Adapted from <sup>[44]</sup>)

have made DNA hairpins ideal model systems to investigate CT in DNA. They are stable<sup>[49]</sup> and stably folded: the assignment of a B-DNA structure (as in Fig. 1.8) in which the stilbene linker is  $\pi$ -stacked with the adjacent base pair was proposed on the basis of spectroscopic data and later supported by X-ray analysis for an analogous hairpin possessing a stilbenediether linker.<sup>[50]</sup> Moreover they are relatively easy to synthesize,<sup>[51]</sup> and they are versatile chromophores systems, which allow for both hole<sup>[44, 47]</sup> and excess electron injection<sup>[52]</sup>.

Finally, in the studies made by Giese, the charge injection is prompted by the photogeneration of a C4' radical from 4'-*tert*-butyl ketones of deoxynucleotides (Fig. 1.9).<sup>[53, 54]</sup> The radical rapidly loses phosphate to generate the enol ether radical cation (the redox potential is unknown), which injects the positive charge (hole injector) into the nearest guanine. As for all the systems described above, but the first one, the generated  $G^{\bullet+}$  can undergo two competing pathways: first it can be trapped irreversibly by water, yielding strand cleavage products in the presence of base; second  $G^{\bullet+}$  can oxidize nearby G, GG doublets or GGG triplets; then the charge undergoes the same trapping process as  $G^{\bullet+}$ .

In another approach Lewis and co-workers,<sup>[44, 45]</sup> used synthetic DNA hairpins, similar to the one depicted in in Fig. 1.8, in which a stilbene dicarboxamide (SA) forms a bridge connecting two oligonucleotide arms. Stilbene is the photoexcitable electron acceptor, which undergoes CT with the oxidizable G,<sup>[44, 46]</sup> GG, and GGG<sup>[47]</sup> electron donor nucleobases. In this case the charge transfer was detected by fluorescence and transient absorption spectroscopy: the transient spectrum is initially dominated by the SA excited state ( $\text{SA}^*$ ) and then evolves to the radical anion  $\text{SA}^-$  as the charge transfer proceeds.<sup>[44]</sup> Many hairpin linkers have been used<sup>[48]</sup> and many features



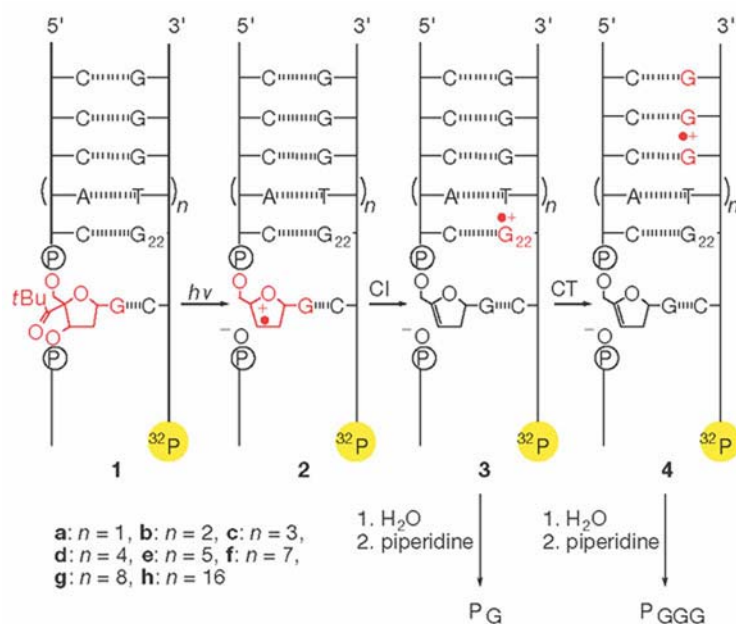


**Fig. 1.9** Charge injection and charge transfer in DNA strands. Illustrated are the method of charge injection into  $G_{22}$  (2→3) and charge transfer (CT) to the GGG sequence (3→4), starting from DNA strands **1a-h** that contain a 4'-acylated deoxyguanoside (in red). Photolyses of **1a-h** were performed at pH 5.0 (citrate buffer) with a 500-W, high-pressure Hg lamp (320 nm cut-off filter) in the absence of oxygen at 15 °C. Trapping by water of the charge at  $G_{22}$  and GGG leads to cleavage products  $P_G$  and  $P_{GGG}$ , respectively, after piperidine (base) treatment. The nucleotides in red indicate the charge precursor (1), the injection site (2), the charge donor (3), and the charge acceptor (4). (Taken from <sup>[53]</sup>)

With this assay the CT absolute rates cannot be determined, contrary to the cases (see above) where time resolved measurements are performed. The relative rate for CT in DNA may be ascertained by determining the product yield ratio of the irreversible reactions products by means of gel electrophoresis and measuring it as a function of D-Ac distance. One advantage of the assay used by Giese and co-workers is that the guanine radical cation is irreversibly generated and there is no competition from the back electron transfer reaction (which takes place instead in the experiments with 2Ap and SA), since the injection system (enol ether radical) oxidizes the DNA bases from its ground state.<sup>[46, 55]</sup> In this way it is easier to detect not only the charge injection step but also the next HT process from one guanine to the other. The latter migration should be independent of the charge injection system, which instead is really dependent on the redox potential of the systems used.<sup>[56]</sup>

### 1.2.3 Mechanistic picture for Hole Transfer in DNA

The results obtained in the studies on HT in DNA are usually described in terms of the parameter  $\beta_{CT}$ , since the CT rate constant  $k_{CT}$  varies with the donor-acceptor distance  $r_{DA}$  covered by the migrating hole as follows:

$$k_{CT} \propto \exp(-\beta_{CT} r_{DA}) \quad (1.3)$$

This proportionality is derived from the Marcus-Levich-Jortner theory, which is based on the superexchange mechanism, and the parameter  $\beta$  reflects the distance dependence of the electronic coupling (see section 1.2.3a).  $\beta$  is estimated to be  $3.4 \text{ \AA}^{-1}$  for CT in a vacuum, while for proteins the value seems to fall in the range  $0.8\text{-}1.2 \text{ \AA}^{-1}$ <sup>[57]</sup>. In the early 90's were published extremely low values for  $\beta_{CT} (< 0.2 \text{ \AA}^{-1})$  in DNA.<sup>[38]</sup> Such values of  $\beta_{CT}$  are characteristic of electrons in conductors, leading to the proposition of DNA as a "pi-way" or "wire" for electrons. This proposition prompted intense debate and experimental scrutiny, leading to results different from the initial ones (see below).

The more reliable Hole Transfer rate measurements were done on well-defined D-DNA-Ac systems, such as the ones from Zewail, Lewis and Giese (described above), as well as the experiments performed by M.E. Beyerle<sup>[54, 58, 59]</sup>. By changing the parameters of the system, as for example the donor D or the intervening sequence between D and Ac (bridge DNA), the authors were able to measure the influence of these parameters on the charge transfer rate. The following unifying conclusions for HT in DNA have been made:

- a) the charge transfer rates  $k_{CT}$  depend on the free energy driving force  $\Delta G^\circ$ .
- b) the photoinduced CT experiments of Giese, Lewis and Zewail yielded similar  $\beta_{CT}$  of  $0.6\text{-}1.2 \text{ \AA}^{-1}$ <sup>[43, 46, 53]</sup>. The hole transfer proceeds by means of the superexchange mechanism (see also section 1.2.3a for the particular case analysis) if 3 or less intervening (A:T) base pairs are present in the traveling pathway of the hole. In that case a distance dependence  $\beta_{CT} \approx 0.6 \text{ \AA}^{-1}$  is found<sup>[60]</sup>. These values for  $\beta_{CT}$ , but also the optical and the electronic properties of DNA,<sup>[61]</sup> suggest that CT through the DNA  $\pi$ -stack arrangement is not as efficient as in conductors, for example, and show that DNA is not a molecular wire.
- c) there is experimental evidence, for hole transfer over long-range distances of  $40\text{-}200 \text{ \AA}$ , from many biochemical approaches.<sup>[38, 55, 62, 63]</sup> The mechanism involved in this long range

CT is a hopping. In particular hopping among intervening guanines and adenines (see also section 1.2.3b for the explanation of the particular case), as showed by Giese and co-workers<sup>[55, 64-66]</sup>, and polaron-like hopping of delocalised radical cations, in the model suggested by Schuster<sup>[67, 68]</sup> (see also section 1.2.3c for the explanation of the particular case).

d) for long-charge transfer to occur, it is essential that D-DNA-Ac are well stacked and posses a strong  $\pi$ -interaction. In fact, the introduction of structure disturbing base mismatch or loops leads to a decrease in the efficiency of the long-range charge transfer.<sup>[56, 60, 69]</sup>

In the following the mechanistic aspects of HT in DNA are described in better detail.

### 1.2.3a Superexchange

The Marcus-Levich-Jortner equation for a nonadiabatic ET tunneling process between a donor D and an acceptor Ac is:<sup>[70, 71]</sup>

$$k_{CT} = \frac{2\pi}{\hbar} H_{DA}^2 F \quad (1.4)$$

$$F = \frac{1}{\sqrt{4\pi\lambda_s k_B T}} \exp(-S_c) \sum_n \frac{S_c^n}{n!} \times \exp\left(-\frac{(\lambda_s + \Delta G^0 + n\hbar\langle\omega_c\rangle)^2}{4\lambda_s k_B T}\right), \quad S_c = \frac{\lambda_i}{\hbar\langle\omega_c\rangle} \quad (1.5)$$

where  $\hbar = h/2\pi$  ( $h$  is Planck's constant),  $F$  is the Franck-Condon factor with  $\Delta G^0$  the redox free energy for the charge transfer reaction,  $k_B$  the Boltzmann constant,  $T$  the temperature,  $S_c$  the Huang-Rhys factor,  $\lambda_i$  the nuclear reorganization energy,  $\lambda_s$  the solvent reorganization energy, and  $\omega$  the average high-frequency vibrational frequency.<sup>[65, 71, 72]</sup> In this form of the Frank-Condon term both medium and intramolecular vibrational modes are taken into account. This is important for highly exothermic reactions.<sup>[73]</sup>

The electronic matrix element coupling the donor and acceptor  $H_{DA}^2$  describes the effective donor-acceptor interaction:

$$H_{AD} = H_{AD}^0 \exp^{-\beta_{CT}(r_{DA}-r_0)} \quad (1.6)$$

where  $r_0$  is the center-to-center distance of the donor-acceptor pair at contact and  $\beta_{CT}$  is a constant, reflecting the rapidity at which the exponential wave function decays. Eq. (1.4) has the correct form for a through space (tunneling) coupling mechanism. Substituting eq.(1.6) in eq. (1.4) one can express the tunneling process in terms of eq. (1.3).

However in a molecule like DNA the intervening bases (bridge) between D and Ac have a role in providing the coupling and reducing the energy barrier that the electron has to overcome in the tunneling process. This phenomenon, known as superexchange, was first studied by McConnell.<sup>[74]</sup> The role of the bridge electronic structure in a [donor D-DNA bridge (B1,B2,...B<sub>n</sub>)-acceptor Ac] sequence is taken into account in the McConnell expression of the electronic matrix element  $H_{DA}$  coupling, in the limit of weak interactions between bridging units and assuming only one orbital per bridge:

$$H_{AD} = \frac{H_{D1}H_{NA}}{\delta E} \prod_{i=1}^{N-1} \frac{H_{i,i+1}}{\delta E_i} \quad (1.7)$$

Where  $H_{Di}$  and  $H_{iN}$  are Hamiltonian terms describing the D-B<sub>i</sub> and the B<sub>i</sub>-Ac interactions, respectively, and  $\delta E$  is the energy gap between donor/acceptor and the bridge (see Fig. 1.10).

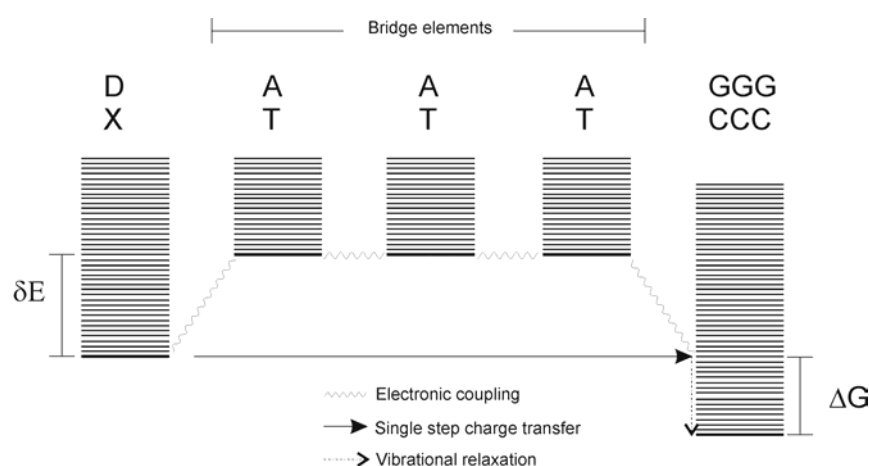


**Fig. 1.10** Vibronic level scheme for unistep charge transfer via superexchange. A possible sequence for such a process is depicted above.

In the superexchange mechanism the hole states of the (T:A) bridges are virtual, they are not a chemical intermediate (or, to say, the hole is not going onto the bridge states).<sup>[75]</sup> It

has been demonstrated that in duplex DNA the superexchange mechanism occurs only at short distances, below 10 Å or 4 (A:T) base pairs. If the intervening bases between the G bases (Gs) are more than 3 then the extent of the electronic coupling dies off exponentially with distance making the exothermic tunnelling to the Gs less efficient.

It should be noted that at very short distances, below 6 Å, and in highly polar solvents also the solvent reorganization energy  $\lambda_s$  has to be considered D-Ac distance dependent and should be counted in eq. (1.5)<sup>[59, 60]</sup>: the solvent reorganization energy is small for charge shifts over short distances, and it increases with the distance until it reaches a plateau. This implies an increase in the  $k_{CT}$  at short distances, as observed by M.E. Michel-Beyerle<sup>[59]</sup> and B. Giese<sup>[66, 76]</sup>.

### 1.2.3b Hopping mechanism between guanines

The observation that the single guanines are carriers for positive charge led to the proposition of a G hopping mechanism to explain long distance CT through DNA.<sup>[42, 62, 67, 77]</sup> Once the positive charge has been injected into DNA, the next guanine can be oxidized, forming a guanine radical cation  $G^{\bullet+}$  that can oxidize, if not trapped by water, another guanine, so that a positive charge can be transported by several superexchange mediated steps over guanines till is trapped by the final acceptor, or by water (see Fig. 1.11).<sup>[56, 65, 75]</sup>

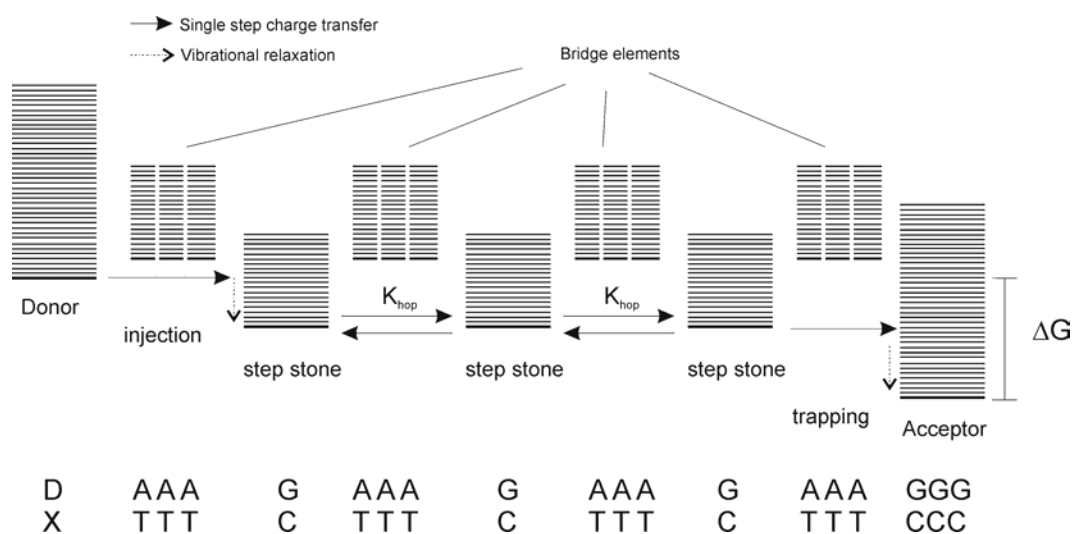


**Figure 1.11** Vibronic level scheme for multistep charge transport via hopping and trapping. A possible sequence for such a process is depicted below.

This process takes place when in the DNA sequence the potential guanine donors ( $G_n$ , where  $n$  is an integer number) and the potential guanine acceptors ( $G_{n+1}$ ) are separated by  $(T:A)_i$  bridges with  $i < 3-4$ . Each hopping step is induced by superexchange, off-resonance coupling between  $G_n$  and  $G_{n+1}$  via the  $(T:A)$  bridges. The energetic difference to the superexchange mechanism is that the stepping-stones of the bridge are lower in energy than the donor states, leading to an occupation of the bridge by the charge (Fig. 1.11). This process occurs only if the water trapping reaction is so slow that the charge transfer can compete with it.

In the hopping mechanism, the apparent overall electronic coupling is increased with respect to a possible long single tunnelling process  $D$  to  $A_c$ , since each short step has a big coupling  $H_{DA}$ . Also the overall rate of hole transport is increased, because is not exponentially distance dependent as in the superexchange case (eq. 1.3), but depends on the number of hopping steps  $N$ :

$$k_{CT} \propto N^{-\eta} \quad (1.8)$$

where  $\eta$  is a constant.<sup>[77]</sup>

The limit of this mechanism is that a single hop between two guanine bases cannot exceed a distance of 3 base pairs, since the single step is governed by the superexchange mechanism. In that case the CT rate should become should be too small to compete with the water trapping reaction.<sup>[78]</sup> Nevertheless experiments showed that hole transfer also occurs over long range  $(T:A)_i$  sequences, following different distance dependencies from the hopping mechanism.<sup>[53, 63]</sup> Thus Giese postulated a A-hopping mechanism in order to interpretate long range hole transport over  $(T:A)_i$  bridges with  $i > 4$ .<sup>[53]</sup>

### 1.2.3c Hopping mechanism between adenines

When the distance between two guanine base is more than 3 base pairs, then the endothermic oxidation of the adjacent adenine may become a competing reaction, if the lifetime of the guanine radical cation is long enough to oxidize the adjacent A:T base pair in a thermally activated step.<sup>[56]</sup> Once the adenine is oxidized (the oxidation is the rate determining step), the charge travels very rapidly the A:T base pairs until decays to the G, GG, or GGG, or is trapped by water.<sup>[53, 60]</sup> This mechanism has been validated by Giese in

---

experiments in which the positive charge was directly injected into an adenine.<sup>[79]</sup> However there is still not spectroscopic evidence for adenin bases as charge carriers.

### *1.2.3c Polaron assisted mechanism*

Another interpretation of the charge transfer between distant Gs has been given by Schuster. He proposed that the charge is not simply present on a guanine base, but is delocalised and extends over the nearby sequence.<sup>[67]</sup> The delocalisation is accomplished by the distortion of the DNA: in order to stabilize the radical cation, the neighbour base pairs are brought closer to the charge, thus delocalising it. The distorted section of duplex DNA around the radical cation is called polaron and its extension stops when the distorting energy is balanced by the stabilization.

In this picture the delocalised hole can also migrate along DNA, by means of a phonon (thermal)-assisted polaron hopping.<sup>[63, 67, 68]</sup> Thermal (phonon) activation will cause base pairs in and near the structural distortion to leave or join the polaron. The delocalised positive charge hops from having its centre on a G to have its centre on the next G base.

This mechanism has been used to explain long-range radical cation migration in DNA.<sup>[63, 68, 80]</sup>

### *1.2.3d Proton coupled electron transfer*

In biological redox reactions electron transfer may be coupled to proton transfer. Such reactions can occur either in a concerted or in a sequential fashion. Steenken postulated that during an CT process the base pairing in DNA could induce rearrangements, i.e. proton transfer within the base pairs.<sup>[25]</sup> The proton transfer leads to a separation of charge from spin: cations or anions are converted into neutral radical, while the charge is transferred to the opposite strand<sup>[25, 30]</sup>(Fig. 1.10).

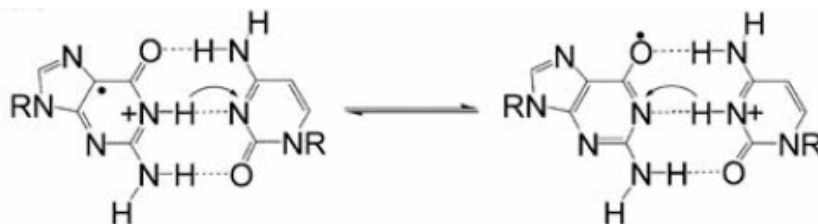


**Figure 1.10** Proton shift from the  $G^+$  radical cation to cytosine and separation of the charge from spin. In this way the charge is stabilized and, as a consequence, the driving force for the hole transfer should increase if proton and hole transfer are coupled together. (Adapted from<sup>[60]</sup>)

This process is driven by the changes in acidity or basicity that result from loss or uptake of an electron from or by a base in a base pair in DNA.<sup>[81, 82]</sup> In the (GC) base pair the driving force of the proton transfer is the increased acidity of  $G^{\bullet+}$  (pKa= 3.9 in neutral solutions of free nucleosides)<sup>[83]</sup> The deprotonated form of  $G^{\bullet+}$  in duplex DNA has been detected by means of EPR spectroscopy in neutral solution at room temperature<sup>[84, 85]</sup> The protonated form of the pyrimidine bases has been already detected by the radiation biologists (see section 1.2.1). If such proton shifts are coupled with the charge shift along the DNA, then it may be possible to speak of charge transfer coupled with a proton transfer. Giese and co-workers<sup>[86]</sup> as well as Shafirovich and co-workers<sup>[87, 88]</sup> speculated that proton coupled charge transfer processes might occur in DNA.

#### 1.2.4 Excess Electron Transfer in DNA

Similar to the approach used in HT in DNA, also for the investigation of EET it is necessary to utilize suitable injector systems and defined Donor-DNA-Acceptor assays. Studies in this field have been done systematically since only few years.<sup>[89-93]</sup> Carell and co-workers, for example, used flavin derivatives as electron donors to repair thymine dimers.<sup>[90, 94]</sup> Recently also the injector system analyzed here (chapter 6) has been used for the same kind of studies.<sup>[95]</sup>

From the studies on EET in DNA a mechanistic picture is also emerging. Recent investigations have shown similarities with the HT process. Also electrons travel over long distances by hopping.<sup>[96, 97]</sup> In EET however, the pyrimidine bases (C,T) were supposed to be temporary charge carriers.<sup>[54]</sup> Nevertheless recently Wagenknecht<sup>[92]</sup> and Rokita<sup>[93]</sup>



suggested that the radical anion of  $C^{\bullet-}$  may not play a major role as an intermediate charge carrier due to its protonation and consequent stabilization of the radical.

### 1.2.5 Biradicals in DNA? Possible correlation between charge transfer rate and exchange coupling

A physical phenomenon that is repeatedly related to  $k_{CT}$  is the spin-spin exchange coupling constant  $J$  between two unpaired electrons, which depends as  $k_{CT}$  on the mediation properties of the bridge connecting the two radical centers.  $J$  is the coupling between two unpaired electrons in a biradical and is measurable by means of EPR. Its expression is given below <sup>[98-100]ii</sup>.

$$J = 2.5(\langle a|\hat{h}|a\rangle + \langle b|\hat{h}|b\rangle)S_{ab}^2 - \langle aa|bb\rangle S_{ab}^2 + \langle ab|ba\rangle \quad (1.9)$$

where  $a$  and  $b$  are the singly occupied molecular orbitals,  $S_{ab} = \int a^* b d\tau$  is the overlap integral between  $a$  and  $b$ ,  $\langle a|\hat{h}|a\rangle = \int a^*(1)\hat{h}a(1)d\tau(1)$  and  $\langle b|\hat{h}|b\rangle = \int b^*(1)\hat{h}b(1)d\tau(1)$  are the one-electron-coulomb integrals,  $\langle aa|bb\rangle = \iint a^*(1)a(1)(\frac{1}{r_{12}})b^*(2)b(2)d\tau(1)d\tau(2)$ , and  $\langle ab|ba\rangle = \iint a^*(1)b(1)(\frac{1}{r_{12}})b^*(2)a(2)d\tau(1)d\tau(2)$ , are the two-electron-coulomb integral and the two-electron-exchange integral, respectively.

In the literature it is frequently speculated that the charge transfer  $k_{CT}$  and the  $J$  coupling may have several determining factors in common.<sup>[101-105]</sup> In particular correlations between  $J$  and  $H_{DA}$  have been established.<sup>[106-111]</sup>  $H_{DA}$  and  $J$  differ by being one- and two-electron quantities, respectively, but both are measures of long-range electronic interactions and should scale together as functions of molecular structure. As an example Forbes et al. used the spin exchange interaction  $J$  in flexible alkane chain biradicals as a model for  $H_{DA}$  in D/Ac complexes.<sup>[104]</sup> They also gave an exponential function for  $J$  with distance similar to the one described in eq. (1.6) for  $H_{DA}$ :<sup>[104]</sup>

$$J = J_0 \exp(-\lambda(r - r_0)) \quad (1.10)$$

$J_0$  is the value of  $J$  at the distance of closest approach of the radical centers ( $r_0=3.5 \text{ \AA}$ ) and  $\lambda$  is a falloff parameter generally accepted to be about  $1.0 \text{ \AA}^{-1}$ . More recently Calvo, Lubitz et al.<sup>[112]</sup> were able to measure  $J$  with EPR and to correlate it with charge transfer parameters for two semiquinone radicals  $Q_A^{\bullet-}$  and  $Q_B^{\bullet-}$  in *Rhodobacter sphaeroides*:

$$H_{DA}^2 \approx (\beta_{CT}) \approx (\lambda_s + \Delta G^0) |J| \quad (1.11)$$

In conclusion this kind of correlation could help to state the value of  $H_{DA}$  and hence of  $k_{CT}$  in case where these values cannot be determined from kinetic experiments, since  $J$  can be inquired with EPR.

In the specific case of the topics treated here, there are no reports about this correlation in DNA neither about  $J$  in DNA. The knowledge of  $J$  would be useful, since its analysis may yield a deeper understanding of the exchange mechanism and of the coupling between the bases. To be able to perform these studies it is necessary to introduce two stable radicals in DNA in a known position and to inquire the  $J$  coupling by multifrequency continuous wave (cw) and modern pulsed electron paramagnetic resonance (EPR) spectroscopic methods. These measurements should be then compared with ET investigations on a system with the donor and the Ac situated in the same position of the two radicals.

---

<sup>ii</sup> There are different definitions of the exchange interaction parameter, as given in<sup>[85]</sup>

---

### 1.3 REFERENCES

- [1] M. Friedrich, *Hoppe-Seyler's medicinisch-chemische Untersuchungen* **1871**, 4, 441.
- [2] M. Friedrich, *Verhandlungen der naturforschenden Gesellschaft in Basel* **1874**, 6, 138–208.
- [3] O. T. Avery, C. M. MacLeod, M. McCarty, *Journal of Experimental Medicine* **1944**, 79, 137.
- [4] J. D. Watson, F. H. C. Crick, *Nature* **1953**, 171, 737.
- [5] A. Kornberg, T. A. Baker, *DNA Replication*, W.H. Freeman & Company, New York, **1991**.
- [6] D. D. Eley, D. I. Spivey, *Transactions of the Faraday Society* **1962**, 58, 411.
- [7] R. S. Smart, *Transactions of the Faraday Society* **1963**, 59, 754.
- [8] N. J. Turro, J. K. Barton, *Journal of Biological Inorganic Chemistry* **1998**, 3, 201.
- [9] P. O'Neill, E. M. Frieden, *Advances in Radiation Biology* **1993**, 17, 53 – 120.
- [10] B. Armitage, *Chemical Reviews* **1998**, 98, 1171 – 1200.
- [11] C. J. Burrows, J. G. Muller, *Chemical Reviews* **1998**, 98, 1109 – 1151.
- [12] D. Wang, D. A. Kreuzer, J. M. Essigmann, *Mutation Research* **1998**, 400, 99 – 115.
- [13] S. Kawanashi, Y. Hiraku, S. Oikawa, *Mutation Research* **2001**, 488, 65 – 76.
- [14] E. Winfree, F. Liu, L. A. Wenzler, N. C. Seeman, *Nature* **1998**, 394, 539.
- [15] H.-W. Fink, C. Schonenberger, *Nature* **1999**, 398, 407.
- [16] D. Porath, A. Bezryadin, S. De Vries, C. Dekker, *Nature* **2000**, 403, 635.
- [17] E. Braun, Y. Eichen, U. Silvan, G. Ben-Joseph, *Nature* **1998**, 391, 775.
- [18] H. J. Muller, *Amer. Nat.* **1926**, 60.
- [19] S. Steenken, *Biology and Chemistry* **1997**, 378, 1293.
- [20] J. Hüttermann, *Radical ions and their reactions in DNA and its constituents. Contribution of electron spin resonance spectroscopy.*, Kluwer, Dordrecht, The Netherlands, **1991**.
- [21] S. Gregoli, M. Olast, A. Bertinchamps, *Radiation Research* **1982**, 89, 238.
- [22] A. Gräslund, Ehrenber.A, Rupprech.A, G. Strom, *Biochimica Et Biophysica Acta* **1971**, 254, 172.

- [23] J. Hüttermann, K. Voit, H. Oloff, W. Kohnlein, A. Gräslund, A. Rupprecht, *Faraday Discussions* **1984**, 135.
- [24] W. A. Bernhard, *Advances in Radiation Biology* **1981**, 9.
- [25] S. Steenken, *Chemical Reviews* **1989**, 89, 503.
- [26] D. M. Close, *Magnetic Resonance Reviews* **1991**, 15, 241.
- [27] D. Becker, M. D. Sevilla, *Advances in Radiation Biology, Vol 17* **1993**, 17, 121.
- [28] J. P. Barnes, W. A. and Bernhard, *Journal of Physical Chemistry* **1995**, 99, 11248.
- [29] C. A. M. Seidel, A. Schulz, S. Sauer, *Journal of Physical Chemistry* **1996**, 100, 5541.
- [30] S. Steenken, S. V. Jovanovic, *Journal of the American Chemical Society* **1997**, 119, 617.
- [31] A. A. Voityuk, M. E. Michel-Beyerle, N. Roosch, *Chemical Physics Letters* **2001**, 342, 231.
- [32] Z. L. Cai, X. F. Li, M. D. Sevilla, *Journal of Physical Chemistry B* **2002**, 106, 2755.
- [33] A. Messer, K. Carpenter, K. Forzley, J. Buchanan, S. Yang, Y. Razskazovskii, Y. L. Cai, M. D. Sevilla, *Journal of Physical Chemistry B* **2000**, 104, 1128.
- [34] Z. L. Cai, M. D. Sevilla, *Journal of Physical Chemistry B* **2000**, 104, 6942.
- [35] E. Meggers, M. E. Michel-Beyerle, B. Giese, *Journal of the American Chemical Society* **1998**, 120, 12950.
- [36] S. O. Kelley, R. E. Holmlin, E. D. A. Stemp, J. K. Barton, *Journal of the American Chemical Society* **1997**, 119, 9861.
- [37] M. Pascaly, J. Yoo, J. K. Barton, *Journal of the American Chemical Society* **2002**, 124, 9083.
- [38] C. J. Murphy, M. R. Arkin, Y. Jenkins, N. D. Ghatlia, S. H. Bossmann, N. J. Turro, J. K. Barton, *Science* **1993**, 262, 1025.
- [39] M. E. Núñez, J. K. Barton, *Current Opinion in Chemical Biology* **2000**, 4, 199.
- [40] C. Turro, A. Evenzahav, S. H. Bossmann, J. K. Barton, N. J. Turro, *Inorganica Chimica Acta* **1996**, 243, 101.
- [41] S. O. Kelley, J. K. Barton, *Chemistry & Biology* **1998**, 5, 413.
- [42] F. D. Lewis, R. L. Letsinger, M. R. Wasielewski, *Accounts of Chemical Research* **2001**, 34, 159.

- 
- [43] C. Z. Wan, T. Fiebig, O. Schiemann, J. K. Barton, A. H. Zewail, *Proceedings of the National Academy of Sciences of the United States of America* **2000**, *97*, 14052.
- [44] F. D. Lewis, T. F. Wu, Y. F. Zhang, R. L. Letsinger, S. R. Greenfield, M. R. Wasielewski, *Science* **1997**, *277*, 673.
- [45] F. D. Lewis, X. B. Zuo, J. Q. Liu, R. T. Hayes, M. R. Wasielewski, *Journal of the American Chemical Society* **2002**, *124*, 4568.
- [46] F. D. Lewis, T. F. Wu, X. Y. Liu, R. L. Letsinger, S. R. Greenfield, S. E. Miller, M. R. Wasielewski, *Journal of the American Chemical Society* **2000**, *122*, 2889.
- [47] F. D. Lewis, X. Y. Liu, J. Q. Liu, S. E. Miller, R. T. Hayes, M. R. Wasielewski, *Nature* **2000**, *406*, 51.
- [48] F. D. Lewis, R. S. Kalgutkar, Y. S. Wu, X. Y. Liu, J. Q. Liu, R. T. Hayes, S. E. Miller, M. R. Wasielewski, *Journal of the American Chemical Society* **2000**, *122*, 12346.
- [49] R. L. Letsinger, T. Wu, *Journal of the American Chemical Society* **1995**, *117*, 7323.
- [50] F. D. Lewis, X. Y. Liu, Y. S. Wu, S. E. Miller, M. R. Wasielewski, R. L. Letsinger, R. Sanishvili, A. Joachimiak, V. Tereshko, M. Egli, *Journal of the American Chemical Society* **1999**, *121*, 9905.
- [51] F. D. Lewis, E. Wasielewski, in *Topics in Current Chemistry, Vol. 236*, Springer-Verlag, Berlin, Heidelberg, **2004**, pp. 45.
- [52] F. D. Lewis, X. Y. Liu, S. E. Miller, R. T. Hayes, M. R. Wasielewski, *Journal of the American Chemical Society* **2002**, *124*, 11280.
- [53] B. Giese, J. Amaudrut, A. K. Kohler, M. Spormann, S. Wessely, *Nature* **2001**, *412*, 318.
- [54] B. Giese, S. Wessely, M. Spormann, U. Lindemann, E. Meggers, M. E. Michel-Beyerle, *Angewandte Chemie-International Edition* **1999**, *38*, 996.
- [55] B. Giese, *Current Opinion in Chemical Biology* **2002**, *6*, 612.
- [56] B. Giese, *Annual Review of Biochemistry* **2002**, *71*, 51.
- [57] R. Langen, J. L. Colon, D. R. Casimiro, T. B. Karpishin, J. R. Winkler, H. B. Gray, *Journal of Biological Inorganic Chemistry* **1996**, *1*, 221.
- [58] W. B. Davis, S. Hess, I. Naydenova, R. Haselsberger, A. Ogrodnik, M. D. Newton, M. E. Michel-Beyerle, *Journal of the American Chemical Society* **2002**, *124*, 2422.
- [59] S. Hess, M. Gotz, W. B. Davis, M. E. Michel-Beyerle, *Journal of the American Chemical Society* **2001**, *123*, 10046.

- 
- [60] B. Giese, in *Topics in Current Chemistry, Vol. 236*, Springer-Verlag, Berlin, Heidelberg, **2004**, pp. 27.
- [61] D. N. Beratan, S. Priyadarshy, S. M. Risser, *Chemistry & Biology* **1997**, *4*, 3.
- [62] B. Giese, *Accounts of Chemical Research* **2000**, *33*, 631.
- [63] P. T. Henderson, D. Jones, G. Hampikian, Y. Kan, G. B. Schuster, *Proceedings of the National Academy of Sciences of the United States of America* **1999**, *96*, 8353.
- [64] B. Giese, *Chemistry in Britain* **2000**, *36*, 44.
- [65] M. Bixon, B. Giese, S. Wessely, T. Langenbacher, M. E. Michel-Beyerle, J. Jortner, *Proceedings of the National Academy of Sciences of the United States of America* **1999**, *96*, 11713.
- [66] B. Giese, A. Biland, *Chemical Communications* **2002**, 667.
- [67] G. B. Schuster, *Accounts of Chemical Research* **2000**, *33*, 253.
- [68] D. Ly, L. Sani, G. B. Schuster, *Journal of the American Chemical Society* **1999**, *121*, 9400.
- [69] M. A. O'Neill, J. K. Barton, in *Topics in Current Chemistry, Vol. 236*, Springer-Verlag, Berlin, Heidelberg, **2004**, p. 67–115.
- [70] R. A. Marcus, N. Sutin, *Biochimica Et Biophysica Acta* **1985**, *811*, 265.
- [71] J. Jortner, *Journal of Chemical Physics* **1976**, *64*, 4860.
- [72] J. Ulstrup, J. Jortner, *Journal of Chemical Physics* **1975**, *63*, 4358.
- [73] G. L. Closs, J. R. Miller, *Science* **1988**, *240*, 440.
- [74] H. M. McConnell, *Journal of Chemical Physics* **1961**, *35*, 508.
- [75] J. Jortner, M. Bixon, A. A. Voityuk, N. Rösch, *Journal of Physical Chemistry A* **2002**, *106*, 7599.
- [76] E. Meggers, D. Kusch, M. Spichty, U. Wille, B. Giese, *Angewandte Chemie-International Edition* **1998**, *37*, 460.
- [77] J. Jortner, M. Bixon, T. Langenbacher, M. E. Michel-Beyerle, *Proceedings of the National Academy of Sciences of the United States of America* **1998**, *95*, 12759.
- [78] B. Giese, M. Spichty, *Chemphyschem* **2000**, *1*, 195.
- [79] T. Kendrick, B. Giese, *Chemical Communications* **2002**, 2016.
- [80] G. B. Schuster, U. Landman, in *Topics in Current Chemistry, Vol. 236*, Springer-Verlag, Berlin, Heidelberg, **2004**, p. 139–161.
- [81] S. Steenken, *Free Radical Research Communications* **1992**, *16*, 349.

- 
- [82] S. Steenken, J. P. Telo, H. M. Novais, L. P. and Candeias, *Journal of the American Chemical Society* **1992**, *114*, 4701.
- [83] L. P. Candeias, S. Steenken, *Journal of the American Chemical Society* **1989**, *111*, 1094.
- [84] O. Schiemann, N. J. Turro, J. K. Barton, *Journal of Physical Chemistry B* **2000**, *104*, 7214.
- [85] K. Hildenbrand, D. and Schulte-Frohlinde, *Free Radical Research Communications* **1990**, *11*, 195.
- [86] B. Giese, S. Wessely, *Chemical Communications* **2001**, 2108.
- [87] V. Shafirovich, N. E. Geacintov, in *Topics in Current Chemistry, Vol. 237*, Springer-Verlag, Berlin, Heidelberg, **2004**, pp. 129.
- [88] V. Shafirovich, A. Dourandin, N. P. Luneva, N. E. Geacintov, *Journal of Physical Chemistry B* **2000**, *104*, 137.
- [89] F. D. Lewis, X. Y. Liu, S. E. Miller, M. R. Wasielewski, *Journal of the American Chemical Society* **1999**, *121*, 9746.
- [90] C. Behrens, L. T. Burgdorf, A. Schwogler, T. Carell, *Angewandte Chemie-International Edition* **2002**, *41*, 1763.
- [91] M. K. Cichon, C. H. Haas, F. Grolle, A. Mees, T. Carell, *Journal of the American Chemical Society* **2002**, *124*, 13984.
- [92] H. A. Wagenknecht, *Angewandte Chemie-International Edition* **2003**, *42*, 2454.
- [93] T. Ito, S. E. Rokita, *Angewandte Chemie International Edition English* **2004**, *43*, 1839.
- [94] C. Behrens, M. Ober, T. Carell, *European Journal of Organic Chemistry* **2002**, 3281.
- [95] B. Giese, B. Carl, T. Carl, T. Carell, C. Behrens, U. Hennecke, O. Schiemann, E. Feresin, *Angewandte Chemie* **2004**, *116*, 1884.
- [96] T. Ito, S. E. Rokita, *Journal of the American Chemical Society* **2003**, *125*, 11480.
- [97] T. Carell, C. Behrens, J. Gierlich, *Organic & Biomolecular Chemistry* **2003**, *1*, 2221.
- [98] O. Kahn, *Molecular Magnetism, Vol. 135*, VCH Publishers, **1993**.
- [99] J. Fritscher, Master Thesis, Johann Wolfgang Goethe-Universität (Frankfurt am Main), **2000**.

- [100] K. Yoshizawa, R. Hoffmann, *Journal of the American Chemical Society* **1995**, *117*, 6921.
- [101] R. Ramasami, J. F. Endicott, *Journal of the American Chemical Society* **1985**, *107*, 389.
- [102] P. Bertrand, *Chemical Physic Letters* **1985**, *113*, 104.
- [103] G. Blondin, J.-J. Girerd, *Chemical Reviews* **1990**, *90*, 1359.
- [104] M. D. E. Forbes, J. D. Ball, N. I. Avdievich, *Journal of the American Chemical Society* **1996**, *118*, 4707.
- [105] R. E. Coffmann, G. R. Beuttner, *Journal of Physical Chemistry* **1979**, *83*, 2387.
- [106] M. D. E. Forbes, *Journal of Physical Chemistry* **1993**, *97*, 3390.
- [107] J. J. Hopfield, *Tunneling in biological systems*, Academic Press, New York, **1979**.
- [108] M. Y. Okamura, R. A. Isaacson, G. Feher, *Biochimica Et Biophysica Acta* **1979**, *546*, 394.
- [109] M. Redi, J. J. Hopfield, *Journal of Chemical Physics* **1980**, *72*, 6651.
- [110] R. Haberkorn, M. E. Michel-Beyerle, R. A. Marcus, *Proceedings of the National Academy of Sciences of the United States of America* **1979**, *76*, 4185.
- [111] M. D. E. Forbes, *Journal of Physical Chemistry* **1993**, *97*, 3396.
- [112] R. Calvo, E. C. Abresch, R. Bittl, G. Feher, W. Hofbauer, R. A. Isaacson, W. Lubitz, M. Y. Okamura, M. L. Paddock, *Journal of the American Chemical Society* **2000**, *122*, 7327.



---

## 2. EPR THEORY AND MODEL SPECTRA

In this chapter an overview of the basic theory of Electron Paramagnetic Resonance (EPR) spectroscopy is given. Particular emphasis will be devoted to the explanation of the isotropic hyperfine coupling and the mechanisms involved, spin polarization and hyperconjugation. The theoretical description of these phenomena will be correlated with examples of EPR spectra from organic radicals that are important in this thesis.

### 2.1 INTRODUCTION

EPR spectroscopy deals with the interaction of electromagnetic radiation with magnetic moments that arise from electrons.

Electromagnetic radiation in free space may be regarded classically as coupled electric ( $\mathbf{E}_1$ ) and magnetic ( $\mathbf{B}_1$ ) fields perpendicular to each other and to the direction of propagation. Both oscillate at some frequency  $\nu$ . In optical spectroscopy it is the electric-field component of the radiation that interacts with molecules. For absorption to occur, two conditions must be fulfilled: (i) the energy  $h\nu$  of a quantum of radiation must correspond to the separation between the considered energy levels in the molecule, and (ii) the oscillating electric-field component  $\mathbf{E}_1$  must interact with an oscillating electric-dipole (or multipole) moment. As the basis for magnetic resonance spectroscopy, the magnetic dipole of a molecule interacts with the magnetic component  $\mathbf{B}_1$  of electromagnetic radiation. Herein we are concerned with permanent dipole moments, that is, those existing in the absence of external fields. However, in EPR, a static magnetic field  $\mathbf{B}_0$  is applied (in addition to  $\mathbf{B}_1$ ) to align the magnetic moments and shift the energy levels in order to achieve conveniently measured splitting. The most common EPR spectrometers work at  $\mathbf{B}_1$  frequency of 9.5 GHz (X-band frequency: 8.2 ÷ 12.4 GHz), corresponding to the splitting induced by  $\mathbf{B}_0 \approx 0.34$  T.<sup>i</sup>

---

<sup>i</sup> EPR spectrometers working at different frequencies up to 360 GHz can be also found. For example in Frankfurt, in Prof. Prisner's group, the following spectrometers are available: S-band (~1.5 GHz), X-band, and G-band (~180 GHz).

## 2.2 SPIN AND ZEEMAN INTERACTION

Each electron possesses an internal degree of freedom, called *spin*. This degree of freedom has the properties of an angular momentum and can be denoted by  $\mathbf{S}$ , the spin angular momentum vector. Quantum theory demands that the magnitude of  $\mathbf{S}$  is quantized in units of  $\hbar$ , and is equal to  $[S(S+1)]^{1/2}\hbar$ , where  $S=1/2$  is the electron spin quantum number. Also the two projections of  $\mathbf{S}$  onto an arbitrarily chosen z-axis are quantized: the z component of  $\mathbf{S}$ , denoted  $S_z = m_s \hbar$ , can have only two values corresponding to the magnetic quantum numbers  $m_s = +1/2$  and  $m_s = -1/2$ . These two values, also called spin states, are denoted  $|\alpha\rangle$  and  $|\beta\rangle$ , respectively, in bra-ket notation. Moreover, in quantum mechanics the spin vector  $\mathbf{S}$  is represented by the spin operator  $\hat{S}$ . This operates on wave functions expressed in terms of spin variables only (e.g.  $|\alpha\rangle$  and  $|\beta\rangle$ , and  $|\psi_s\rangle$  for a general spin wave function).

Electrons possess also a permanent magnetic moment which is related to the spin angular momentum  $\mathbf{S}$  by the following relation:

$$\boldsymbol{\mu}_e = -\frac{e}{2m_e}\mathbf{S} = -g_e\beta_e\mathbf{S} \quad (2.1)$$

where  $g_e \approx 2.0023193043737$  <sup>[1]</sup> (see also section 2.4.1) is a dimensionless constant called the free electron g-factor,  $\beta_e$  is the electronic Bohr magneton ( $\beta_e = 9.274026 \cdot 10^{-24}$  J/T),  $e$  is the electronic charge and  $m_e$  is the mass of the electron.

In the absence of an external magnetic field the quantum mechanical states  $|\alpha\rangle$  and  $|\beta\rangle$  for an electron spin and hence for the spin magnetic moments are degenerate in energy. The application of an external static magnetic field  $\mathbf{B}_0$  breaks the degeneracy of the two magnetic moment quantum states (see also Fig. 2.1). The interaction between the electron magnetic moment and the external field is called electron Zeeman interaction (see section 2.4.1) and is represented by the spin Hamiltonian operator:

$$\hat{H}_{EZ} = -\hat{\mu}_e B_0 = g_e\beta_e B_0 \hat{S} \quad (2.2)$$

If the direction of the magnetic field is defined to be along the z direction, equation (2.2) can be rewritten as:

$$\hat{H}_{EZ} = g_e \beta_e B_0 \hat{S}_Z \quad (2.3)$$

where  $\hat{S}_Z$  is the operator for the component of the electron spin in the z direction. Application of the time independent Schrödinger equation  $\hat{H}_{EZ} \psi_s = E \psi_s$  to a simple system given by an isolated electron leads to two allowed energy levels (see also Fig. 2.1):

$$\hat{H}_{EZ} |\alpha\rangle = g_e \beta_e B_0 \hat{S}_Z |\alpha\rangle = +\frac{1}{2} g_e \beta_e B_0 |\alpha\rangle \Rightarrow E_{|\alpha\rangle} = +\frac{1}{2} g_e \beta_e B_0 \quad (2.4)$$

$$\hat{H}_{EZ} |\beta\rangle = g_e \beta_e B_0 \hat{S}_Z |\beta\rangle = -\frac{1}{2} g_e \beta_e B_0 |\beta\rangle \Rightarrow E_{|\beta\rangle} = -\frac{1}{2} g_e \beta_e B_0 \quad (2.5)$$

The lower energy level corresponds to the situation in the state  $|\beta\rangle$  in which the spin vector  $\mathbf{S}$  is antiparallel to  $\mathbf{B}_0$  while the magnetic moment  $\boldsymbol{\mu}$  is parallel. In the upper energy level, state  $|\alpha\rangle$ , the spin vector  $\mathbf{S}$  is parallel to  $\mathbf{B}_0$  while the magnetic moment  $\boldsymbol{\mu}$  is antiparallel. The energy difference between the two spin states is:

$$\Delta E = g_e \beta_e B_0 \quad (2.6)$$

During an EPR experiment a macroscopic assembly containing a generic number N of electrons is analyzed, not only a single spin. In thermal equilibrium the distribution of spins over the possible states is statistical and governed by the *Boltzmann's law*, which for a two spin level system is:

$$\frac{N_\alpha}{N_\beta} = e^{-\Delta E / kT} \quad (2.7)$$

where  $N_\alpha$  and  $N_\beta$  are the number of  $\alpha$  spins and  $\beta$  spin in the sample respectively,  $\Delta E$  is the energy difference given in eq. (2.6), k is the Boltzmann's constant and T is the absolute temperature. Eq. (2.7) indicates that there is a slight excess of spins in the  $\beta$  state. For

electrons in a field of 0.34 T and at room temperature (298 K), it can be calculated that the populations of the two spin states differ by only 1.5 parts in  $10^3$ .

In most systems, electrons occur in pairs such that the net magnetic moment is zero. Hence only species that contain one or more unpaired electrons possess the net spin necessary for suitable interaction with an electromagnetic field.

EPR transitions between the electron spin levels occur provided there is a population difference between the spin states, the magnetic component of the electromagnetic radiation  $\mathbf{B}_1$  is perpendicular to the steady field  $\mathbf{B}_0$  and the following selection rule is fulfilled (see also section 2.3.2):

$$\Delta m_s = \pm 1 \tag{2.8}$$

Moreover an EPR signal appears only if the frequency  $\nu$  of the oscillating field satisfies the resonance condition:

$$h\nu = g_e \beta_e B_0 \tag{2.9}$$

There are two alternative methods to obtain EPR signals: applying a constant magnetic field and scanning the frequency of the electromagnetic radiation; alternatively, applying a constant electromagnetic radiation frequency and scanning the magnetic field. Owing to the limitations of microwave electronics, the latter method offers better performance and it is normally used in EPR spectrometers. A peak in the absorption will occur when the magnetic field tunes the two spin states so that their energy difference matches the energy of the radiation (see Fig. 2.1). This field is called the resonance field.

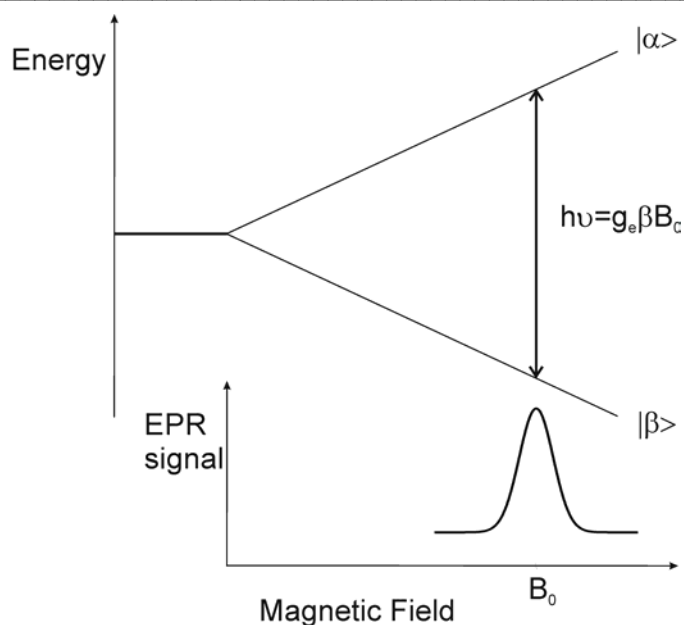


**Figure 2.1** Schematic representation of the electron Zeeman splitting versus field strength. When the resonance condition is fulfilled an EPR signal in absorption is detected corresponding to the resonance magnetic field<sup>i</sup>.

Similarly to electrons, also some nuclei can have the property of *spin*. In this case the spin angular momentum vector  $\mathbf{I}$  has magnitude  $[I(I+1)]^{1/2} \hbar$  and z component  $I_z = m_I \hbar$ . The spin quantum number  $I$  of a nucleus may have one of the following values  $I=0, 1/2, 1, 3/2, 2, \dots$ , with quantum numbers greater than 4 being rather rare. The magnetic quantum number  $m_I$  can only have one of a set of discrete values which are  $+I, (I-1), \dots, -I$ . Nuclei involved in the analysis of EPR spectra in this thesis are hydrogen atoms ( $\text{H}^1, I=1/2$ ) and nitrogens ( $\text{N}^{14}, I=1$ ).

The interaction between the magnetic moment of a nucleus and the applied field  $\mathbf{B}_0$  is called the nuclear Zeeman interaction, which is represented by an expression, analogous to eq. (2.2):

<sup>i</sup> To optimize the signal to noise ratio, a special detection scheme has been developed so that EPR spectra are normally detected as absorption derivative signals. The magnetic field strength is modulated sinusoidally at a certain modulation frequency (usually 100 KHz). In the presence of an EPR signal, the field modulation quickly sweeps through part of the signal and the microwaves reflected from the cavity are amplitude modulated at the same frequency. The EPR signal is transformed into a sine wave with amplitude proportional to the slope of the signal. As a result an EPR derivative signal appears.

$$\hat{H}_Z = -g_N \beta_N B_0 \hat{I} \quad (2.10)$$

Where  $\beta_N$  is the nuclear magneton ( $\beta_N = 5.050824 \cdot 10^{-27}$  J/T) and  $g_N$  is a dimensionless constant called the nuclear g-factor.  $g_N$  is an intrinsic property of a nucleus ( for  $H^1$ ,  $g_N=5.585$ ; for  $N^{14}$   $g_N=0.403$ ).

### 2.3 STATIC SPIN HAMILTONIAN AND ITS COMPONENTS

The transition energies of an electron spin  $S_1$  in a constant magnetic field  $B_0$ , interacting with  $n$  magnetic nuclei with spin  $I$  and with another electron spin  $S_2$ , can be calculated from the static spin Hamiltonian operator:<sup>[2]</sup>

$$\begin{aligned} \hat{H} &= \beta_e B_0 \tilde{g} \hat{S}_1 - \beta_N \sum_{k=1}^n (g_{N,k} B_0 \hat{I}_k) + \sum_{k=1}^n (\hat{S}_1 \tilde{T} \hat{I}_k) + \sum_{I_k > 1/2} (\hat{I}_k \tilde{Q}_k \hat{I}_k) + \hat{S}_1 \tilde{D} \hat{S}_2 - 2J \hat{S}_1 \hat{S}_2 \\ &= \hat{H}_{EZ} + \hat{H}_{NZ} + \hat{H}_{hfs} + \hat{H}_Q + \hat{H}_{SS} + \hat{H}_J \end{aligned} \quad (2.11)$$

The various terms describe the following interactions and magnitudes<sup>[3]</sup> (for general cases):

$\hat{H}_{EZ}$ : describes the general expression for the electron Zeeman interaction and has an energy of magnitude  $0-1 \text{ cm}^{-1}$  (the energy depends on the magnetic field strength  $B_0$ ).  $\tilde{g}$  is a tensor. A detailed explanation of  $\hat{H}_{EZ}$  in eq. (2.11) and of the  $\tilde{g}$  tensor will be given in section 2.3.1.

$\hat{H}_{NZ}$ : describes the nuclear Zeeman interaction and has energy of magnitude  $0-10^{-3} \text{ cm}^{-1}$  (also here the energy depends on the magnetic field strength  $B_0$ ). In the case of protons, the differences both in  $g$  and masses lead to a nuclear Zeeman interaction that is only 1/658 of the electron Zeeman interaction, for all other nuclei it is even less.

$\hat{H}_{hfs}$ : describes the interaction of nuclear spins with an unpaired electron and the energy can span a magnitude of  $0-10^{-2} \text{ cm}^{-1}$ . It produces the so-called hyperfine structure on the EPR spectrum.  $\tilde{T}$  is a tensor. A detailed explanation of  $\hat{H}_{hfs}$  will be given in section 2.3.2.

$\hat{H}_Q$ : describes the quadrupole interaction for nuclei with quantum number  $I \geq 1$  and non-spherical charge distribution. In the Hamiltonian of eq. 2.11  $\tilde{Q}$  is the symmetrical and traceless quadrupole tensor.<sup>[4]</sup> The associated energy can span a magnitude of  $0-10^{-2} \text{ cm}^{-1}$ .

$\hat{H}_{SS}$ : describes the classical magnetic dipolar interaction between two spins  $\mathbf{S}_1$  and  $\mathbf{S}_2$  and can have energy of magnitude  $0-1 \text{ cm}^{-1}$ :

$$H_{SS} = -\frac{\mu_0}{4\pi} g_{e1} \beta_e^2 g_{e2} \left\{ \frac{3(\hat{S}_1 \cdot \hat{r})(\hat{S}_2 \cdot \hat{r})}{r^5} - \frac{\hat{S}_1 \cdot \hat{S}_2}{r^3} \right\} = \hat{S}_1 \tilde{D} \hat{S}_2 \quad (2.12)$$

where  $\tilde{D}$  is a (3x3) antisymmetric and traceless tensor,  $\hat{r}$  is the operator for the vector connecting the two electrons and  $\mu_0$  the vacuum magnetic permeability.

$\hat{H}_J$ : describes the isotropic exchange interaction between two spins  $\mathbf{S}_1$  and  $\mathbf{S}_2$  and can have energy of magnitude  $0-10^3 \text{ cm}^{-1}$ .  $J$  is called the exchange coupling constant and an expression for it has already been given in eq. (1.9).

$\hat{H}_{EZ}$  and  $\hat{H}_{hfs}$  are the interactions contributing to the transition frequencies of the systems described in this work and will be further analyzed in the following.

### 2.3.1 The g tensor

The expression of eq. (2.2) is related to the particular case of  $g$  isotropic. The general expression of the Zeeman interaction is the following:

$$\hat{H}_{EZ} = \beta_e B_0 \tilde{g} \hat{S} \quad (2.13)$$

where  $\tilde{g}$  is a coupling matrix, commonly referred to as the “ $\tilde{g}$ -tensor”, and is one of the EPR observables which can be used to identify paramagnetic species.

Eq. (2.13) refers to an *anisotropic g tensor*, that is, when variability of  $g$  with orientation relative to  $\mathbf{B}_0$  appears. For an anisotropic property to be described, six independent parameters are sufficient.  $\tilde{g}$  can be written as a symmetric tensor with, for example, three principal values  $g_{xx}$ ,  $g_{yy}$ , and  $g_{zz}$  (each of them is the  $g$  factor for  $\mathbf{B}_0$  along one axis of the

paramagnetic entity) and three Euler angles describing the orientation of the principal axes of the  $\tilde{g}$ -tensor with respect to the laboratory frame. Usually the  $\tilde{g}$  principal axes frame is fixed within the molecular frame by the symmetry of the molecular orbitals and all other tensors are referred to this frame. As a consequence the resonant field value is a function of the field orientation relative to the crystal (or molecular) axes.

The anisotropy arises from the fact that the angular momentum of a system more complex than a single atom is not solely due to spin angular momentum (“pure spin state”), where the  $g$  value is isotropic and equal to the scalar factor for a free electron  $g_e \approx 2.0023$ . Any deviation or anisotropy from this value is the result of the so-called spin orbit coupling between the spin angular momentum  $\mathbf{S}$  and the orbital angular momentum  $\mathbf{L}$ . In organic radicals the spin orbit coupling is usually small and therefore the  $g$  anisotropy is small, while in transition metal ions the deviations from  $g_e$  can be larger.

An *isotropic  $g$  value* is observed in dilute liquid solutions of low viscosity. In this solutions, when the rotation correlation time is in the range of the EPR time scale the measured  $g$  factor is to be considered as an effective value averaged over all orientations, which is equal to 1/3 of the trace of the  $g$  tensor, i.e.:

$$g_{iso} = \frac{1}{3}(g_{xx} + g_{yy} + g_{zz}) \quad (2.14)$$

For several systems the differences  $\Delta g$  between the tensor components are too small to be resolved at low frequencies, e.g. at X band. Therefore it is useful to make experiments at higher fields in order to achieve an accurate resolution of the principal values of  $\tilde{g}$  (see Fig. 2.2).



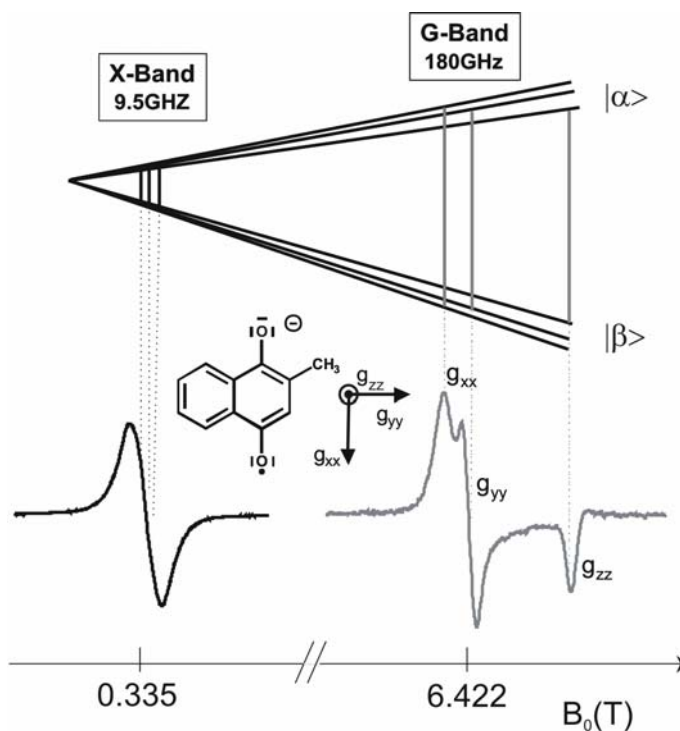


**Figure 2.2** Upper panel: dependence of the Zeeman term on  $B_0$ . Lower panel: EPR spectra of a quinone molecule detected at different mw frequencies corresponding to the frequency band depicted in the upper panel. [With courtesy of Dr. Oliver Brüggmann<sup>[5]</sup>]

### 2.3.2 The hyperfine tensor

The general Hamiltonian for one electron spin coupled to a single nucleus is:

$$\hat{H} = \beta_e B_0 \tilde{g} \hat{S} + \hat{S} \tilde{T} \hat{I} \quad (2.15)$$

For such a Hamiltonian EPR transitions appear for  $\Delta m_s = \pm 1$ ,  $\Delta m_l = 0$  (see Fig. 2.3). The first term is the Zeeman interaction and has already been explained in section 2.3.1. The second term in eq. (2.15) is the hyperfine term  $\hat{H}_{hfs} = \hat{S} \tilde{T} \hat{I}$  and describes the interaction between the magnetic moments of the electron and nuclei.

In particular  $\tilde{T}$  is the hyperfine coupling tensor, which may be decomposed into the sum of two terms:

$$\tilde{T} = a_{iso} \hat{S} \hat{I} + \hat{S} \tilde{A} \hat{I} \quad (2.16)$$

The first term is the *isotropic hyperfine* coupling, also called Fermi-contact interaction. It is a pure quantum mechanical term and occurs only when the electron has a finite probability density at the nucleus. The expression of the coupling constant  $a_{iso}$ , which has the dimensions of energy, is:

$$a_{iso} = \frac{2\mu_0}{3} g_e \beta_e g_N \beta_N |\psi(0)|^2 \quad (2.17)$$

where  $|\psi(0)|^2$ , the electron probability distribution, is the squared amplitude of the electronic wave function of the unpaired electron at a distance  $r = 0$  from the nucleus. Hence contact interaction can only occur when the electronic wavefunction has some s-orbital character. Although p-, d- or f-orbitals, have nodes at the nucleus, they can have a significant contribution by the configuration interactions or spin-polarization mechanisms (see section 2.4.1) and the isotropic hf-interaction can be either positive or negative, depending on its quantum mechanical origin.

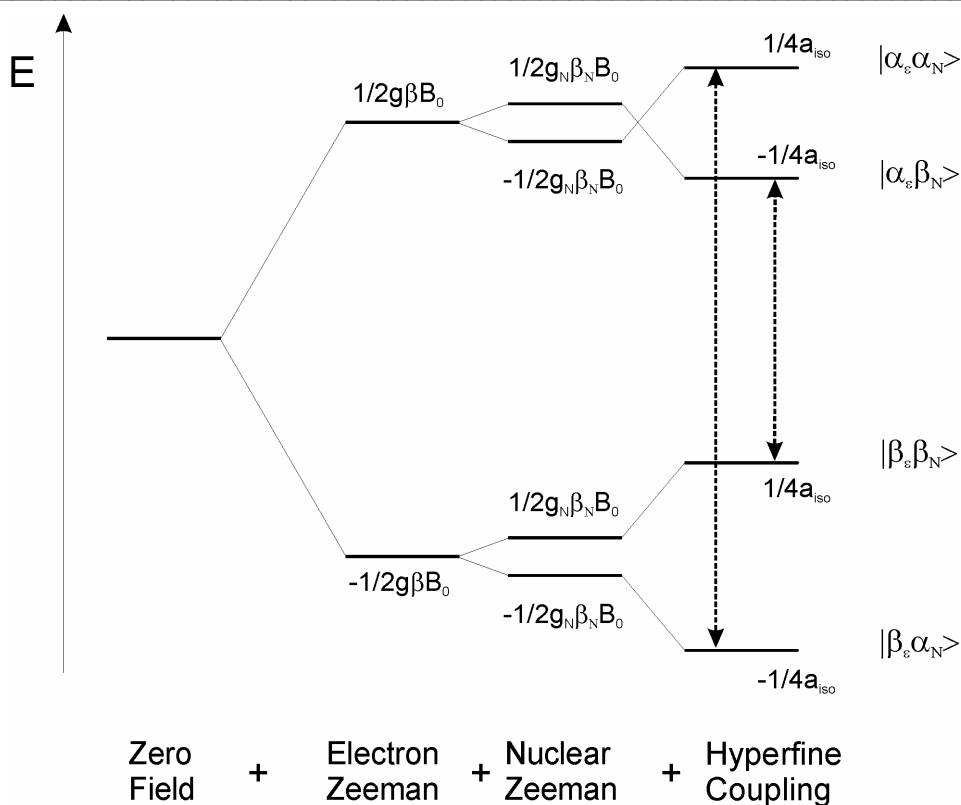


**Figure 2.3** Energy level diagram of hyperfine interactions on a system with one unpaired electron and one nucleus with  $I = 1/2$  and  $a_{iso} > 0$ ,  $a_{iso}/2 > \nu_n = (g_N\beta_N B_0)/h$ . Dotted line arrows indicate the allowed EPR transitions. [Adapted from <sup>[6]</sup>]

The second term in equation (2.16) is the *anisotropic hf* dipolar interaction, which arises from the classical magnetic coupling between two magnetic moments  $\mu_e$  and  $\mu_N$  and can be described by a Hamiltonian analogous to eq. (2.10):

$$H_{hfs}^{dip} = \frac{\mu_0}{4\pi} g_e \beta_e g_N \beta_N \left\{ \frac{3(\hat{I} \cdot \hat{r})(\hat{S} \cdot \hat{r})}{r^5} - \frac{\hat{I} \cdot \hat{S}}{r^3} \right\} = \tilde{S} \hat{A} \hat{I} \quad (2.18)$$

where  $\hat{r}$  is the operator for the vector connecting the electron and the nuclear spin and  $\mu_0$  the vacuum magnetic permeability.

$\hat{A}$  is the so-called dipolar hyperfine coupling tensor. Because it is traceless,  $\hat{A}$  vanishes when averaged over all orientations, as it is usually the case in liquids due to the rapid tumbling of molecules.

## 2.4 SPECTRAL ANALYSIS OF ISOTROPIC HYPERFINE PATTERNS

In this thesis we will encounter systems where: the tensor  $\tilde{g}$  is not resolved and only a  $g$  factor defined as the zero-crossing value from the center line can be assigned; the dipolar hyperfine tensor  $\hat{A}$  is averaged to zero and the observed splittings between the lines give the isotropic coupling constant  $a_{iso}$  directly. In the following paragraphs the explanation of the hyperfine coupling mechanisms are given together with the interpretation of some spectra from organic radicals. As we will see, the interpretation of the EPR patterns of such systems will become useful in the spectral analysis presented in the following results chapters.

### 2.4.1 $\pi$ -type organic radicals: spin density and spin polarization

In aliphatic systems, the observable hf interaction occurs mainly with nuclei in positions  $\alpha$  and  $\beta$  to the atom primarily associated with the unpaired electron. The following notation defines proton positions:

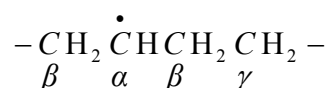


**Figure 2.4** Notation for proton positions in aliphatic radicals.

Hf couplings with the  $\gamma$  protons are usually small and not resolved at X-band frequency<sup>[7, 8]</sup>. According to eq. (2.17), the isotropic hyperfine coupling is proportional to  $|\psi(0)|^2$ , the probability of finding the unpaired electron at the position of the nucleus. Nevertheless it is worth noting that this explanation is oversimplified and only valid for a hydrogen like nucleus.

In fact a molecule contains many electrons, whose spins are coupled together, and it is not in general possible to say that there is just one unpaired electron in a certain orbital, while the other electrons are paired together. The correct and general expression for the coupling constant  $a_{iso}$  is then the following:

$$a_{iso} = \frac{4\mu_0}{3} g_e \beta_e g_N \beta_N \rho(\vec{r}_N) \quad (2.19)$$

where  $\rho(\vec{r}_N)$  is the unpaired electron spin density at the nucleus. It is normalized to one for  $S=1/2$  and can be positive or negative. By definition it is a probability density, measured in electrons/(Ångstroms)<sup>3</sup>, arising from the difference between the electron spin density of  $\alpha$  and  $\beta$ :

$$\rho(\vec{r}_N) = P^\alpha(\vec{r}_N) - P^\beta(\vec{r}_N) \quad (2.20)$$

the  $P^i(\vec{r})$  contributions, when summed, define the electron density  $P(\vec{r})$ , which is measured directly in X-ray diffraction experiments:

$$P(\vec{r}) = P^\alpha(\vec{r}) + P^\beta(\vec{r}) \quad (2.21)$$

Connected with the quantity above and also widely used is the spin density in an orbital,  $\rho_H$ , representing the fractional population of unpaired electrons on an atom.

In the case of aromatic radicals, it is difficult to think in terms of the Fermi contact interaction (eq. (2.17)) for the ring hydrogen atoms. Since the electron occupies the molecular  $\pi$  orbital, formed by overlap of the carbon  $2p_z$  orbitals, there is a node in the plane of the molecule, where the  $1s$  orbital of the H atoms are. One should account for an indirect coupling through a C-H bond, via the so-called *spin polarization* effect.

The phenomenon of spin polarization at the origin of the isotropic hyperfine splitting can be illustrated on the simple example of a  $C_\alpha$ -H fragment and was explained by McConnell<sup>[9]</sup> and other authors<sup>[10-12]</sup>. Qualitatively, one can account for spin polarization on the basis of Hund's rules. The exchange interaction between unpaired electrons in different atomic orbitals having the same energy is lowest when the electrons have parallel spins. Hence the parallel alignment of the spins in different orbitals is favored, as indicated by Hund's rule. A similar exchange interaction between the  $P^\alpha(\vec{r}_N)$  density on the  $C_\alpha$  and the paired electrons of the  $\sigma$ -bond would cause the spin-up alignment to have the greater probability at the  $C_\alpha$  end of the  $\sigma$ -bond, and hence the spin-down alignment to have the greater probability in the  $1s$  H-orbital (Fig.2.5). The spin density thus induced on the proton would

be negative relative to the  $P^{\alpha}(\vec{r}_N)$  density on the C, as was originally shown by McConnell [9].

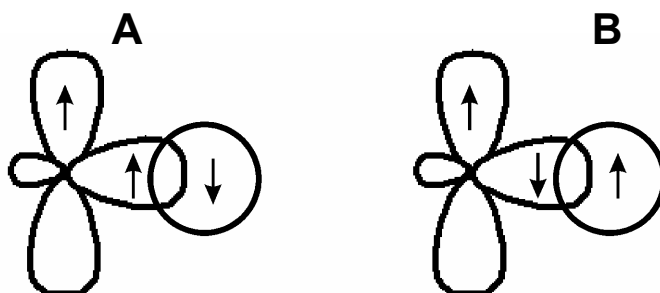


**Figure 2.5** Polarization in  $\dot{C}-H$  fragment. Due to the interaction between  $\sigma$  and  $\pi$  electrons, structure (A) is energetically more favored than structure (B). The  $\pi$ -electron induces a deviation from perfect pairing which results in a finite unpaired spin density at both the hydrogen and carbon nuclei. Note that spin density is being induced at the proton without any transfer of electron density. As a consequence, the isotropic hyperfine coupling constants of carbon and proton have opposite signs.

In the case of  $\alpha$ -protons of  $\pi$ -type organic radicals, a linear relation between the isotropic proton hyperfine splitting parameters of proton  $k$  ( $a_{iso,k}$ ), and the unpaired  $\pi$ -electron populations of the carbon atoms has been theoretically predicted by McConnell and Chesnut [13] and is expressed by the McConnell relation [9]:

$$a_{iso,k} = Q\rho_k \quad (2.22)$$

where  $\rho_k$  is the unpaired  $\pi$ -electron population at the adjacent carbon atom  $k$  and  $Q$  is a proportionality constant (expressed in frequency or magnetic-field units).

#### 2.4.2 *Tert*-butyl radical: hyperconjugation

A typical example of hyperconjugation in EPR is the *tert*-butyl radical and other similar alkyl radicals that are involved as intermediates during fast photochemical or thermal reactions.<sup>[7, 8, 14-20]</sup> An example of a typical 10 lines spectrum of this species, as it appears at the classical X-band frequency around 9.5 GHz, is given in Fig. 2.6:

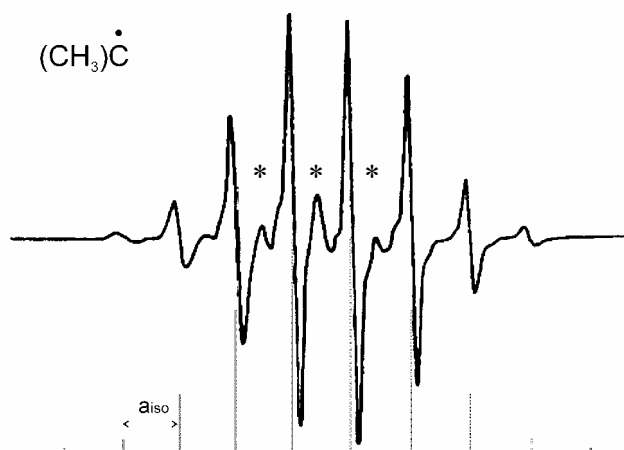


**Figure 2.6** Ten-line spectrum of the tert-butyl radical with approximately the binomial distribution of intensity coming from X-irradiated polycrystalline ammonium salt. Only the central eight lines are visible, the other two are too broad, and thus too weak to be seen. The weaker pattern indicated by \* does not belong to the tert-butyl radical. (Adapted from <sup>[19]</sup>, p 817)

The  $\tilde{g}$  tensor is not resolved at X-band frequency, since the  $\Delta g$  differences between the tensor components are too small, and only a  $g$ -factor close to 2,0026 could be obtained from the EPR spectrum<sup>[15]</sup>.

The spectrum in Fig. 2.6 is dominated by the *hyperfine pattern*. The ten lines spectrum arises from the isotropic hyperfine coupling between the unpaired electron on the 2pz orbital of the tertiary carbon atom with the 9 equivalent protons of the 3 rapidly rotating methyl groups. If the methyl group is rotating at a frequency greater than the hf separation expressed in frequency units ( $s^{-1}$ ), then the  $\beta$  hydrogens appear equivalent. Thus the anisotropic contribution is averaged out to zero, due to this fast motion.

To understand this pattern it is necessary to introduce the phenomenon of spin density induced by hyperconjugation.

The elucidation of the coupling's origin for the  $\beta$  protons, which are not confined to the nodal plane of the  $\pi$  system, as in 2.4.1, can be given by molecular orbital theory.<sup>[4]</sup>

Considering the electronic structure of a  $\dot{C}-C'H_3$  fragment of the tert-butyl radical it is possible to construct group orbitals of the methyl hydrogen 1s orbitals  $\phi_i$ , e.g. for one methyl group in figure:

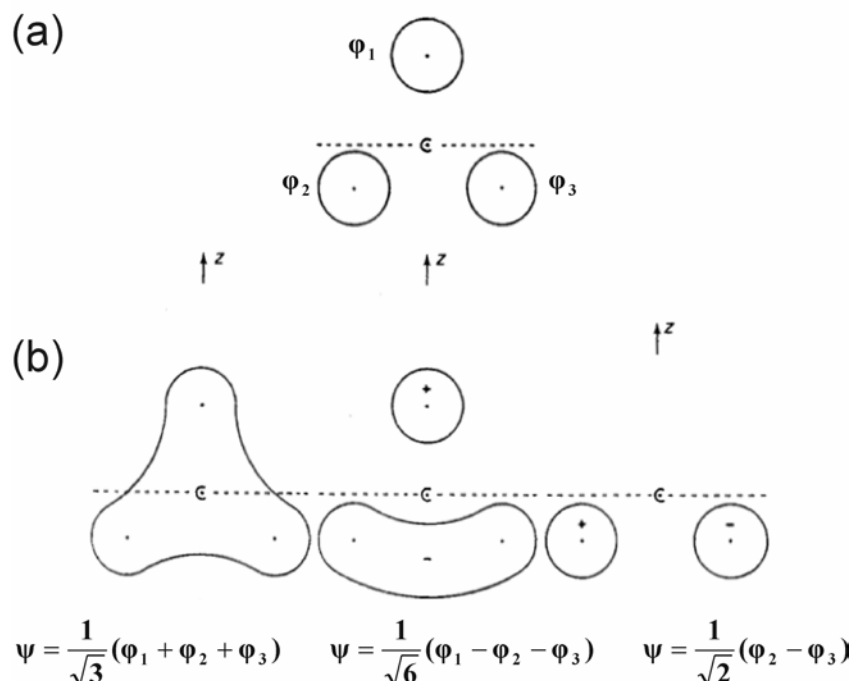


**Figure 2.7** The atomic (a) and group (b) orbitals for the hydrogen atoms in a methyl group. In this figure the methyl group is viewed along the connecting C-C bond. The dashed lines indicate the nodal plane of the  $\pi$  system and  $z$  indicates the axis of the  $2p$ -orbital on the substituted carbon atom. (Figure taken from<sup>[4]</sup>, p 106)

From Fig. 2.7 it can be seen that  $\psi_2$  has the correct symmetry to overlap with the  $2p_z$  orbital on C' ( $\phi'$ ). Thus the singly occupied  $\pi$ -type orbital has the form:

$$\Psi = c\phi + c'\phi' + s\psi_2 \quad (2.23)$$

where  $\phi$  and  $\phi'$  are the  $2p$  orbitals on C and C', respectively. It is clear that this orbital gives, directly, positive spin density at the methyl groups.

This view indicates a mechanism, called hyperconjugation, which explains how spin density from the odd electron could be found at the methyl protons. It also implies that the beta proton coupling constant should be positive, as confirmed by NMR experiments.

The  $\beta$  hyperfine coupling constant can be described by a relationship that has been suggested by Heller and McConnell<sup>[21]</sup>:

$$a_\beta = (B_0 + B_2 \cos^2 \theta) \rho_\phi \quad (2.24)$$



The  $\cos^2$  dependence of the splitting accounts for the geometry dependence of the hyperconjugation, as shown in Fig. 2.7, from which the spin density at proton 1 ( $\psi_2$  group orbital) is predicted to be greater because of the more favorable overlap with  $\phi'$  of the singly occupied molecular orbital  $\Psi$  (eq. (2.23)).  $\theta$  is the dihedral angle as described in Fig. 2.8. The expression above emphasizes the dependence of the spin population  $\rho_\phi$  on  $\theta$ . Finally  $B_2$  reflects the spin density arising from hyperconjugation while  $B_0$  accounts for the spin density arising from orientation independent mechanisms, such as spin polarization, and it is expected to be small (a few Gauss or less).

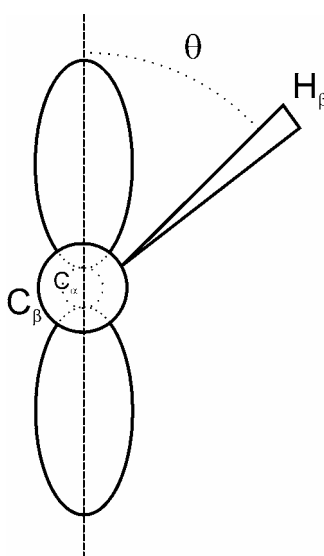


**Figure 2.8** Definition of the dihedral angle  $\theta$  specifying the position of a  $\beta$ -proton relative to the axis of the  $2p$ -orbital.

A methyl group is usually free to rotate about the C-C' bond, thus giving an orientationally averaged coupling for each proton:

$$a_\beta = B_0 + \frac{1}{2}B_2 \quad (2.25)$$

These kind of protons are termed “equivalent”. Equivalent protons can also be found in aromatic radicals and also when the protons occupy symmetrically equivalent positions in the molecule.

To calculate the spin density on the C attached to rotating methyl groups a formula similar to (2.22) can be used <sup>[8]</sup>:

$$a_{\beta} = Q_{\beta}(\text{CH}_3)\rho \quad (2.26)$$

Fessenden and Schuler<sup>[8]</sup> gave  $Q_{\beta} = 29,30$  G for the *tert*-butyl radical, and a calculated value of the unpaired spin density on the adjacent carbon  $\rho = 0,776$ .

The interaction of the unpaired electron with  $n$  equivalent protons results in  $n+1$  lines whose relative intensities are proportional to the coefficients of the binomial expansion of  $(1+x)^n$ . The methyl radical  $\text{CH}_3$  gives a 1:3:3:1 proton hyperfine spectrum with a splitting constant of 23.04 Gauss <sup>[8]</sup>, while for the *tert*-butyl radical the nine equivalent protons give a proton hyperfine spectrum of 10 lines which have the first order relative intensities 1:9:36:84:126:126:84:36:9:1, with a coupling constant  $a_{\text{iso}} \approx 22.72$  <sup>[8]</sup>. In the latter case the hf coupling constant is smaller than for the methyl radical, since the spin density on the central atom is reduced as the number of methyl substituents increases. <sup>[22]</sup>

If the methyl rotation is not confined or restricted, the coupling constants of  $\beta\text{-CH}_3$  do not depend significantly on the nature of the solvent or on the temperature. More strictly, the hf coupling depends on such parameters in the measure that they affect the random and spin independent methyl rotation.

Eq. (2.26) is also valid at very low temperatures (e.g. 4.2 K) because of the tunnel effect averaging the angles  $\theta$  for each proton as in a free rotation <sup>[23]</sup>.

### 2.4.3 The thymyl radical

Historically, several radicals located on the thymine base could be detected by EPR spectroscopy after irradiation of both DNA and single nucleosides/nucleotides with  $\gamma$  rays, X-rays or UV light <sup>[24-35]</sup>. The thymine anion radical  $\text{T}^{\bullet-}$  and the so-called 5-thymil radical  $\text{TH}^{\bullet}$  (also called 5-6 dihydro-5-thymil radical <sup>[29]</sup>) are depicted in Fig.2.9:

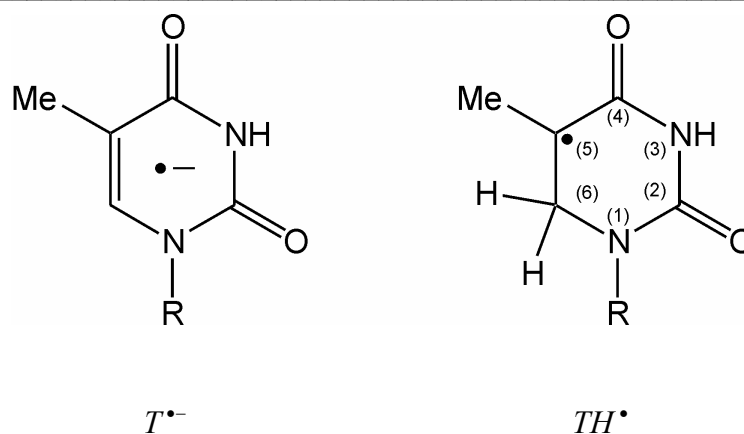


**Figure 2.9** Thymine radical structures. The carbon positions on the base are specified.

The  $T^{\bullet-}$  has been isolated at low temperatures (e.g. 77 K) [27, 29, 30, 32-35]. At X-band, the spectrum is a doublet with  $a_{\text{iso}}=14$  G [36]. A  $g_{\text{iso}}$  of 2.00299 can be calculated from the  $\tilde{g}$  tensor given by Weiland et al. [27].

$TH^{\bullet}$  is one of the important species that will be encountered during this thesis.  $TH^{\bullet}$  may be formed as a secondary radical by conversion of  $T^{\bullet-}$  radical after temperature annealing [27-30, 33-35] or as a primary radical in single crystals of thymidine, [24] in both cases by means of high energy radiation ( $\gamma$  and X rays). It can also be obtained as a primary radical after UV light irradiation of frozen (77 K) aqueous solutions of DNA [25, 35] or frozen (77 K) aqueous  $\text{MgCl}_2$  solutions of proflavine and dTMP [29].

The analysis of the  $TH^{\bullet}$  EPR spectrum at X-band is here briefly summarized. The typical “octet fingerprint” of the thymyl radical, reported in Fig. 2.10, is the result of a hf structure arising from sets of three and of two hydrogens with equivalent couplings (20.5 G and 40.5 G respectively) [24, 25]:

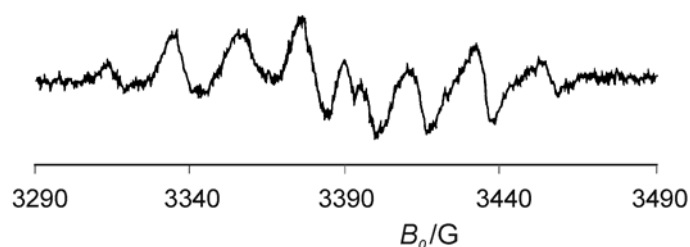


**Figure 2.10** Eight-line spectrum of the Thymyl radical. (Adapted from [33], p 351)

Recently Weiland et al. were able to resolve the  $g$ -tensor from the eleven lines of the spectrum at 245 GHz<sup>[27]</sup>. The  $g$ -tensor for non single crystal samples is not resolved at 9.5 GHz, where only a  $g$ -factor of 2.0035 could be measured<sup>[25]</sup>.

The hf coupling of the protons could be obtained directly by measurement of the spacings of the components of the hyperfine structure. The set of the three equivalent couplings is given by the methyl group rotating about the C(5)-C(methyl) bond. Pruden et al. used eq. (2.26) and estimated a value of  $\rho=0.70$  for the spin density in the  $2\pi$  orbital of the C(5) of the ring. They also stated that the coupling of the C(6)H<sub>2</sub> hydrogens on the ring arises mostly from hyperconjugation with the spin density on the C(5), and partly from  $\pi$  orbital density which circulates in the ring. Finally they were able to conclude that the ring structure of the radical must lie in a plane, with the two C(6)H bonds oriented symmetrically above and below the ring. The two C(6)H bonds should form similar angles of approximately 35° with the normal to the plane of the ring, thus accounting for the equivalent couplings.

Lately Hole et al. obtained, from ENDOR measurements, more accurate values for the hf  $\tilde{T}$  tensor of the C(6)H<sub>2</sub> hydrogens<sup>[26]</sup>, which are in agreement with the isotropic values reported above.

## 2.5 RELAXATION PHENOMENA

In a sample with a large number of non-interacting dipoles (spin  $S=1/2$ ), and with  $N$  the number of magnetic moments  $\mu_i$  per unit volume, *the macroscopic magnetization vector  $\mathbf{M}$*  can be introduced:

$$\mathbf{M} = \sum \mu_i \quad (2.27)$$

The presence of the magnetic field  $\mathbf{B}_0$  induces a torque on  $\mathbf{M}$  of strength  $\tau = \mathbf{M} \times \mathbf{B}_0$ . This torque forces the spin vector to precess round a cone anticlockwise at a uniform angular velocity  $\omega_0$ , making a constant angle with the field. This motion is called the Larmor precession (see Fig. 2.11) of the spin, and  $\omega_0 = \gamma B_0$  is known as the Larmor frequency ( $\gamma$  is the gyromagnetic ratio). In conditions of thermal equilibrium, the  $z$  component of  $\mathbf{M}$  has a steady value  $M_z$ .

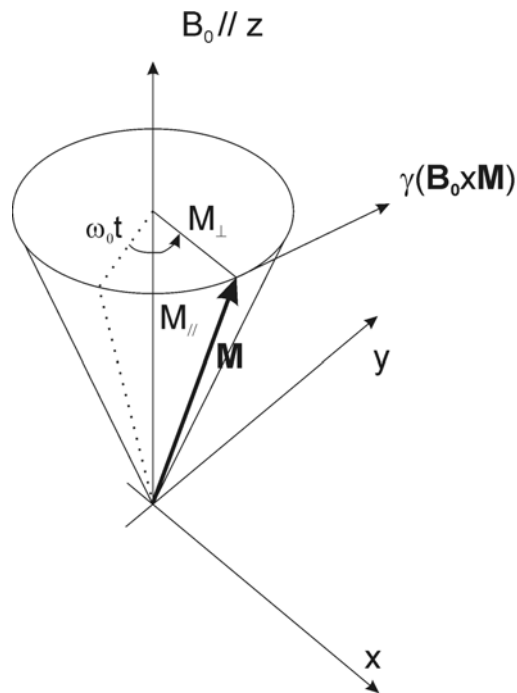


**Fig. 2.11** Precession of electron magnetic moments about a steady magnetic field.

If  $\mathbf{M}$  is not at thermal equilibrium, because for example a magnetic resonance experiment has been performed, then relaxation effects have to be taken into account. The *Bloch equations* of motion for the three components of the magnetization,  $M_x$ ,  $M_y$ ,  $M_z$ , collect the effects of Larmor precession and of relaxation:

$$\begin{aligned}
 \frac{dM_x}{dt} &= \gamma(\mathbf{B} \times \mathbf{M})_x - \frac{M_x}{T_2} = \omega_0 M_y - \frac{M_x}{T_2} \\
 \frac{dM_y}{dt} &= \gamma(\mathbf{B} \times \mathbf{M})_y - \frac{M_y}{T_2} = -\omega_0 M_x - \frac{M_y}{T_2} \\
 \frac{dM_z}{dt} &= \gamma(\mathbf{B} \times \mathbf{M})_z - \frac{M_z - M_0}{T_1} = -\frac{M_z - M_0}{T_1}
 \end{aligned} \tag{2.28}$$

The spin-lattice *relaxation* time, which is a measure of the time taken for the spin system to approach thermal equilibrium by means of non-radiative processes of energy transfer from the spins to other degrees of freedom (“lattice”) of the system.  $T_2$ , often called the spin-spin relaxation time or transverse relaxation time, is the time taken for the spin system to vary the relative energies of the spin levels, rather than their lifetimes.

In the form eq. (2.28) the Bloch equations give a phenomenological description of relaxation: they explain how, after a time dependent magnetic component  $\mathbf{B}_1$  of mw electromagnetic radiation is quickly applied, the transverse components of  $\mathbf{M}$  ( $M_x$  and  $M_y$ ) decay to zero with a characteristic time  $T_2$  while  $M_z$  relaxes towards its equilibrium value  $M_0$  with a decay time  $T_1$ .

Moreover the Bloch equations can describe in detail the macroscopic behavior of magnetic resonance absorption, when a radio frequency field  $\mathbf{B}_1$  is applied. Such a treatment is not an object of this thesis (for further reading see <sup>[6, 37]</sup>). In the following only the predictions arising from the mathematical treatment of eq. (2.28) are reported.

As results from eq. (2.28), the spin-lattice relaxation causes the spins to achieve thermal equilibrium according to the Boltzmann law, so that the population difference between the spin energy levels is re-established. On the other hand, if during continuous wave irradiation the microwave power becomes high enough, so that the relaxation is slow compared with the transition rate, finally an equal population of the spin energy levels will occur. In particular, *saturation* occurs under the following condition::

$$\gamma^2 B_1^2 T_1 T_2 \geq 1 \quad (2.29)$$

where each term has the meaning already given above. In the non-saturating regime the square of the double integral over the intensity  $I$  of a derivative signal is proportional to the microwave power irradiated. If the line width does not change, one can write this as:

$$I \propto \sqrt{P} \quad (2.30)$$

As the line is saturating the signal intensity does not grow as fast as  $\sqrt{P}$  anymore and finally decreases. The power, where the quotient out of  $I$  and  $\sqrt{P}$  has been reduced to one half of its non-saturating value, is called half saturation power  $P_{1/2}$ . The saturation curve usually obeys the empirical law:<sup>[38]</sup>

$$\frac{I}{\sqrt{P}} = c \frac{1}{\left(1 + \frac{P}{P_{1/2}}\right)^{b/2}} \quad (2.31)$$

where  $c$  is a constant,  $b = 1$  in case of a inhomogeneous line broadening and  $b = 2$  for a homogeneously broadened line (see below.) *Signal intensities* do not depend solely on the microwave power. They also depend on the concentration of the EPR active species (spins) in the sample. The integrated intensity of an EPR absorption signal is proportional to the spin concentration and can therefore be used as an estimation for the concentration of the paramagnetic species <sup>[39]</sup>. A useful quantitation method is to compare the integral absorption of the unknown sample with that of a sample of known spin concentration, measured under exactly the same, non-saturating, conditions. However, due to baseline errors, and sample filling factors, the error of this method is 5-10 %, or more.

Under not saturating conditions the Bloch equations can be also used to predict a definite kind of *line shape* <sup>[6]</sup>, the Lorentz line, described by the distribution:

$$L(\omega) = \frac{T_2}{\pi} \frac{1}{1 + T_2^2(\omega - \omega_0)^2} \quad (2.32)$$

where the distribution function  $L$  is given in terms of angular frequency,  $L(\omega) = (L(\nu) / 2\pi)$ , and  $\omega_0$  is the resonance frequency. Lorentzian lines are usually observed in solution spectra.

If the line width is determined by inhomogeneous broadening due to unresolved hyperfine splittings, the line shapes will be Gaussian:

$$G(\omega) = \frac{A}{\sigma\sqrt{2\pi}} \exp - \frac{(\omega - \omega_0)^2}{2\sigma^2} \quad (2.33)$$

For solid concentrated free radicals where the electron exchange with neighbors narrows the resonance lines, Lorentzian lines are observed. For single crystals containing paramagnetic centers, the line shapes will vary from roughly Gaussian at high concentration to approximately Lorentzian at low concentrations.

## **2.6 CW X-BAND EPR SPECTROMETER**

All the spectra presented in this thesis are recorded with a conventional cw X-band spectrometer working at 9.5 GHz. The advantage of using the cw X-band approach is twofold: the relative simple and fast measurement procedure and the fact that the resulting spectra can be compared with similar EPR studies typically performed at that band.

EPR spectra were detected on a Bruker ESP300E EPR spectrometer equipped with a TM<sub>102</sub> rectangular resonator and a cryostat from Oxford for measurements between 77 K and 4 K. The parameters used for acquiring the spectra presented are given for each case.

A sample of DPPH, which has a known  $g$ -factor of 2.0036, was used as a standard for  $g$ -factor calibration purposes after the experimental measurements. A magnetic field offset  $B_{off}$  was calculated from the DPPH acquired spectrum. Assuming that the conditions for the calibration and the experimental measurement were the same, the  $g$ -factor of the EPR signals detected was calculated with the following simplified equation, rearranged from eq. (2.9) of the resonance condition:

$$g = \frac{h\nu}{\beta_e B_0'} = 0.07144775 \frac{\nu [MHz]}{B_0' [mT]} \quad (2.34)$$

$\nu$  is simply obtained from the frequency counter of the spectrometer, while  $B_0' = B_0 + B_{off}$  ( $B_0$  is the zero crossing of the center line of the spectrum under analysis).



---

## 2.7 REFERENCES

- [1] J. Schwinger, *Phys. Rev.* **1948**, 73, 416.
- [2] A. Schweiger, G. Jeschke, *Principles of pulse electron paramagnetic resonance*, Oxford University Press, New York, **2001**.
- [3] C. P. Poole, *Electron Spin Resonance*, Wiley, New York, **1967**.
- [4] N. M. Atherton, *Principles of Electron Spin Resonance*, Ellis Horwood Ltd, Chichester, **1993**.
- [5] O. Brüggmann, PhD Thesis, J. W. Goethe-University, Marie Curie-Strasse 11 (Frankfurt/Main (Germany)), **2003**.
- [6] A. Carrington, A. D. McLachlan, *Introduction to Magnetic Resonance*, Harper & Row, London, **1967**.
- [7] H. Fischer, *Journal of Physical Chemistry* **1969**, 73, 3834.
- [8] R. W. Fessenden, R. H. Schuler, *Journal of Chemical Physics* **1963**, 39, 2147.
- [9] H. M. McConnell, *Journal of Chemical Physics* **1956**, 24, 764.
- [10] S. J. Weissmann, *Journal of Chemical Physics* **1956**, 25, 890.
- [11] R. Bersohn, *Journal of Chemical Physics* **1956**, 24, 1066.
- [12] H. S. Jarret, *Journal of Chemical Physics* **1956**, 25, 1289.
- [13] H. M. McConnell, D. B. Chesnut, *Journal of Chemical Physics* **1958**, 28, 107.
- [14] P. J. Krusic, J. K. Kochi, *Journal of the American Chemical Society* **1968**, 90, 7155.
- [15] H. Paul, H. Fischer, *Helvetica Chimica Acta* **1973**, 56, 1575.
- [16] H. Schuh, E. J. Hamilton, H. Paul, H. Fischer, *Helvetica Chimica Acta* **1974**, 57, 2011.
- [17] D. E. Wood, R. F. Sprecher, *Molecular Physics* **1973**, 26, 1311.
- [18] D. E. Wood, L. F. Williams, R. F. Sprecher, W. A. Lathan, *Journal of the American Chemical Society* **1972**, 94, 6241.
- [19] Y. D. Tsvetkov, J. R. Rowlands, D. H. Whiffen, *Journal of the Chemical Society* **1964**, 810.
- [20] P. B. Ayscough, C. Thomson, *Transactions of the Faraday Society* **1962**, 58, 49.
- [21] C. Heller, H. M. McConnell, *Journal of Chemical Physics* **1960**, 32, 1535.
- [22] D. B. Chesnut, *Journal of Chemical Physics* **1958**, 29, 43.

- [23] C. Heller, *Journal of Chemical Physics* **1962**, 36, 175.
- [24] B. Pruden, W. Snipes, W. Gordy, *Proceedings of the National Academy of Sciences of the United States of America* **1965**, 53, 917.
- [25] P. S. Pershan, R. G. Shulman, B. J. Wyluda, J. Eisinger, *Science* **1965**, 148, 378.
- [26] E. O. Hole, E. Sagstuen, W. H. Nelson, D. M. Close, *Journal of Physical Chemistry* **1991**, 95, 1494.
- [27] B. Weiland, J. Hüttermann, J. vanTol, *Acta Chemica Scandinavica* **1997**, 51, 585.
- [28] R. A. Holroyd, J. W. Glass, *International Journal of Radiation Biology and Related Studies in Physics Chemistry and Medicine* **1968**, 14, 445.
- [29] S. Gregoli, M. Olast, A. Bertinchamps, *Radiation Research* **1976**, 65, 202.
- [30] J. Hüttermann, M. Rohrig, W. Kohnlein, *International Journal of Radiation Biology* **1992**, 61, 299.
- [31] M. Lange, B. Weiland, J. Hüttermann, *International Journal of Radiation Biology* **1995**, 68, 475.
- [32] M. D. Sevilla, R. Failor, C. Clark, R. A. Holroyd, M. Pettei, *Journal of Physical Chemistry* **1976**, 80, 353.
- [33] B. Weiland, J. Hüttermann, *International Journal of Radiation Biology* **1998**, 74, 341.
- [34] A. Gräslund, Ehrenber.A, Rupprech.A, G. Strom, *Biochimica Et Biophysica Acta* **1971**, 254, 172.
- [35] P. M. Cullis, J. D. McClymont, M. E. Malone, A. N. Mather, I. D. Podmore, M. C. Sweeney, M. C. R. Symons, *Journal of the Chemical Society-Perkin Transactions 2* **1992**, 1695.
- [36] M. D. Sevilla, Vanpaeme.C, C. Nichols, *Journal of Physical Chemistry* **1972**, 76, 3571.
- [37] G. E. Pake, T. L. Estle, *The Physical Principles of Electron Paramagnetic Resonance*, Benjamin, W.A., Reading, Massachusetts, **1973**.
- [38] J. R. Pilbrow, *Transition Ion Electron Paramagnetic Resonance*, Clarendo Press, Oxford, **1990**.
- [39] R. Aasa, T. and Vänngård, *Journal of Magnetic Resonance* **1975**, 19, 308.

### 3. EPR SPECTROSCOPIC STUDY OF NOVEL AROMATIC NITROXIDES AS POTENTIAL DNA INTERCALATORS

One way to incorporate radicals into DNA in order to study the spin-spin exchange coupling constant  $J$  between two unpaired electrons is to link stable nitroxides to DNA. Nevertheless, since spin labelling on the periphery of DNA may yield erroneous results in this kind of studies, a better choice would be to use nitroxides that intercalate between two base pairs.<sup>[1]</sup> These intercalating nitroxides need to be stable in liquid solution and to possess extended planar and heterocyclic  $\pi$ -systems. They should also be polarizable and polar or charged, as the well-known diamagnetic intercalators ethidium<sup>[2]</sup> or acridine<sup>[3]</sup>. Furthermore, to investigate  $J$  coupling in biradical DNA generated with stable intercalated nitroxides, it is necessary for the interacting spins to be well inside the DNA base stack. For this reason, intercalation ought to occur with the N-O group between the bases or, if this does not happen, the spin density should be delocalised into the intercalating part of the nitroxide. Aromatic nitroxides<sup>[4, 5]</sup> may be a class of substances, which could match these criteria.

Herein five aromatic nitroxides are studied (depicted in Fig. 3.1; synthesized by Mario Beyer) which are potentially capable of intercalating into DNA. Among them, two were described earlier in the literature: the carbazole-9-oxyl **1**<sup>[6-8]</sup>, which showed a delocalization of the N-O spin density over the whole aromatic ring system, and the 9,9-diphenylacridane-10-oxyl **2**<sup>[9, 10]</sup>.

In this chapter the spin density distribution of the five aromatic nitroxides is studied by means of spectral simulations of the EPR spectra recorded by Mario Beyer at room temperature, in order to show if and to which extent the spin delocalisation is present. Spin delocalization would make the nitroxides under investigation suitable candidates to selectively inject two radicals in DNA for future studies on the  $J$  coupling. Comparison of the simulated hyperfine coupling constants with the results obtained from DFT calculation (performed by Jörg Fritscher) is also presented.

### 3.1 MATERIALS AND METHODS

#### 3.1.1 Sample preparation

The carbazole-based aromatic nitroxides **1**<sup>•</sup> and **3**<sup>•</sup> as well as the acridane-based nitroxides **4**<sup>•</sup> and **5**<sup>•</sup> were synthesized as described in Beyer al.<sup>[1]</sup>, **2**<sup>•</sup> was synthesized according to Greci.<sup>[10]</sup>

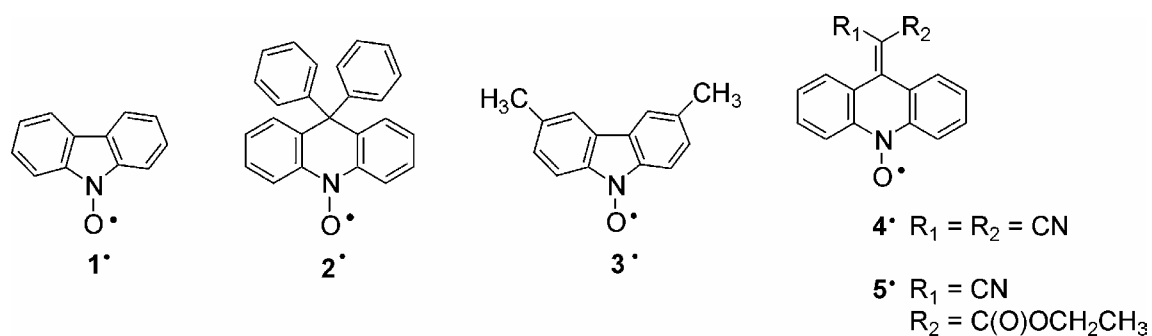


**Figure 3.1** Structures of compounds **1**<sup>•</sup> - **5**<sup>•</sup>.

#### 3.1.2 Simulation and fit program

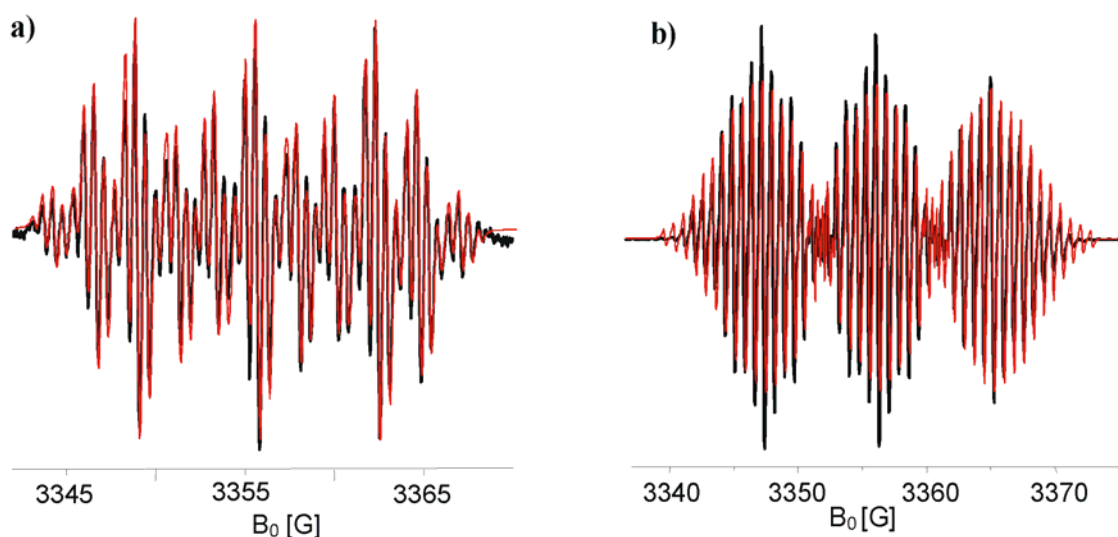
The simulation program<sup>i</sup> used in the following is based on MATLAB. The isotropic spin Hamiltonian, describing the spin system under study, includes the electron Zeeman and electron-nuclear spin-spin interactions. Input data needed for describing the spectrum are fixed values as center field and microwave frequency, and variable parameters as  $g_{\text{iso}}$ , hyperfine coupling constants  $a_{\text{iso}}$ , and the peak-to-peak line width  $\Delta H_{\text{pp}}$ . The line width was added by means of a convolution procedure in the Fourier transform space. The variable parameters are optimized by a simplex fit routine minimizing the root-mean-square values.

<sup>i</sup> Prof. T. F. Prisner wrote and provided the fit program.

## 3.2 RESULTS AND DISCUSSION

### 3.2.1 EPR spectroscopy and simulations of the experimental spectra

The cw X-band EPR spectra of substances **1**<sup>•</sup>-**5**<sup>•</sup> measured at room temperature are depicted in Fig. 3.2 together with the simulated spectra. The simulations were performed with a home-written program and fit to the experimental spectra utilizing a simplex fit routine. The obtained <sup>1</sup>H and <sup>14</sup>N hf coupling constants are summarized in Table 3.1 together with the  $g_{\text{iso}}$  values.<sup>ii[11]</sup>



<sup>ii</sup> Further analysis on the  $\tilde{g}$  tensor of samples **2**<sup>•</sup> and **4**<sup>•</sup> by means of both DFT calculations and G-band EPR spectroscopy has been recently done by Bela Bode.<sup>[11]</sup>

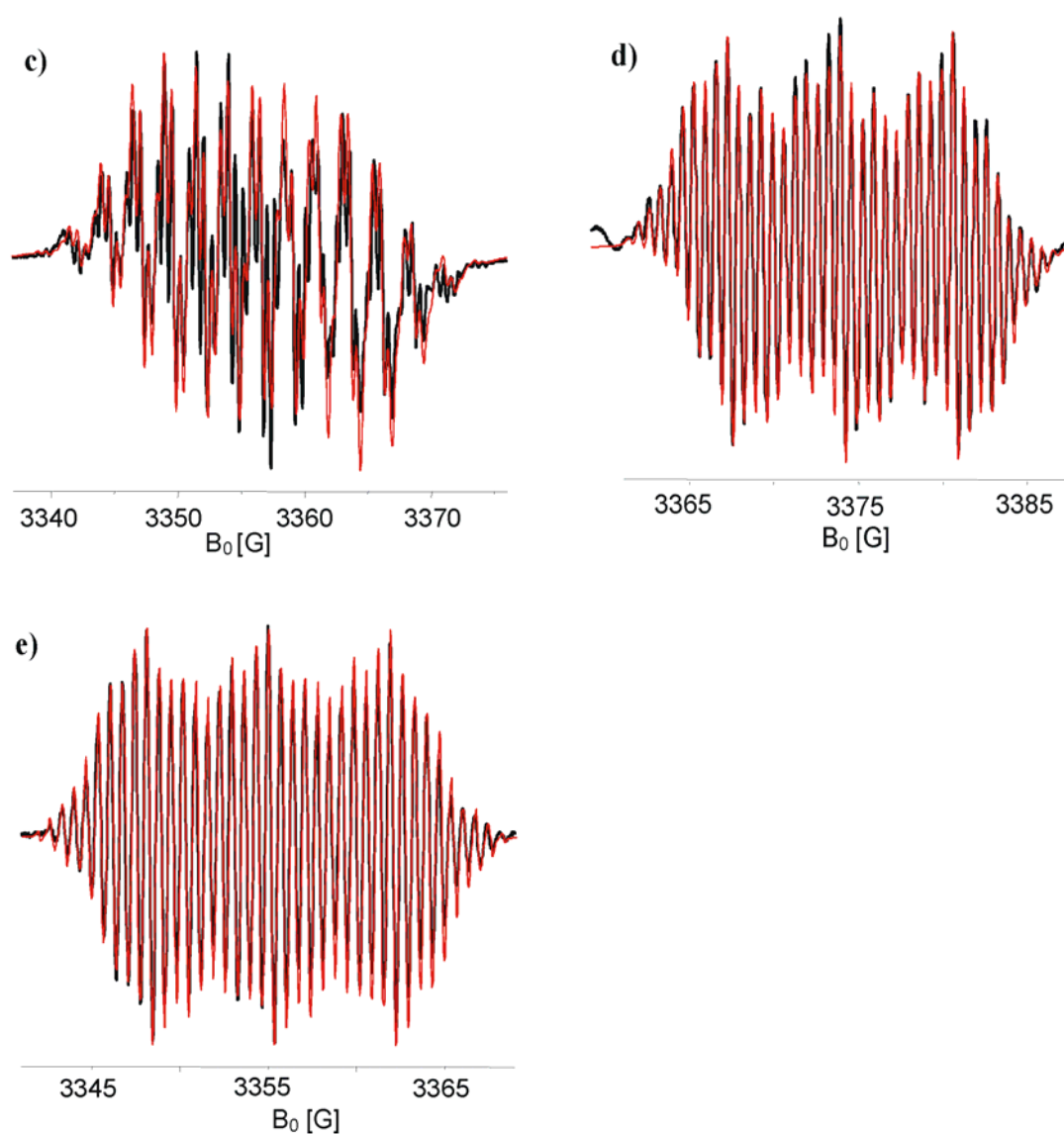


**Figure 3.2** CW X-band EPR spectra of (a)  $1^\bullet$  ( $\nu_0 = 9.4270$  GHz), (b)  $2^\bullet$  ( $\nu_0 = 9.4270$  GHz), (c)  $3^\bullet$  ( $\nu_0 = 9.4270$  GHz), (d)  $4^\bullet$  ( $\nu_0 = 9.4777$  GHz), and (e)  $5^\bullet$  ( $\nu_0 = 9.4270$  GHz) in benzene- $d_6$ . All spectra were recorded at room temperature. The red curves represent the simulated spectra.

**Table 3.1** EPR parameters of **1<sup>•</sup>**, **2<sup>•</sup>**, **3<sup>•</sup>**, **4<sup>•</sup>** and **5<sup>•</sup>** as obtained from fits of the experimental spectra.<sup>a</sup>

	<b>g<sub>iso</sub></b>	<b>a<sub>iso</sub>(<sup>14</sup>N) [G]</b>	<b>a<sub>iso</sub>(<sup>1</sup>H) [G]</b>	<b>ΔH<sub>pp</sub> [G]</b>
<b>1<sup>•</sup></b>	2.0072	6.73 / +5.37 (NO)	2.36 / -2.86 (H6,6') 2.27 / -2.76 (H4,4') 0.59 / +1.05 (H5,5') 0.50 / +0.98(H3,3')	0.17
<b>2<sup>•</sup></b>	2.0066	8.92 / +7.57 (NO)	3.03, 3.10 / -3.09 (H6,6') 2.39, 2.28 / -2.99 (H4,4') 1.58, 1.52 / +1.50 (H5,5') 0.80, 0.71 / +1.42 (H3,3')	0.17
<b>3<sup>•</sup></b>	2.0061	6.98 / +5.48 (NO)	2.52 / -2.86 (H6,6') 2.47 / +2.50 (CH <sub>3</sub> ) <sup>b</sup> 0.61 / +1.12 (H5,5') 0.61 / +0.93 (H3,3')	a = 0.19 <sup>c</sup> b = -0.04 <sup>c</sup> c = 0.01 <sup>c</sup>
<b>4<sup>•</sup></b>	2.0067	6.91 / +5.56 (NO) 0.61 / +0.76 (2xCN)	2.10 / -2.89 (H6,6') 2.06 / -2.64 (H4,4') 0.71 / +1.60 (H5,5') 0.17 / +1.37 (H3,3')	0.19
<b>5<sup>•</sup></b>	2.0075	6.90 / +6.11 (NO) 0.70 / +0.79 (CN)	2.07 / -2.98 (H6,6') 2.00 / -2.80 (H4,4') 0.81 / +1.69 (H5,5') 0.66 / +1.57 (H3,3')	0.14

<sup>a</sup> The hyperfine coupling constants following the slash are the ones obtained from the unrestricted PBE0/6-31G(d) DFT calculations. The numbering of the protons follows the numbering scheme given in Fig. 3.1. <sup>b</sup> The isotropic <sup>1</sup>H hyperfine coupling constants of CH<sub>3</sub> in **3<sup>•</sup>** were calculated by averaging over the three methyl hydrogens:  $a_{iso} = (a_{iso,1} + a_{iso,2} + a_{iso,3})/3$ . <sup>c</sup>  $m_I$ -dependence of the line width of the <sup>14</sup>N hyperfine couplings according to  $\Delta H_{pp} = a + bm_I + cm_I^2$ .

Generally, cw X-band EPR spectra of alkyl nitroxides in fluid solutions are characterized by three lines due to the isotropic  $^{14}\text{N}$  hf coupling of  $\cong 14\text{-}15$  G as well as small and usually not resolved hyperfine couplings to nearby  $^1\text{H}$  nuclei.<sup>[4, 5]</sup> The reason for this is the localization of spin density to over 95% on the N-O group. The aromatic nitroxides studied here showed, in contrast to alkyl nitroxides, resolved hyperfine couplings for all the ring protons and for  $\mathbf{3}^\bullet$ ,  $\mathbf{4}^\bullet$ , and  $\mathbf{5}^\bullet$  even to the methyl and nitrile substituents, respectively. This delocalization of spin density from the N-O group into the ring system decreased the  $^{14}\text{N}$  hyperfine coupling to about 7 G for  $\mathbf{1}^\bullet$ ,  $\mathbf{3}^\bullet$ ,  $\mathbf{4}^\bullet$ , and  $\mathbf{5}^\bullet$  and to 9 G for  $\mathbf{2}^\bullet$ , leaving only roughly 50% of the spin density on the N-O nitrogen. The hyperfine coupling constants for  $\mathbf{2}^\bullet$  found here slightly differ from the ones reported in literature.<sup>[6-10]</sup> The line broadening with increasing field observable for  $\mathbf{3}^\bullet$  was accounted for by incorporating a  $m_I$ -dependence of the line width for the  $^{14}\text{N}$  hyperfine couplings (see also Table 3.1).

### **3.2.2 DFT calculations**

For a specific assignment of the hf coupling constants the DFT calculations are useful. Geometry optimizations of all five nitroxides revealed that the carbazole nitroxides  $\mathbf{1}^\bullet$  and  $\mathbf{3}^\bullet$  are planar (Fig. 3.3a). On the other hand, the three acridane nitroxides  $\mathbf{2}^\bullet$ ,  $\mathbf{4}^\bullet$ , and  $\mathbf{5}^\bullet$  deviate from planarity by an angle of  $22^\circ$  for  $\mathbf{2}^\bullet$  and of  $17^\circ$  in the case of  $\mathbf{4}^\bullet$  and  $\mathbf{5}^\bullet$  (Fig. 3.3b).



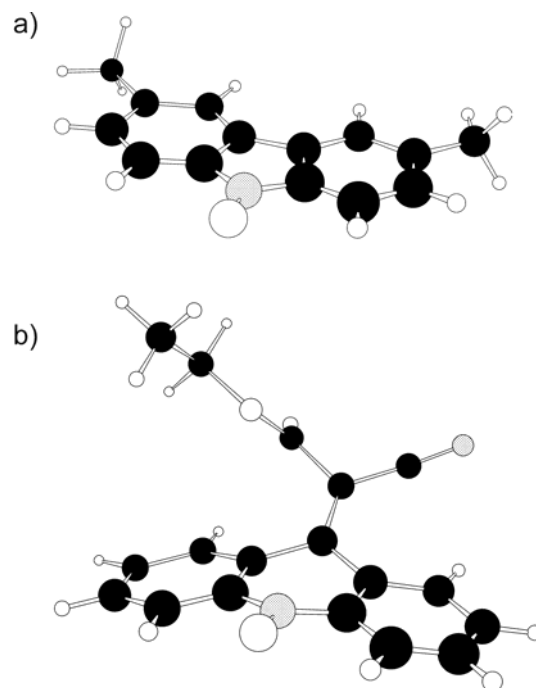


**Figure 3.3** Geometry-optimized molecular structures of a)  $3^\bullet$  and b)  $5^\bullet$ .

Moreover, the substituents at the double bond between the carbon atoms 7 and 8 are not in plane but bent above and below the double bond plane. These deviations from planarity are thought to be induced by a steric interaction of the hydrogens in the 3 and 3' positions with the phenyl, nitrile, or ester substituents.

The geometry-optimized structures were then used to calculate the electronic and EPR properties. These calculations showed that in contrast to the localized singly occupied molecular orbitals (SOMOs) of alkyl nitroxides<sup>[12, 13]</sup> the SOMOs of all five aromatic nitroxides are extended over the whole  $\pi$ -system and even onto the substituents in the case of  $3^\bullet$ ,  $4^\bullet$ , and  $5^\bullet$  as shown for  $3^\bullet$  and  $5^\bullet$  in Fig. 3.4a and 3.4c. The positive spin density distribution follows the shape of the SOMOs (Fig. 3.4b and 3.4d). Due to spin polarization, negative spin density is induced at those carbon atoms of the rings for which the SOMOs possess a node.<sup>[14]</sup> The spin density on the ring hydrogens is also caused by spin polarization, as indicated by the opposite sign of the spin density at the corresponding carbon atom (Fig. 3.4b and 3.4d).

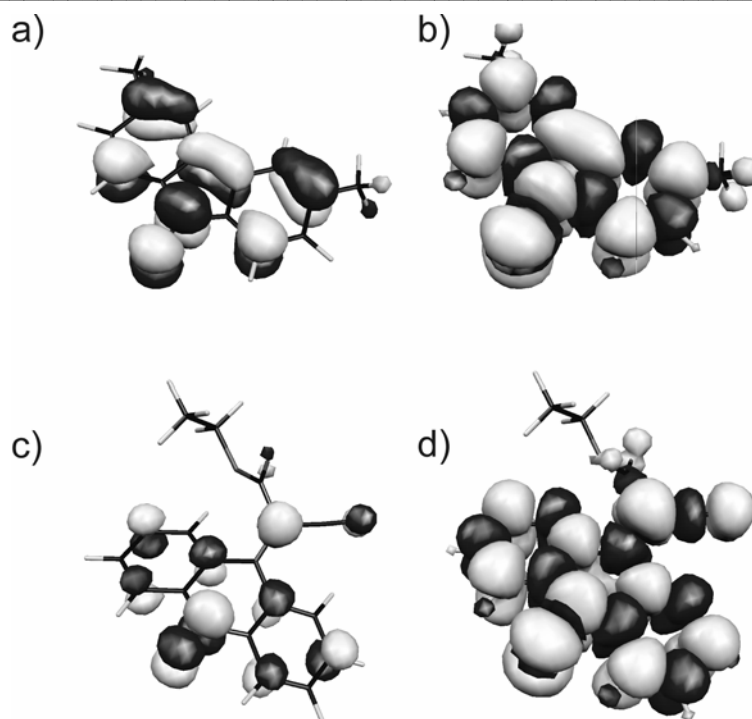


**Figure 3.4** Singly occupied molecular orbitals (SOMOs; a and c) and spin density distributions (b and d) of  $3^\bullet$  and  $5^\bullet$ , respectively, showing the delocalization of the unpaired electron due to the heterocyclic  $\pi$ -system. Positive spin densities are shown in light gray and negative ones in dark gray.

On the other hand the spin density at the hydrogens of the methyl groups of  $3^\bullet$  is transferred by hyperconjugation, leading to the same sign for the spin density as for the methyl substituted ring carbon atoms. A considerable amount of spin density was also found on the nitrile groups in  $4^\bullet$  and  $5^\bullet$  (Fig. 3.4d) as expected from the shape of the SOMOs and in agreement with the EPR measurements. Finally, it should be mentioned that the total atomic spin density of about +0.50 on the oxygen of the N-O group observed for the aromatic nitroxides is comparable to those found in alkyl nitroxides, whereas the spin density on the nitrogen (+0.25) is diminished by 50%.

With these spin density distributions, isotropic  $^{14}\text{N}$  and  $^1\text{H}$  hyperfine coupling constants were calculated that are in very good agreement with the ones obtained by simulation of the experimental EPR spectra, allowing a reliable assignment of the experimental hyperfine couplings to the respective nuclei (Table 3.1). Yet, the calculated isotropic  $^{14}\text{N}$  hyperfine coupling constants of the N-O group are slightly smaller than the experimental

ones, as commonly found in DFT calculations of nitroxides,<sup>[15]</sup> whereas the calculated isotropic <sup>1</sup>H hyperfine couplings are slightly larger.

### 3.3 CONCLUSIONS

Simulations of the room temperature cw X-band EPR spectra of the aromatic nitroxides **1**<sup>•</sup>, **2**<sup>•</sup>, **3**<sup>•</sup>, **4**<sup>•</sup> and **5**<sup>•</sup> were successfully performed. These aromatic nitroxides show resolved hyperfine couplings for all the ring protons and, in the case of **3**<sup>•</sup>, **4**<sup>•</sup> and **5**<sup>•</sup>, even to the methyl and nitril substituents, respectively. DFT studies on the hyperfine coupling constants of the same compounds are in good agreement with the simulated data and allow a specific assignment of the couplings. These investigations show that the spin density in the nitroxides under investigation is delocalised into the  $\pi$ -system. Thus such stable aromatic nitroxides could be in principle used to investigate J coupling in DNA when intercalated into the double helix.

### 3.4 REFERENCES

- [1] M. Beyer, J. Fritscher, E. Feresin, O. Schiemann, *Journal of Organic Chemistry* **2003**, *68*, 2209.
- [2] C. Z. Wan, T. Fiebig, S. O. Kelley, C. R. Treadway, J. K. Barton, A. H. Zewail, *Proceedings of the National Academy of Sciences of the United States of America* **1999**, *96*, 6014.
- [3] W. B. Davis, S. Hess, I. Naydenova, R. Haselsberger, A. Ogrodnik, M. D. Newton, M. E. Michel-Beyerle, *Journal of the American Chemical Society* **2002**, *124*, 2422.
- [4] L. B. Volodarsky, V. A. Reznikov, V. I. Ovcharenko, *Synthetic Chemistry of Stable Nitroxides*, CRC Press: Boca Raton, New York, **1994**.
- [5] J. K. Kochi, *Free Radicals, Vol. Volumes 1 and 2*, Wiley-Interscience, New York, **1973**.
- [6] H. G. Aurich, G. Bach, K. Hahn, G. Kuettner, W. J. Weiss, *Journal of Chemical Research, Miniprint* **1977**, 1541.
- [7] H. R. Falle, G. R. Luckhurst, *Molecular Physics* **1967**, *12*, 493.

- [8] H. G. Aurich, W. J. Weiss, *Chemistry Berlin* **1973**, 106, 2408.
- [9] C. Berti, M. Colonna, L. Greci, L. Marchetti, *Gazzetta Chimica Italiana* **1978**, 108, 659.
- [10] P. Carloni, L. Greci, A. Mar'in, P. Stipa, *Polym. Degrad. Stab.* **1994**, 44, 201.
- [11] B. E. Bode, Master Thesis, J. W. Goethe-University, Marie Curie-Strasse 11 (Frankfurt/Main (Germany)), **2004**.
- [12] R. Improta, G. Scalmani, V. Barone, *Chemical Physics Letters* **2001**, 336, 349.
- [13] J. Fritscher, M. Beyer, O. Schiemann, *Chemical Physics Letters* **2002**, 364, 393.
- [14] J. A. Weil, J. R. Bolton, J. E. Wertz, *Electron Paramagnetic Resonance. Elementary Theory and Practical Applications*, Wiley-Intescience, New York, **1994**.
- [15] V. Barone, *Recent Advances in Density Functional Methods*, World Scientific, Singapore, **1995**.

---

## 4. EPR DETECTION OF SELECTIVELY GENERATED GUANINE RADICALS IN DNA

In this chapter one method to introduce transient radicals into DNA using cw UV-light is presented. In a previous report, guanine radicals were generated within DNA at ambient temperature using the Flash-Quench Technique<sup>[1]</sup>, and detected by EPR. The aim of this chapter is to study if a transient guanine radical generated in DNA by the Flash-Quench Technique, can be trapped in glassy solution and detected by cw X-band EPR spectroscopy. In particular the extent of selectivity involved in the guanine radical formation is addressed. The selectivity is the determining factor in deciding whether this method can be successfully applied to generate two radicals in DNA. This represents the first step of the long-term goal of measuring the exchange coupling constant  $J$  in biradical DNA and correlating it with the charge transfer rate  $k_{CT}$  (see also section 1.2.5).

### 4.1 MATERIALS AND METHODS

#### 4.1.1 Sample preparation and irradiation

Poly(dG-dC), Poly(dA-dT), and Poly(dI-dC)<sup>i</sup> were purchased from Amersham Pharmacia Biotech and were exchanged into standard aqueous buffer solution (50 mM Tris, pH 7) by ultrafiltration prior to use. The ruthenium intercalator  $[\text{Ru}(\text{phen})_2(\text{dppz})]\text{Cl}_2$  (dppz= dipyridophenazine, phen= 1,10-phenanthroline, see Fig. 4.1 for the structure) was prepared as described previously.<sup>[2]</sup> Cobalt  $[\text{Co}(\text{NH}_3)_3\text{Cl}]\text{Cl}_3$ , and ruthenium  $\text{Ru}(\text{NH}_3)_6\text{Cl}_3$  were purchased from Aldrich and used without further treatment as quenchers (see section 4.1.2).

All samples contained 5 mM DNA, 0.5 mM quencher and 0.05 mM  $\text{Ru}^{2+}$ -intercalator in an aqueous buffer solution (50 mM Tris, pH 7). The concentrations are calculated based on the extinction coefficients of  $\epsilon_{440}=21000 \text{ M}^{-1}\text{cm}^{-1}$ ,  $\epsilon_{254}=8400 \text{ M}^{-1}\text{cm}^{-1}$ ,  $\epsilon_{251}=6900 \text{ M}^{-1}\text{cm}^{-1}$ , and  $\epsilon_{262}=6600 \text{ M}^{-1}\text{cm}^{-1}$  for  $[\text{Ru}(\text{phen})_2(\text{dppz})]\text{Cl}_2$ , Poly(dG-dC), Poly(dI-dC), and Poly(dA-

---

<sup>i</sup> The following nomenclature is used: d, deoxy; G, C, A, T are the normal DNA bases (see chapter 1); I, Inosine.

dT), respectively. The solutions were transferred into standard X-band EPR tubes (quartz, outer diameter 4 mm, internal diameter 2.4 mm) and deoxygenated by repeated argon flushing. Still under argon the samples were irradiated with an Osram Hg-ShortArc lamp of 100 W and simultaneously cooled to 77 K. The contemporary irradiation and freezing was done by slowly placing the sample into a "cold finger" transparent quartz dewar, which was previously filled with liquid nitrogen (77 K) and mounted in the focus of the UV-visible light source. The optimization of the beam geometry was achieved by visual inspection of the focus of the source after a 5 cm diameter quartz lens.

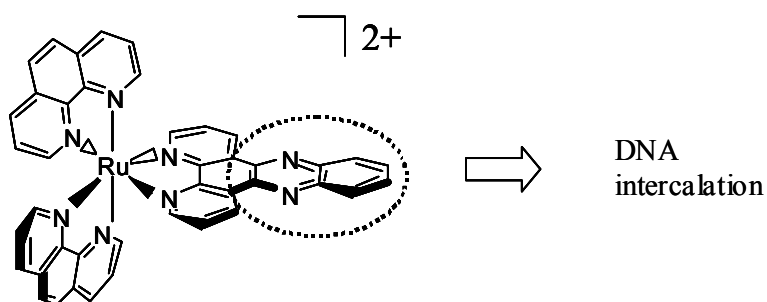


**Figure 4.1** Structure of the  $Ru(phen)_2(dppz)^{2+}$ , showing the phz (=phenazine) part of the dppz ligand (dashed circle) and the direction of DNA intercalation of the dppz ligand. <sup>[3]</sup>

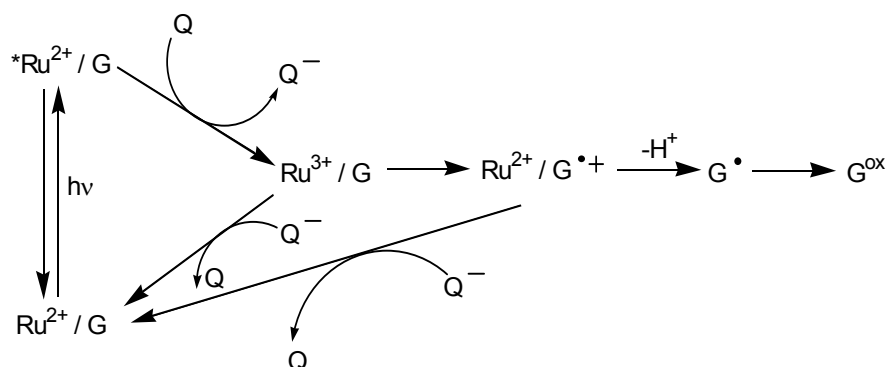
#### 4.1.2 The flash quench-technique

A useful method to generate guanine radicals within DNA duplexes is the flash-quench technique (Scheme 4.1)<sup>[4, 5]</sup>. A key role in this method is exerted by the complex  $[Ru(phen)_2(dppz)]Cl_2$ , which can intercalate with the planar dppz ligand between the base pairs of DNA (see Fig. 4.1).<sup>[3, 6-8]</sup> In the flash quench cycle the DNA intercalated  $[Ru(phen)_2(dppz)]^{2+}$  ( $Ru^{2+}$ ) is excited with visible light yielding  $*[Ru(phen)_2(dppz)]^{2+}$  ( $*Ru^{2+}$ ). By ET from  $*Ru^{2+}$  to a non-intercalating electron acceptor (quencher, Q),  $[Ru(phen)_2(dppz)]^{3+}$  ( $Ru^{3+}$ ) is formed in its ground state, which is a powerful oxidant ( $E_{Ru^{3+}/Ru^{2+}}^0 = 1.6 V^{ii}$ )<sup>[9, 10]</sup>.  $Ru^{3+}$ , if intercalatively bound to DNA,<sup>[3]</sup> is capable of oxidizing guanine ( $E_{G^{+\bullet}/G} = 1.3 V^{iii}$ )<sup>[11]</sup> leading to the guanine radical cation  $G^{+\bullet}$ . The latter is then rapidly deprotonated on the microsecond time scale<sup>[12]</sup>, due to its low  $pK_a$  value of 3.9<sup>[13]</sup>.

<sup>ii</sup> The redox potentials here reported are expressed in V versus NHE

<sup>iii</sup> Value in aqueous solution at pH=7

The neutral guanine  $G^{\bullet[4, 5]}$  may then react irreversibly with water and/or oxygen to form stable oxidized products,  $G^{\text{ox}}$ , which can be further analyzed using biochemical methods.



**Scheme 4.1** The Flash-Quench Cycle. For the nomenclature see the text.

## 4.2 RESULTS AND CONCLUSIONS

A sample of poly(dG-dC) was prepared and irradiated as described above. Simultaneous irradiation and cooling of the poly(dG-dC) sample to 77 K was necessary in order to obtain an EPR signal. In this way the quencher was still mobile, as needed for the flash-quench cycle to be active, but the generated radicals were rapidly trapped. As a consequence the cw X-band EPR signal displayed in Fig. 4.2 was recorded.

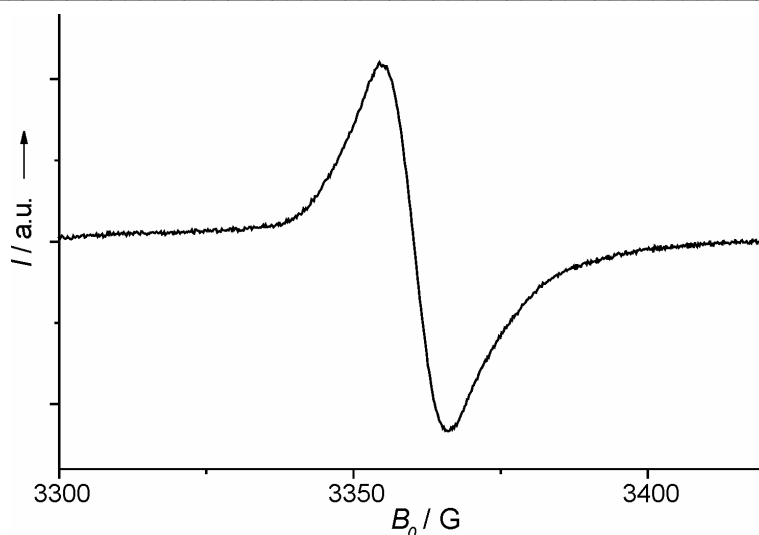


**Figure 4.2** CW X-band EPR signal from a sample of 5 mM poly(dG-dC), 0.5 mM  $[\text{Co}(\text{NH}_3)_5\text{Cl}]\text{Cl}_2$ -quencher and 0.05 mM  $[\text{Ru}(\text{phen})_2(\text{dppz})]\text{Cl}_2$ -intercalator in 10 mM Tris HCl buffer solution (pH = 7) detected at 80 K. A microwave power of 10 mW, a modulation amplitude of 5 G, a receiver gain of  $5 \cdot 10^4$ , a conversion time of 20.48 ms, a time constant of 1.28 ms and 50 scans were used.

The singlet in Fig. 4.2 shows no resolved hyperfine structure and is characterized by a zero crossing at  $g$ -factor =  $2.004 \pm 0.001$ , a half width at half height linewidth  $\Delta H_{1/2} = 12.5$  G. The  $g$ -factor is the same as in the liquid state, while the increased line width of 4 Gauss compared to the signal at room temperature<sup>[1]</sup> is attributed to  $g$ - or hyperfine anisotropy. The EPR signal intensity is still weak (5 G modulation amplitude had to be used, see Fig. 4.2) but it is increased by a factor of 40 with respect to the room temperature.<sup>[1]</sup> The signal is detectable for several days due to the increased lifetime of the radical at low temperature. The signal obtained is comparable in spectral shape and parameters to the singlet attributed by Weiland and Hüttermann to the neutral guanine radical  $\text{G}^\bullet$  at 77 K.<sup>[14]</sup> No EPR signal at 80K was observed using the  $[\text{Co}(\text{NH}_3)_5\text{Cl}]^{2+}$ -quencher and poly(dA-dT) or poly(dI-dC). This demonstrates that no adenine, thymine, inosine, cytosine, sugar or metal complex radicals are generated/detectable, and therefore proves that the observed signal is due to guanine radicals  $\text{G}^\bullet$  (Fig. 4.3).



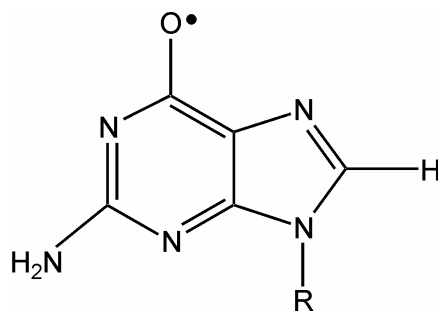


**Figure 4.3** Chemical structure of the guanine radical  $G^\bullet$ .

Attempts were made to see if the forbidden transitions  $\Delta m_s = \pm 2$  at half-field ( $g \approx 4$ ,  $B_0 \approx 0.17$  T) could be detected. The detection of such transitions is characteristic of a triplet state ( $S=1$ ) or higher multiplet state of radical pairs, and hence of an exchange coupling interaction  $J$ . No half-field signal neither by using a rectangular or a dual mode resonator could be observed nor any indications for an exchange coupling were found from the main field signal. The non-observability of the  $g = 4$  signal can be attributed to its inherent weak intensity and the random distribution of guanine radicals within the DNA duplexes, leading to radical-radical distances too long for an exchange coupling measurable via the half-field signal.

### 4.3 REFERENCES

- [1] O. Schiemann, N. J. Turro, J. K. Barton, *Journal of Physical Chemistry B* **2000**, *104*, 7214.
- [2] E. Amouyal, A. Homsy, J. C. Chambron, J. P. Sauvage, *Journal of the Chemical Society-Dalton Transactions* **1990**, 1841.
- [3] W. Chen, C. Turro, L. A. Friedman, J. K. Barton, N. J. Turro, *Journal of Physical Chemistry B* **1997**, *101*, 6995.
- [4] E. D. A. Stemp, M. R. Arkin, J. K. Barton, *Journal of the American Chemical Society* **1997**, *119*, 2921.
- [5] M. R. Arkin, E. D. A. Stemp, S. C. Pulver, J. K. Barton, *Chemistry & Biology* **1997**, *4*, 389.

- [6] A. E. Friedman, J. C. Chambron, J. P. Sauvage, N. J. Turro, J. K. Barton, *Journal of the American Chemical Society* **1990**, *112*, 4960.
- [7] Y. Jenkins, A. E. Friedman, N. J. Turro, J. K. Barton, *Biochemistry* **1992**, *31*, 10809.
- [8] C. Turro, S. H. Bossmann, Y. Jenkins, J. K. Barton, N. J. Turro, *Journal of the American Chemical Society* **1995**, *117*, 9026.
- [9] A. Juris, V. Balzani, F. Barigelletti, S. Campagna, P. Belser, A. von Zelewsky, *Coordination Chemistry Reviews* **1988**, *84*, 85.
- [10] C. J. Murphy, M. R. Arkin, N. D. Ghatlia, S. Bossmann, N. J. Turro, J. K. Barton, *Proceedings of the National Academy of Sciences of the United States of America* **1994**, *91*, 5315.
- [11] S. Steenken, S. V. Jovanovic, *Journal of the American Chemical Society* **1997**, *119*, 617.
- [12] S. Steenken, *Chemical Reviews* **1989**, *89*, 503.
- [13] L. P. Candeias, S. Steenken, *Journal of the American Chemical Society* **1989**, *111*, 1094.
- [14] B. Weiland, J. Hüttermann, *International Journal of Radiation Biology* **1998**, *74*, 341.

## 5. THE 4'-PIVALOYL SUBSTITUTED THYMIDINE AS PRECURSOR FOR THE THYMYL RADICAL

In this chapter the EPR study of *in situ* radical formation upon irradiation of the photocleavable 4'-pivaloyl substituted thymidine **1** (Fig. 5.1) is presented.

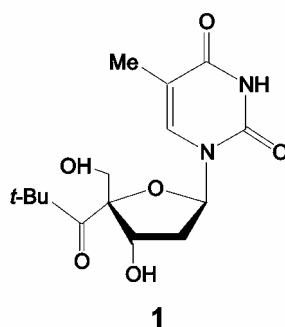
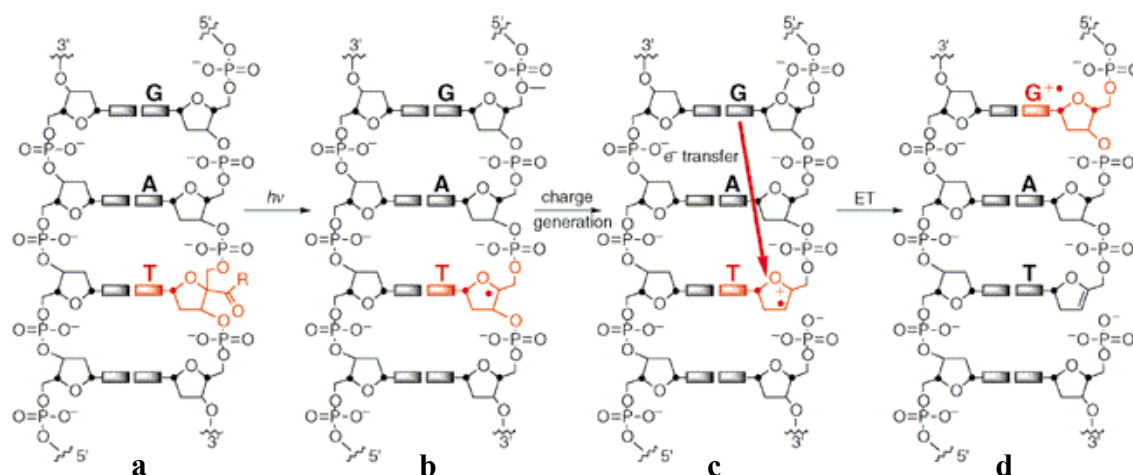


**Figure 5.1** Structure of the 4'-pivaloyl substituted thymidine **1**. The tert-butyl group is depicted as “t-Bu”.

Based on product analysis it was suggested that the UV-vis irradiation of compound **1** leads to a homolytic C-C bond cleavage (Norrish type I) at the pivaloyl site and thereby to radical formation of two radicals: a tert-butyl radical and a 4' sugar radical.<sup>[1, 2]</sup> Moreover, DNA modified with the nucleotide derivative of **1** were used by Giese and co-workers to generate site selectively, upon irradiation, a guanine radical cation  $G^{\bullet+}$  and to study HT processes in DNA.<sup>[3-8]</sup> In that case the following mechanism for the charge transfer reaction was suggested:



**Scheme 5.1** Photolytic generation of the 4'-DNA radical **b** from **a**: charge generation (sugar radical cation  $C3'^{\bullet+}$ ) by heterolytic cleavage ( $b \rightarrow c$ ), and electron transfer (ET) through DNA ( $c \rightarrow d$ ). The hole transfer occurs in the opposite direction. This assay was used for site-selective charge injection into a single G. (Adapted from <sup>[3]</sup>)

Here for the first time EPR spectroscopy is used to analyze the radicals formed upon irradiation of **1** and to study the mechanism involved in their generation.<sup>[9]</sup>

## 5.1 MATERIALS AND METHODS

### 5.1.1 Sample preparation

The *thymidine derivative 1* (Fig 5.1) was prepared by Giese and co-workers as described previously.<sup>[1]</sup>

Appropriate amounts of **1** were dissolved in dry acetonitrile ( $CH_3CN$ ) or in  $H_2O$  or  $D_2O$  yielding final concentrations of 20 mM if not stated otherwise. The samples were transferred into standard X-band EPR tubes, deoxygenated by repeated argon flushing, and then, still under argon, frozen in liquid nitrogen (77 K). The electron scavenger  $K_3[Fe(CN)_6]$  (Sigma-Aldrich) was added in a concentration of 1 mM (see section 5.2.2) according to Hüttermann et al. <sup>[10]</sup>(see also section 5.1.4).

Samples of thymine, thymidine and di-*tert*-butylketone (Fig 5.2) were purchased from Sigma-Aldrich and used as model samples (see section 5.2.1) without further purification. They were prepared and treated in the same way as **1**.

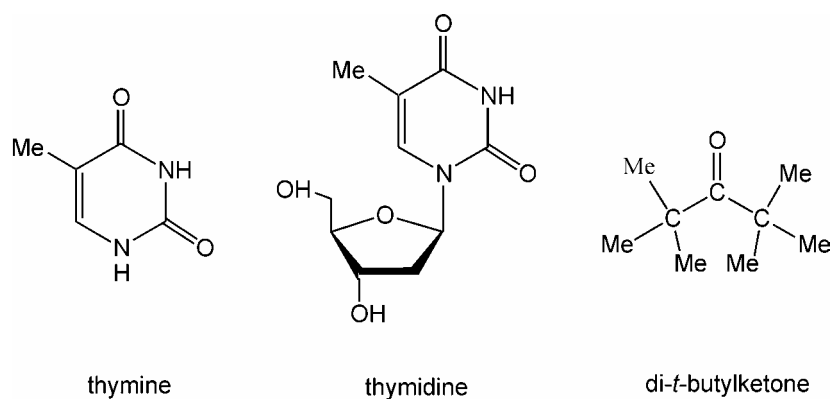


**Figure 5.2** Structures of thymine, thymidine and di-*tert*-butylketone. Methyl groups are depicted as “Me”.

The *double stranded DNA* in which a thymine nucleotide in the middle of the sequence was modified at the 4' sugar site with a pivaloyl group was prepared as follows. Two strands, one with the modification and the counter-strand (Fig. 5.3), were synthesized by Giese and co-workers and given to us in an amount of 1.10 nmol the former, 1.21 nmol the latter.



**Figure 5.3** Sequence of the DNA moiety modified with the nucleotide derivative of **1**, which is depicted as T\*.

The duplexes were hybridized by slow cooling (90-20 °C, in 5 min) of equal concentrations of complementary strands in aqueous buffer solution (phosphate buffer, pH 7.0), leading to a final concentration of 15 μM in DNA. Then, the DNA double strands were transferred in the EPR quartz tube and illuminated in the same way as **1**.

### **5.1.2 Generation of radicals by UV Irradiation**

The method used to generate the radicals is UV irradiation, which, as described below (see section 5.1.3), should induce homolytic cleavage of the pivaloyl group.

The EPR tube with the frozen sample was placed into a “cold finger” transparent quartz dewar, filled with liquid nitrogen (77 K) and mounted in the focus of a UV light source. Sample **1**, and also thymine, thymidine and di-*tert*-butylketone were irradiated with an Osram Hg-ShortArc lamp of 100W, equipped with a 320nm cut-off filter, for 200 s. The optimization of the beam geometry was based on visual observation of the focus of the source after a 5 cm diameter quartz lens and the 320 nm cut-off filter. In all experiments particular attention was paid to ensure a homogeneous light intensity distribution over the whole area of the sample inside the EPR quartz tube. This was achieved by continuous and slow rotation of the sample during the whole irradiation period.

Irradiation at temperatures below 77 K was performed directing the UV light beam through the grid of the standard EPR cavity and focusing it on the sample inside the quartz helium cryostat. In order to avoid the beam being obstructed by the arm of the cryostat, it was necessary to turn the cavity by 180° and to position the lamp behind the magnet.

The cryostat (continuous flow ESR900 cryostat from Oxford) allows the cooling of the sample down to 4 K, by means of liquid helium flushing: the experiments were done at temperature values between 4 K and 140 K.

### **5.1.3 Photolysis of the pivaloyl group and radical formation**

The pivaloyl group has been widely used as photolabile radical precursor both in oligonucleotides and model nucleosides/nucleotides [7, 11-16], in solid-phase organic synthesis<sup>[17, 18]</sup> and in the synthesis of hexose radicals<sup>[19]</sup>. The photochemical process that occurs by exposure to UV light is the so-called Norrish type I reaction<sup>[20-22]</sup>, typical for alkyl ketones: a molecule undergoes photolytic generation of a radical pair via cleavage of the  $\sigma$  bond between the carbonyl carbon and an  $\alpha$  carbon (Fig. 5.4a). This primary process originates from the photo-excited  $n\pi^*$  state of the carbonyl group and it is commonly

called homolytic  $\alpha$  cleavage<sup>i</sup>. The products of such a reaction are an alkyl radical and an acyl radical, and the latter eventually decarbonylates.<sup>[23-25]</sup> In the case of the pivaloyl group, the primary radicals are a radical at the site of the pivaloyl group on the modified molecule and a pivaloyl radical,<sup>[16-18]</sup> which eventually decarbonylates to a *tert*-butyl radical and CO<sup>[24, 26]</sup>(Fig. 5.4b).

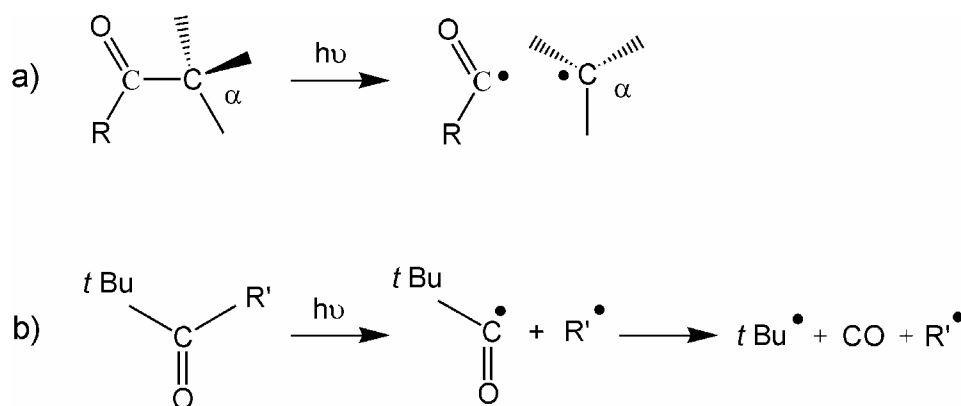


**Figure 5.4** a) Norrish type I  $\alpha$ -cleavage of an excited carbonyl compound leading to an acyl-alkyl radical pair as a primary photoproduct (*R* is a generic alkyl group). b) Structure and photoreaction of the pivaloyl group with a generic molecular fragment *R'*.

The first experimental attempts were carried out with **1** dissolved in acetonitrile and irradiated using the UV lamp in conjunction with a 389 nm cut-off filter: no EPR spectra were detected on such samples, neither from the model compounds in Fig. 5.2. On the other hand, when the irradiation was performed using the lamp without any filtering of the UV light, all the samples gave very intense and complicated EPR signals, probably arising from damage by short-wavelength UV light. Finally the sample was irradiated for 200 s using a 320 nm cut-off filter, optimal conditions found to obtain intense EPR spectra from **1** (see section 5.2). This is in agreement with the findings on similar carbonyl compounds showing a  $n\pi^*$  absorption band below 340 nm, which undergo  $\alpha$  cleavage when exposed to UV light below 340 nm,<sup>[18, 25]</sup> e.g. di-*tert*-butylketone<sup>[20, 26]</sup>.

<sup>i</sup> The Norrish type II reaction for alkyl ketones, which doesn't occur herein, originates from the  $n\pi^*$  excited state of the carbonyl group and involves the intramolecular abstraction of a  $\gamma$ -hydrogen from a side chain of the ketone, which leads to formation of an enol (isolated as its tautomeric ketone) and an olefin or cyclobutanol.<sup>[18]</sup>

#### **5.1.4 Component differentiation of composite EPR spectra**

It is well known that the exposure of DNA or single nucleosides/tides to X-rays,  $\gamma$ -rays and UV light can lead to the generation of numerous radicals.<sup>[27-36]</sup> As a consequence, overlap of radical components occurs extensively in a very narrow magnetic field range at typical X-band EPR frequency, since the  $g$  and the hyperfine parameters of many species are comparable. Diverse chemical, physical and computer aided tools can be however used to differentiate and assign the radical species present in the samples.

*Thermal annealing* is a powerful tool in case of radicals that are stable at certain temperatures (e.g. 77 K) but can undergo thermally induced reactions and can be converted into secondary radical species or into non-paramagnetic species. This technique has been widely used in studies on DNA base radicals: typical is the case (already presented in section 2.5.3) of the thymine anion radical, which is stable at low temperatures and can be protonated under heat treatment to form the thymyl radical<sup>[28, 29, 31, 34-37]</sup>.

*Electron scavengers*, like  $K_3[Fe(CN)_6]$ , can change the proportions of reduced and oxidized components, acting as electron gain species. Electron scavengers have been used to prevent the formation of the thymine anion and of the thymyl radical<sup>[29, 32, 34]</sup>.

*Different solvents* can be also used in order to eliminate radicals that are solvent sensitive or to avoid indirect effects. For example alkyl and other organic free radicals are short lived in aqueous solutions. On the other hand water radiolysis products (e.g.  $H^\bullet$ ,  $OH^\bullet$ ), can also react with the substrate (e.g. DNA)<sup>[38, 39]</sup> or give overlapping spectra<sup>[31, 34, 40]</sup>.

*Microwave power dependent EPR measurements* can be done in order to recognize paramagnetic species with similar power saturation characteristics<sup>[41]</sup> or to enhance some patterns with respect to others if a species saturates at lower power than others<sup>[36]</sup>.

*Computer reconstruction of experimental and simulated data* was made by linear combination of the weighted individual components. The determination of the best matching reconstructed spectra, with respect to the experimental one, was made by visual inspection. Simulations, baseline corrections, spectra subtraction and addition and further data processing were performed with the software Simfonia and WinEPR from Bruker. Components were isolated also by suitable spectra subtraction.



## 5.2 RESULTS

### 5.2.1 Sample dissolved in CH<sub>3</sub>CN

The first measurements were carried out with the pivaloylated thymidine **1** dissolved in acetonitrile. After 200 seconds of irradiation at 77 K the 165 G broad EPR spectrum displayed in Fig. 5.5 was detected.

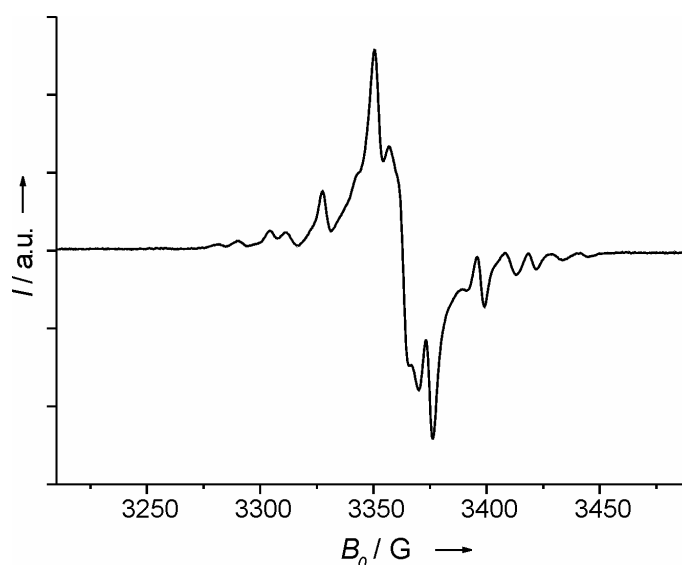


**Figure 5.5** EPR spectrum of a 0.12 M solution of **1** in CH<sub>3</sub>CN irradiated and measured at 77 K. The spectrum was acquired at a microwave power of 1 mW. 50 scans were accumulated. All the spectra presented in this chapter were acquired at a modulation amplitude of 0.7 G, a receiver gain of  $1 \times 10^5$ , a conversion time of 40.96 ms and a time constant of 40.96 ms, if not stated otherwise.

No signal was obtained with thymine or thymidine photolyzed under the same conditions. A negligible signal was detected from unmodified thymidine in the presence of di-*tert*-butylketone (see Appendix A, Fig. A.1). These control measurements reveal that the radical formation is not due to direct UV damage of the thymine base but to a homolytic C,C-bond cleavage at the site of the pivaloyl substituent, which is the photolabile radical precursor, as already stated (see section 5.1.3).

Power saturation measurements were then performed to obtain a first impression of whether all of the observed lines belong to only one or more radical species (Fig. 5.6).

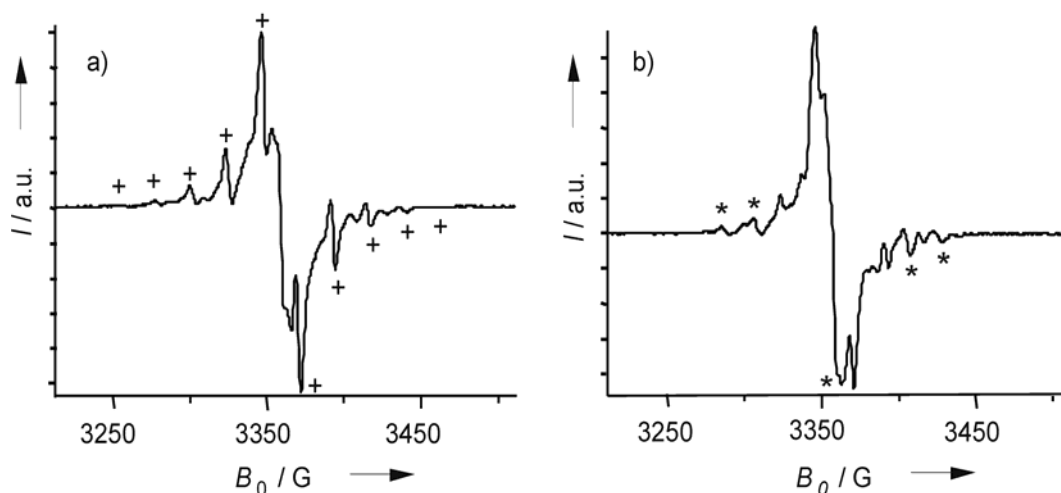


**Figure 5.6** a) EPR spectrum of **1** in  $\text{CH}_3\text{CN}$  detected at 77 K after 200 seconds of irradiation and using a microwave power of 15 mW (the + indicate the 10-line spectrum attributed to the *tert*-butyl radical). b) The same sample detected with a microwave power of 40  $\mu\text{W}$  (the \* indicate some of the lines that are more evident at low power than at high power).

The spectra detected at high and low power are different. In particular the lines indicated by + in Fig 5.6a are more intense at high power than at low power, while other lines, for example the ones indicated by \* in Fig 5.6b, are more evident at low power. Such observations suggested that these two groups of lines belong to different paramagnetic species. Subtracting the low power (Fig. 5.6b) from the high power (Fig. 5.6a) spectrum yielded the 10-line spectrum depicted in Fig. 5.7 (indicated by +) with a splitting of 22.7 G, which resembles the *tert*-butyl radical spectrum known from literature<sup>[42, 43]</sup> (see also Fig. 2.6).

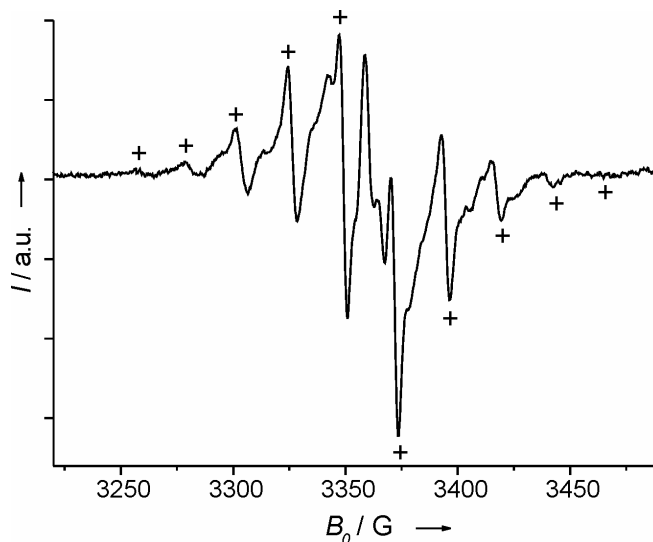


**Figure 5.7** 10-line spectrum (indicated by +) generated by subtraction of the low power spectrum from the high power spectrum, after normalizing the four outer lines indicated by \* in the low-power spectrum to the corresponding lines present in Fig. 5.6a. It should be noted that the 1<sup>st</sup> and the 10<sup>th</sup> lines are hardly visible, as already seen in Fig. 2.6.

To get rid of the *tert*-butyl radical species, very pronounced in the high power spectrum, and still present at low power, the subtraction of the high power from the low power spectrum has been done, and yielded a spectrum (Fig. 5.8) with a pronounced central part and clear side bands.

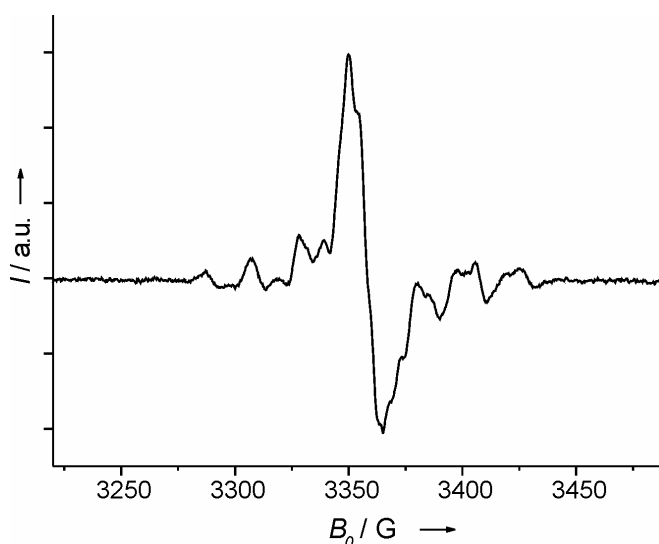


**Figure 5.8** Spectrum generated by subtraction of the high power spectrum from the low power spectrum, after normalizing the 10 line spectrum (indicated by + in Fig. 5.6a) to the corresponding lines still present in Fig. 5.6b.

These spectra alone are not very informative, nevertheless they indicate that the spectrum in Fig. 5.5 is a superposition of spectra belonging to different radicals.

### 5.2.2 Sample dissolved in H<sub>2</sub>O and in D<sub>2</sub>O

Experiments with **1** dissolved in water were also carried out to suppress the *tert*-butyl radical signal, which is known to be water sensitive, and hence to simplify the pattern of Fig. 5.5. The spectrum detected at 80 K (see Fig. 5.9) shows that the 10-line spectrum of the *tert*-butyl radical is almost completely suppressed leaving a spectrum displaying eight well-resolved lines (indicated by #) with a clear splitting of 20.4 G and an intense "central part" which partially superimposes to the two central lines. The eight lines spectrum can be attributed to the thymyl radical (*TH*<sup>•</sup>), which has a typical "octet fingerprint" spectrum<sup>[34]</sup> (see also Fig. 2.10). It is worth noting the similarity of this spectrum with the one in Fig. 5.8, obtained by subtraction of the spectra at different powers. No new signals from reactions with water or *OH*<sup>•</sup> radicals<sup>[31, 44]</sup> could be detected.

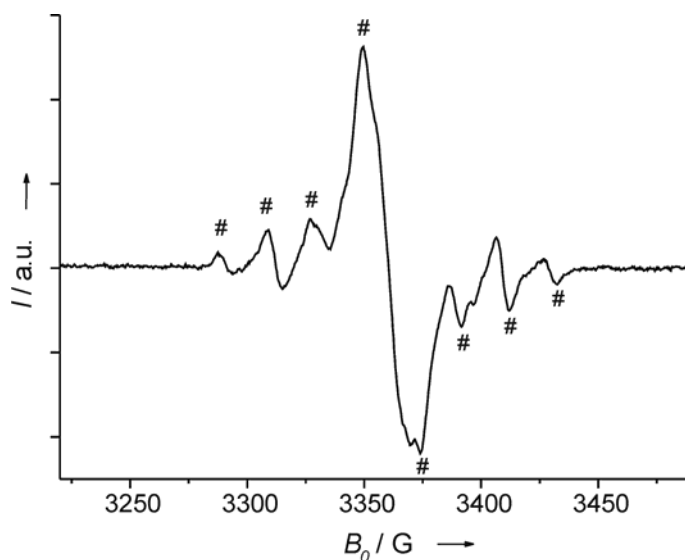


**Figure 5.9** EPR spectrum of the photolysis products of **1** in H<sub>2</sub>O at 80 K using a microwave power of 1 mW. Modulation amplitude of 1 G was used. 625 scans were accumulated. The eight lines attributed to *TH*<sup>•</sup> are indicated by #.

As already explained in section 5.1.4, electron scavengers can be used to prevent the formation of thymine radical anion or thymyl radical (double and octet spectrum, respectively, see also section 2.4.3). Hence, the electron scavenger  $K_3[Fe(CN)_6]$  was added to the solution of **1** in  $H_2O$  in order to try to suppress the 8-line spectrum at 80 K. This treatment in fact gave a spectrum dominated by the “central part” signal (Fig. 5.10a), which appears partially resolved in the 16 G broad line (Fig. 5.10b), whereas the eight lines spectrum is diminished.

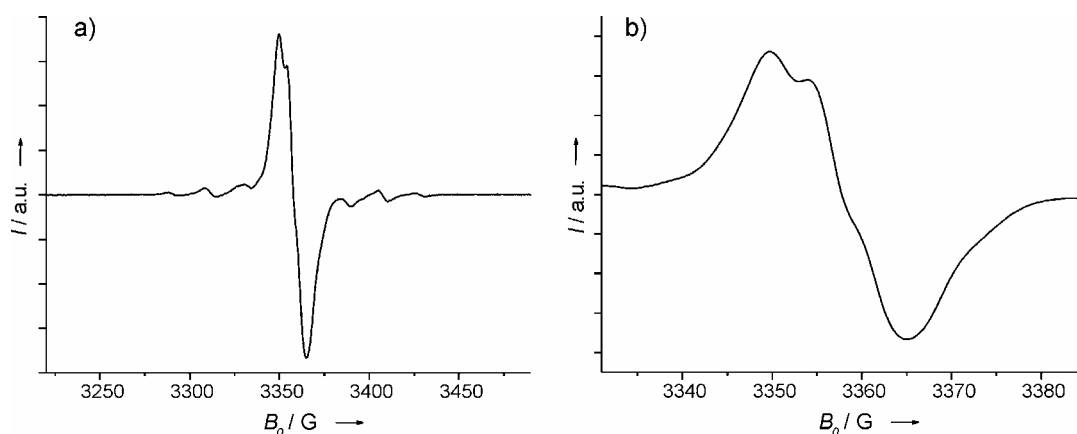


**Figure 5.10** a) EPR spectrum of **1** in  $H_2O$  a sample like in Fig. 5.9 but with 1 mM  $K_3[Fe(CN)_6]$  scavenger. b) Central part of the spectrum magnified. The spectrum was acquired at a microwave power of 1 mW and modulation amplitude of 0.5 G. 50 scans were accumulated.

Subtraction of the "central part" spectrum in Fig. 5.10b, which contains negligible contributions from the 8-line or 10-line spectra, from the spectrum in Fig. 5.9, yielded the pure 8-line spectrum shown in Fig. 5.11.

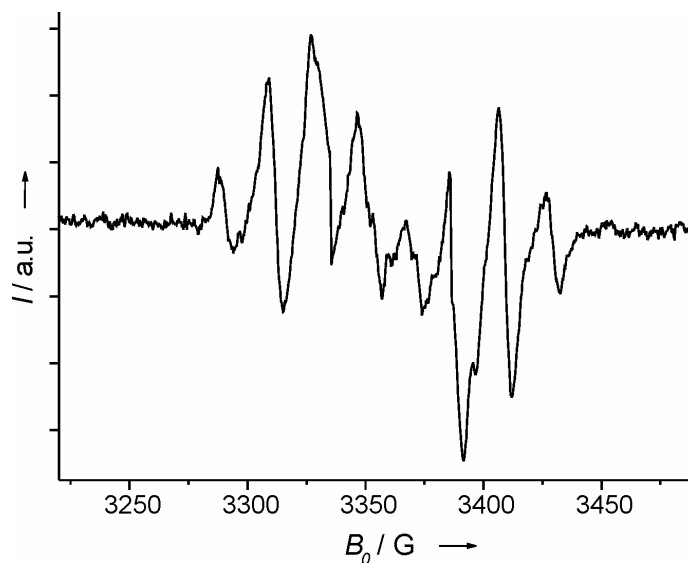


**Figure 5.11** Pure 8-line spectrum obtained after subtracting the "central part" spectrum in Fig. 5.10b from the spectrum in Fig. 5.9. The "central part" spectrum was normalized to the maximum amplitude of the spectrum in Fig. 5.9 prior to subtraction.

This spectrum is clearly the so called "octet-fingerprint" spectrum of the thymyl radical (see Fig. 2.10)<sup>[34, 36]</sup>, whose pattern has already been analyzed in section 2.4.3.

In order to verify eventual temperature effects, direct irradiation of **1** in water at 4 K was done. Interestingly, in that case, only the "central part" spectrum was detected (Fig. 5.12).

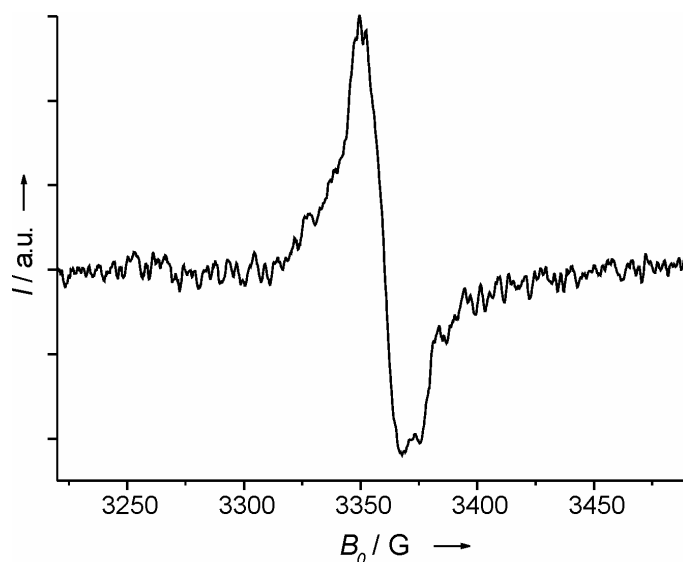


**Figure 5.12** EPR spectrum after photolysis of **1** in H<sub>2</sub>O at 4 K. 64 scans were accumulated at a microwave power of 5  $\mu$ W.

When the solvent was changed to  $D_2O$ , it was possible to narrow the line width and to resolve the "central part" spectrum, displaying three lines with a splitting of 5 G and a shoulder at the high field side. Heating this sample to 140 K in 10 K steps did not change the signal components, but decreased the line width even more to 2.5 G (Fig. 5.13). Above 200 K no signal was observable.

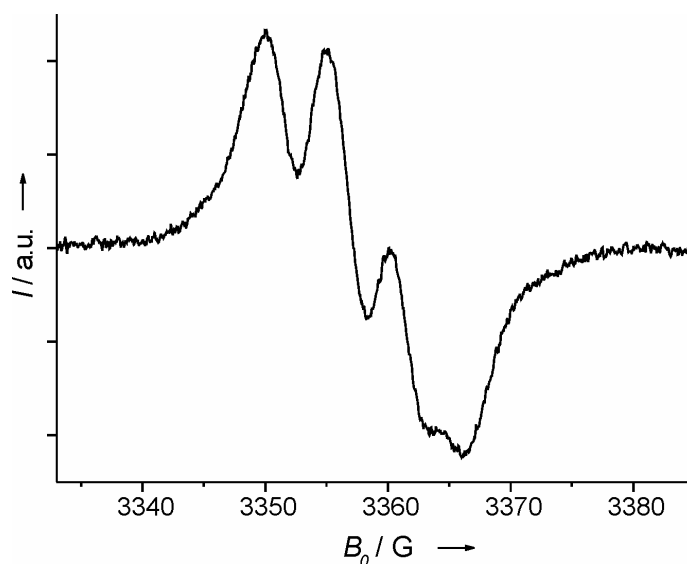


**Figure 5.13** EPR spectrum of the photolysis products of **1** in  $D_2O$  at 140 K after 40 seconds of irradiation at 4 K. The spectrum was recorded using a microwave power of 0.1 mW. Modulation amplitude of 0.5 G was used. 60 scans were accumulated.

### 5.2.3 Simulations and computer reconstructions

Both, the spectrum in Fig. 5.7, which is attributed to the *tert*-butyl radical, and the one in Fig. 5.11, which is attributed to the thymyl radical, were simulated (Fig. 5.14a,b) with the parameters given in Table 5.1, matching the parameters from the literature for the mentioned radicals.

**Table 5.1** Simulation data for the spectra assigned.

Radical	$a_{\text{iso}}$ [G]			g-factor	
	Position	Literature	This work	Literature	This work
<b>tert-butyl</b>	9H (3 Me)	22.74 <sup>[45, 46]</sup>	22.7 ± 0.3	2.0026 <sup>[45]</sup>	2.0032 <sup>b</sup> ± 0.0007
	Lw <sup>a</sup>		6.5 ± 1.0		
<b>thymyl</b>	3H (C5)	20.5 <sup>[47]</sup> , 20.2 <sup>[48]</sup>	20.5 ± 0.5	2.0035 <sup>d[27]</sup>	2.0037 <sup>b</sup> ± 0.0005
	2H (C6)	40.5 <sup>[47]</sup> , 37.6 <sup>[48]</sup>	37.5 ± 1.5		
	Lw <sup>a</sup> [G]		8.0 ± 2.0		

<sup>a</sup> The line components were assumed to be Gaussian and the peak-to-peak linewidth is presented. <sup>b</sup> The  $B_0$  necessary for the calculation of the g-factor (eq.2.36) was calculated as average value from the zero crossing  $B_i$  values of the 3<sup>rd</sup> and 8<sup>th</sup> line of the tert-butyl spectrum (Fig. 5.14a); for the thymyl spectrum lines 2<sup>nd</sup> and 7<sup>th</sup> were considered. <sup>c</sup> The complete hf  $\tilde{T}$  tensor has been given by Hole et al.<sup>[49]</sup>. <sup>d</sup> The complete  $\tilde{g}$  tensor has been given by Weiland et al.<sup>[28]</sup>.

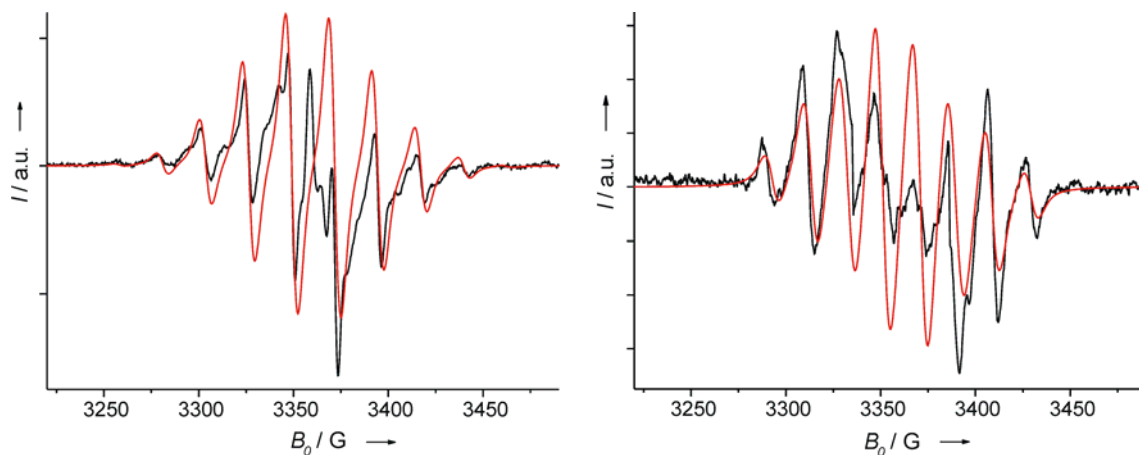


**Figure 5.14** a) Simulation of the tert-butyl spectrum (red curve) using a hyperfine coupling constant of  $a_{\text{iso}}(^1\text{H}) = 22.7$  G for the nine equivalent methyl hydrogens and a line width of 6.5 G. The experimental spectrum (presented in Fig. 5.7) is overlaid in black. b) Simulation (red curve) of the spectrum of thymyl radical using hyperfine coupling constants of  $a_{\text{iso}}(^1\text{H}) = 20.5$  G for the three hydrogens at the methyl group and of 37.5 G for the two methylene hydrogens and a line width of 8 G. The experimental spectrum (presented in Fig. 5.11) is overlaid in black.

Adding the two simulated spectra in a ratio of 1:1 (Fig. 5.15a) and superimposing the result on the “central part” spectrum of Fig. 5.10b with a ratio of 1:4, respectively, constitutes the



total spectrum in Fig. 5.15b<sup>ii</sup>, which very nicely resembles the spectrum generated by photolysis of **1** in acetonitrile. Small differences may be due to different line widths at different microwave powers.

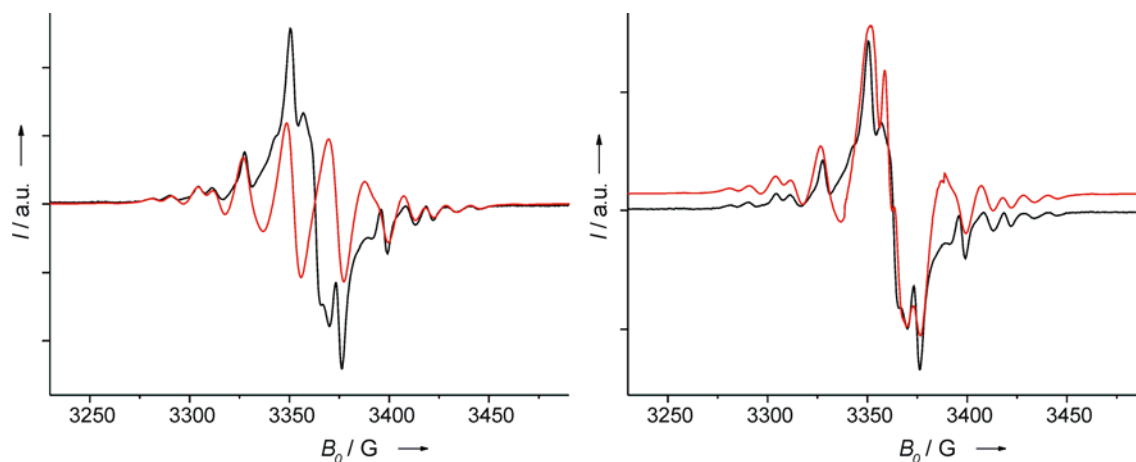


**Figure 5.15** a) Simulated sum spectrum (red curve) obtained from a 1:1 superposition of the simulated spectrum of **2** with the tert-butyl spectrum. The experimental spectrum from Fig. 5.5 is overlaid in black. b) Simulated sum spectrum (red curve) obtained from a 1:4 superposition of the simulated spectrum in a) with the "central part" spectrum of Fig. 5.10b. The experimental spectrum from Fig. 5.5 is overlaid in black.

Moreover, adding the experimentally obtained 8-line (Fig. 5.11) and 10-line (Fig. 5.7) spectra in a ratio 1:0.7 and superimposing the result on the central part spectrum in H<sub>2</sub>O (Fig. 5.10b) with a ratio 1:5 yielded the sum spectrum in Fig. 5.16<sup>iii</sup>, which is almost identical to the spectrum of **1** in acetonitrile.

<sup>ii</sup> The same result is obtained if one sums the normalized spectra of Fig. 5.14a, Fig. 5.14b and Fig. 5.10b with a ratio 1:2:60, respectively.

<sup>iii</sup> The same result is obtained if one sums the normalized spectra of Fig. 5.12, Fig. 5.7 and Fig. 5.13b with a ratio 1:1:20, respectively.

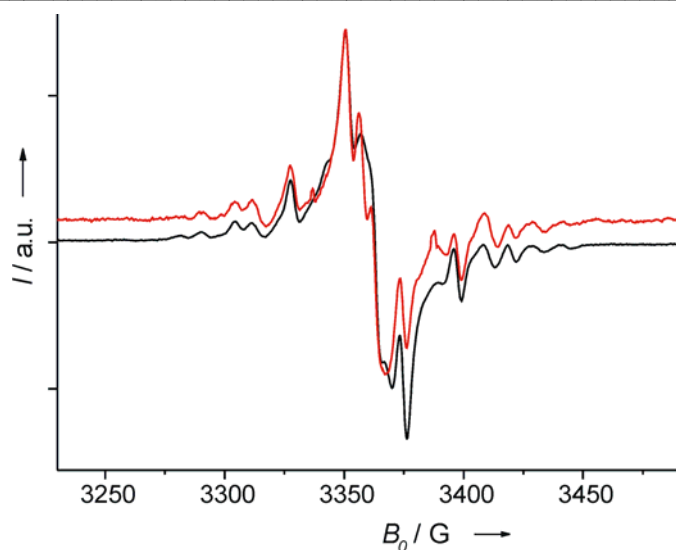


**Figure 5.16** Sum (red curve) of the three spectral components from Fig. 5.11, Fig. 5.7 and Fig. 5.10b in a ratio 1:0.7:5 respectively. The spectrum of **1** in acetonitrile is overlaid in black.

#### 5.2.4 Double strand DNA modified with the nucleotide derivative of **1**

Preliminary results on the double strand DNA modified with the nucleotide derivative of **1** (see Fig. 5.3 for the DNA sequence) are presented here. The spectrum in Fig. 5.17 was acquired at 77 K after irradiating for 10 min at the same temperature.

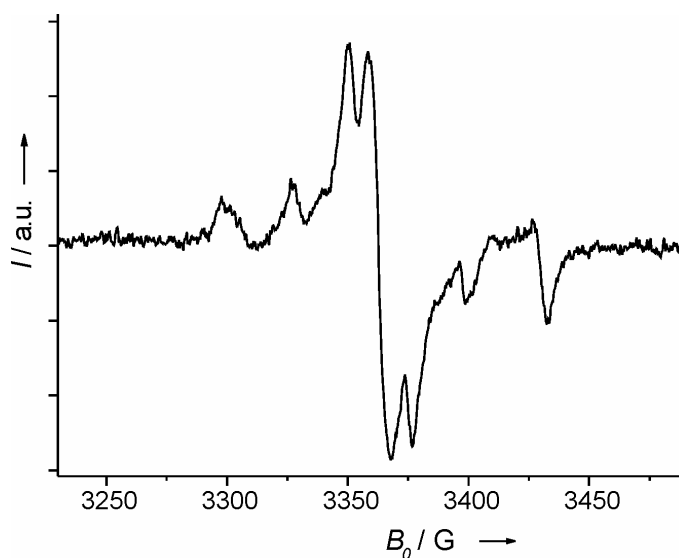


**Figure 5.17** EPR spectrum of modified DNA. The spectrum was recorded using a microwave power of 0.1 mW and modulation amplitude of 1.5 G. 140 scans were accumulated.

In this case no appearance of the eight-line spectrum, also characteristic for a thymyl radical in DNA,<sup>[34]</sup> could be detected. The spectrum shows a different pattern which is not known from the literature. Many attempts were made to simulate all or at least some lines of the spectrum. Simulations from electron loss centers (guanine cation  $G^{\bullet+}$ ) and electron gain centers (cytosine anion  $C^{\bullet-}$  and thymine anion  $T^{\bullet-}$ ) as well as from sugar radicals were done and were superimposed to the spectrum in Fig. 5.17 (see Appendix A, Fig. A.2). From this approach a clear assignment is not possible, although some paramagnetic species may be present, e.g. a guanine radical cation  $G^{\bullet+}$  (singlet line in Appendix, Fig. A.2A) or a cytosine radical anion  $C^{\bullet-}$  (doublet in Appendix, Fig. A.2B).

## 5.3 DISCUSSION AND CONCLUSIONS

### 5.3.1 Components and radical structures

For the first time it was possible to detect an EPR signal from the UV irradiated 4'-Pivaloyl Substituted-Thymidine (**1**). By means of different techniques it was possible to simplify the initial spectrum detected in acetonitrile, assigning the spectral components to specific radicals.<sup>[9]</sup>

It can be concluded from the experiments that three different radicals are generated upon irradiation of the 4'-pivaloylated thymidine **1** giving rise to a 10-line, a 8-line and a "central part" spectrum. The 10-line spectrum shown in Fig. 5.7 can unambiguously be assigned to the *tert*-butyl radical by comparison with spectra from literature.<sup>[42, 43]</sup> The sensitivity to water and the saturation at high microwave power are also characteristic for the *tert*-butyl radical.<sup>[26]</sup> Its formation is due to the Norrish I type cleavage and CO decarbonilation (Scheme 5.2).

The 8-line spectrum is the typical "octet-fingerprint" spectrum of the thymyl radical  $TH^{\bullet}$  (**2**, see scheme 5.2, and also Fig. 2.10).<sup>[34, 36, 47]</sup> This assignment is supported by the suppression of the octet-spectrum in the presence of an electron scavenger.

Both the *tert*-butyl and the thymyl radical spectra were simulated (Fig. 5.14) with the parameters given in Table 5.1 matching the parameters from the literature. Both the spectra reconstruction in Fig. 5.15b and Fig. 5.16, done with the *tert*-butyl (ten lines), the thymyl

(eight lines) and “central part” spectra, are similar to the experimental spectrum of **1** in acetonitrile and show that all spectral components were accounted for.

An assignment of the "central part" spectrum is difficult, but it is clear that this radical is not the precursor of the thymyl radical **2** and hence not the  $C4'$ • sugar radical (Fig. 5.18) because it does not interconvert to **2** by warming up from 4 K to 200 K in 10 K steps. The HPLC analysis (made by Dr. T. Carl in Prof. B. Giese's group, University of Basel, Switzerland) of the irradiated sample **1** showed the presence of the reactant and of a minor peak at the retention time characteristic for deoxyribose derivatives after cleavage of the pivaloyl group (see Appendix B, Fig. B.1). Nevertheless an analysis of this signal by mass spectroscopy was not possible due to the low conversion of the reactant.

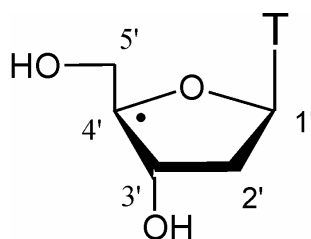


**Figure 5.18** Detailed chemical structure of the  $C4'$ • sugar radical ( $T$ =thymine base). The carbon positions suitable for H- abstraction and subsequent sugar radical formation are numbered.

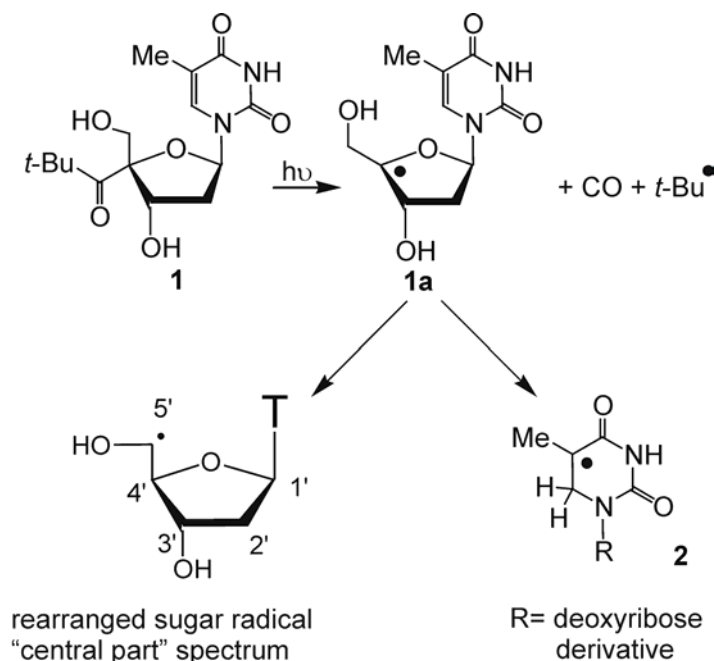
A tentative assignment of the “central part” can be done on the basis of the following considerations. Numerous sugar radicals have been observed by EPR and ENDOR spectroscopy in X-, $\gamma$ - or UV-irradiated nucleosides and nucleotides. However positive radical identification is always quite difficult in sugars for many reasons. First, the radical species are similar, consisting only of carbon, oxygen and hydrogen. Second it is quite likely that several sugar radicals are formed upon high-energy irradiation, giving composite EPR spectra. Finally the variety of conformations of the deoxyribose radicals should influence the  $\beta$  couplings and broaden or change the line components of the EPR spectra.<sup>[50]</sup> To date it seems that a distinction can be made between the EPR spectra of some radical species, in particular for the neutral radicals formed in H-abstraction processes. The  $C1'$ • has previously been observed in  $\gamma$ -irradiated 5'-dAMP (deoxyadenosine monophosphate) frozen solution with two  $\beta$  couplings of  $a_{iso}(^1H) \cong 15$  G, and  $a_{iso}(^1H) \cong 32$  G, resulting in an EPR quartet spectrum.<sup>[51]</sup> Similar assignment with

similar hf couplings has been reported by several authors after experiments on analogous models systems.<sup>[50, 52-55]</sup> The  $C3'^{\bullet}$  spectrum, at 77 K, was first reported in photoionized 5'-dCMP (deoxycytidine monophosphate) as a sextet arising from 3  $\beta$ -protons with  $a_{iso}(2\times(^1H)) \cong 32$  G and  $a_{iso}(^1H) \cong 21$  G.<sup>[54]</sup>  $C3'^{\bullet}$  with the same couplings has also been observed by Weiland et al.<sup>[55]</sup> and recently by Shukla et al.<sup>[53]</sup> Based on DFT model calculations, Becker et al.<sup>[56]</sup> reported that a radical formed by  $-OH$  abstraction at the  $C3'$  carbon of the deoxyribose should have a sextet 134 G broad. The  $C4'^{\bullet}$  spectrum has not been definitively assigned yet, but also in these cases it is supposed that big couplings are involved.<sup>[34, 50]</sup> Finally there is some doubt on the spectra assignment of the  $C2'^{\bullet}$  and  $C5'^{\bullet}$  radicals.<sup>[50]</sup>

At this point, considering the literature findings reported above, the  $C1'^{\bullet}$  and the  $C3'^{\bullet}$  radicals can be immediately discarded as candidates for the assignment of the “central part” in Fig. 5.13, since their spectra don't account for the 16 G broad pattern of the “central part”. The  $C4'^{\bullet}$  has already been discarded as discussed above. Thus only the  $C2'^{\bullet}$  and the  $C5'^{\bullet}$  are suitable candidates. In a detailed study on sugar radicals,<sup>[50]</sup> Close reported that  $C2'^{\bullet}$  should have at least one big hf coupling ( $a_{iso} > 25$  G), while  $C5'^{\bullet}$  should have two small couplings, below 10 G, and pronounced  $g$  anisotropy. Experimental findings reported there also confirmed these values for the hf coupling constants of such sugar radicals. The range of parameter values for  $C5'^{\bullet}$  as reported by Close would fit with the spectrum in Fig. 5.13. Moreover, computational studies on a single nucleotide<sup>[57]</sup> indicate that the  $C5'$ , together with the  $C4'$ , are the most probable sites for H-atom abstraction by radical species. The fact that the  $C5'$  is nearby the  $C4'$ , which is first formed in the reaction mechanism (see also Scheme 5.2), makes  $C5'$  a good candidate for the H-abstraction. As a consequence of these mechanistic and spectroscopic arguments, the  $C5'^{\bullet}$  radical can be favored for the assignment of the “central part” spectrum. Nevertheless further analysis is necessary (see the chapter “Summary and Outlook”).

### 5.3.2 Mechanism of radical formation

On the basis of the results obtained a reaction scheme is proposed.<sup>[9]</sup> We assume that the 4'-nucleoside radical **1a**, formed by Norrish cleavage of **1**, has two pathways, one leading to a rearranged sugar radical (probably C5'•, by H-atom shift) giving the "central part" spectrum and the other one yielding the thymyl radical **2** (Scheme 5.2).



**Scheme 5.2** Mechanism proposed for the radical formation upon irradiation of **1**. Formation of the 4'-nucleoside radical **1a** by photolysis of the 4'-pivaloylated nucleoside **1** and the subsequent formation of the thymyl radical **2** and a rearranged sugar radical (C5'• is the proposed one).

The reaction **1a**→**2** is a proton coupled electron or a hydrogen atom transfer from the 4'-deoxyribosyl radical to the thymine base, similar to the mechanism described by Hüttermann for the X-ray irradiation induced formation of the 5-yl base radicals from 5-chloro and 5-bromodeoxyuridine.<sup>[58]</sup>

Intermolecular reaction pathways leading to the formation of the thymyl radical **2** can be excluded, since a reaction between thymine and the *tert*-butyl or solvent radicals do not yield the octet spectrum and no free electrons are generated with this low energy setup. Furthermore, a direct formation of **2** due to UV damage of the thymine base can also be excluded, because no signal was observed by using thymine or thymidine instead of **1**.

Finally, the weak signal intensity, corresponding to a radical concentration below 1  $\mu\text{molar}$ , as well as the observed linear dependence of the signal intensity on concentration can rule out the possibility of an intermolecular ET between two molecules of **1**.

The assumption that the proton originates from a C, H-bond of the sugar is based on the fact that, exchanging  $\text{H}_2\text{O}$  by  $\text{D}_2\text{O}$ , does not change the octet spectrum, excluding the solvent as a source for the proton. Moreover a doublet spectrum<sup>[36]</sup> of the thymine radical anion was not observed, which may imply that the proton transfer is coupled with the electron transfer, or the reaction occurs directly by hydrogen atom transfer. Also, the doublet of the thymine radical anion cannot be a constituent of the "central part" spectrum, because addition of the electron quencher did not lead to a decrease in intensity for any of the two lines within the "central part" spectrum.

All these experiments and the short distance of about 4 Å between the tertiary  $\beta\text{-C,H}$ -bond of the carbohydrate and the thymine make a proton coupled electron transfer (or hydrogen atom transfer) between the 4'-deoxyribosyl and the thymine plausible.

It should be mentioned that irradiation of the nucleotide derivative of **1** incorporated into DNA oxidizes guanine and does not reduce thymine bases, as mentioned above (see Scheme 5.1) and shown earlier.<sup>[3, 5-8]</sup> This different reaction behavior is based on the presence of different 3'-groups that is hydroxy for the nucleoside **1** and phosphate for the nucleotide of **1** incorporated into DNA. Phosphate is an excellent leaving group, whose immediate heterolytic cleavage from the 3'-site after the formation of the 4'-carbohydrate radical results in the formation of a sugar radical cation,<sup>[11-13, 15]</sup> which is capable to oxidize guanines but not to reduce thymines (see also later in this section). The nucleoside **1** with the poor hydroxyl leaving group in the 3'-position does not form the cation radical but pursues the reaction pathway **1a**→**2** to the thymyl radical.<sup>[9]</sup> Schulte-Frohlinde et al. showed that the 3'-OH group can be protonated and thereby transformed to a good  $\text{H}_2\text{O}$  leaving group at acidic pH values,<sup>[59-61]</sup> however, the experiments reported here were performed at pH 7 or in acetonitrile, which makes a 3'-OH protonation unlikely.

### **5.3.3 Discussion about the modified double strand DNA**

The modified double strand DNA of Fig. 5.3 was measured under the same conditions as **1**. The EPR pattern of Fig. 5.17 is not known in literature and in particular does not show the 8-line spectrum of the thymyl radical. It is worth noting that similar modified DNA molecules were used by Giese and co-workers to generate site selectively a guanine radical cation  $G^{\bullet+}$  and to study HT processes in DNA (see introduction to at the beginning of this chapter).<sup>[4, 7]</sup> In one of these studies<sup>[7]</sup> it is also reported that for DNA sequences where the first G is more than three base pairs away (as in the present case), charge transfer processes are almost absent. In that case reaction pathways other than CT seem to occur, and other reaction intermediates (sugar radicals and phosphate anions) are supposed to be present. Herein, simulations to assign all or at least some lines of Fig. 5.17 were done, but without success. From the simulations it is not possible to confirm if a guanine radical cation  $G^{\bullet+}$  spectrum (single line) is present, although some simple pattern may be there, such as those of  $C^{\bullet-}$  (doublet) or  $G^{\bullet+}$  radical itself. In conclusion, taking into account both the simulations done and the findings in the literature for similar DNA molecules, it can be only assumed that different radicals may be formed upon irradiation, giving rise to a multicomponent spectrum.



---

## 5.4 REFERENCES

- [1] A. Marx, P. Erdmann, M. Senn, S. Korner, T. Jungo, M. Petretta, P. Imwinkelried, A. Dussy, K. J. Kulicke, L. Macko, M. Zehnder, B. Giese, *Helvetica Chimica Acta* **1996**, *79*, 1980.
- [2] S. Korner, A. Bryant-Friedrich, B. Giese, *Journal of Organic Chemistry* **1999**, *64*, 1559.
- [3] B. Giese, *Accounts of Chemical Research* **2000**, *33*, 631.
- [4] E. Meggers, M. E. Michel-Beyerle, B. Giese, *Journal of the American Chemical Society* **1998**, *120*, 12950.
- [5] B. Giese, J. Amaudrut, A. K. Kohler, M. Spormann, S. Wessely, *Nature* **2001**, *412*, 318.
- [6] T. Kendrick, B. Giese, *Chemical Communications* **2002**, 2016.
- [7] E. Meggers, A. Dussy, T. Schäfer, B. Giese, *Chemistry-a European Journal* **2000**, *6*, 485.
- [8] A. Dussy, E. Meggers, B. Giese, *Journal of the American Chemical Society* **1998**, *120*, 7399.
- [9] O. Schiemann, E. Feresin, T. Carl, B. Giese, *Chemphyschem* **2004**, *5*, 270.
- [10] M. Lange, B. Weiland, J. Hüttermann, *International Journal of Radiation Biology* **1995**, *68*, 475.
- [11] B. Giese, A. Dussy, C. Elie, P. Erdmann, U. Schwitter, *Angewandte Chemie-International Edition in English* **1994**, *33*, 1861.
- [12] B. Giese, X. Beyrichgraf, P. Erdmann, L. Giraud, P. Imwinkelried, S. N. Muller, U. Schwitter, *Journal of the American Chemical Society* **1995**, *117*, 6146.
- [13] A. Gugger, R. Batra, P. Rzadek, G. Rist, B. Giese, *Journal of the American Chemical Society* **1997**, *119*, 8740.
- [14] M. Spormann, B. Giese, *Synthesis-Stuttgart* **2001**, 2156.
- [15] S. Peukert, R. Batra, B. Giese, *Tetrahedron Letters* **1997**, *38*, 3507.
- [16] B. Giese, P. Imwinkelried, M. Petretta, *Synlett* **1994**, 1003.
- [17] R. Glatthar, M. Spichty, A. Gugger, R. Batra, W. Damm, M. Mohr, H. Zipse, B. Giese, *Tetrahedron* **2000**, *56*, 4117.
- [18] S. Peukert, B. Giese, *Journal of Organic Chemistry* **1998**, *63*, 9045.

- [19] J. Dupuis, B. Giese, D. Rügge, H. Fischer, H.-G. Korth, R. Sustmann, *Angewandte Chemie International Edition in English* **1984**, *23*, 896.
- [20] C. H. Bamford, R. G. W. Norrish, *J. Chem. Soc.* **1935**, 1504.
- [21] R. G. W. Norrish, C. H. Bamford, *Nature* **1936**, *138*, 1016.
- [22] R. G. W. Norrish, C. H. Bamford, *Nature* **1937**, *140*, 195.
- [23] P. J. Wagner, G. S. Hammond, *Advances in Photochemistry* **1968**, *5*, 87.
- [24] N. J. Turro, *Modern Molecular Photochemistry*, University Science Books, Sausalito, **1991**.
- [25] J. C. Dalton, N. J. Turro, *Annual Review of Physical Chemistry* **1970**, *21*, 499.
- [26] H. Schuh, E. J. Hamilton, H. Paul, H. Fischer, *Helvetica Chimica Acta* **1974**, *57*, 2011.
- [27] P. S. Pershan, R. G. Shulman, B. J. Wyluda, J. Eisinger, *Science* **1965**, *148*, 378.
- [28] B. Weiland, J. Hüttermann, J. vanTol, *Acta Chemica Scandinavica* **1997**, *51*, 585.
- [29] S. Gregoli, M. Olast, A. Bertinchamps, *Radiation Research* **1976**, *65*, 202.
- [30] J. Hüttermann, W. Gatzweiler, M. Lange, B. and Weiland, *Free radical formation in DNA: some new aspects of an old problem.*, Battelle Press, Columbus, Ohio, USA, **1995**.
- [31] J. Hüttermann, M. Rohrig, W. Kohnlein, *International Journal of Radiation Biology* **1992**, *61*, 299.
- [32] M. Lange, B. Weiland, J. Hüttermann, *International Journal of Radiation Biology* **1995**, *68*, 475.
- [33] M. D. Sevilla, R. Failor, C. Clark, R. A. Holroyd, M. Pettei, *Journal of Physical Chemistry* **1976**, *80*, 353.
- [34] B. Weiland, J. Hüttermann, *International Journal of Radiation Biology* **1998**, *74*, 341.
- [35] A. Gräslund, Ehrenber.A, Rupprech.A, G. Strom, *Biochimica Et Biophysica Acta* **1971**, *254*, 172.
- [36] P. M. Cullis, J. D. McClymont, M. E. Malone, A. N. Mather, I. D. Podmore, M. C. Sweeney, M. C. R. Symons, *Journal of the Chemical Society-Perkin Transactions 2* **1992**, 1695.
- [37] R. A. Holroyd, J. W. Glass, *International Journal of Radiation Biology and Related Studies in Physics Chemistry and Medicine* **1968**, *14*, 445.
- [38] D. Becker, M. D. Sevilla, *Advances in Radiation Biology, Vol 17* **1993**, *17*, 121.

- 
- [39] S. Steenken, *Chemical Reviews* **1989**, *89*, 503.
- [40] K. Hildenbrand, D. and Schulte-Frohlinde, *Free Radical Research Communications* **1990**, *11*, 195.
- [41] P. M. Cullis, M. E. Malone, I. D. Podmore, M. C. R. Symons, *Journal of Physical Chemistry* **1995**, *99*, 9293.
- [42] P. B. Ayscough, C. Thomson, *Transactions of the Faraday Society* **1962**, *58*, 49.
- [43] Y. D. Tsvetkov, J. R. Rowlands, D. H. Whiffen, *Journal of the Chemical Society* **1964**, 810.
- [44] K. Hildenbrand, G. Behrens, D. Schulte-Frohlinde, J. N. Herak, *Journal of the Chemical Society Perkin Transaction* **1989**, *2*, 283.
- [45] H. Paul, H. Fischer, *Helvetica Chimica Acta* **1973**, *56*, 1575.
- [46] R. W. Fessenden, R. H. Schuler, *Journal of Chemical Physics* **1963**, *39*, 2147.
- [47] B. Pruden, W. Snipes, W. Gordy, *Proceedings of the National Academy of Sciences of the United States of America* **1965**, *53*, 917.
- [48] M. D. Sevilla, Vanpaeme.C, G. Zorman, *Journal of Physical Chemistry* **1972**, *76*, 3577.
- [49] E. O. Hole, E. Sagstuen, W. H. Nelson, D. M. Close, *Journal of Physical Chemistry* **1991**, *95*, 1494.
- [50] D. M. Close, *Radiation Research* **1997**, *147*, 663.
- [51] W. Wang, M. D. Sevilla, *International Journal of Radiation Biology* **1994**, *66*, 683.
- [52] W. Wang, Y. Razskazovskii, M. D. Sevilla, *International Journal of Radiation Biology* **1997**, *71*, 387.
- [53] L. I. Shukla, R. Pazdro, J. Huang, C. De Vreugd, D. Becker, M. D. Sevilla, *Radiation Research* **2004**, *161*, 582.
- [54] M. E. Malone, P. M. Cullis, M. C. R. Symons, A. W. Parker, *Journal of Physical Chemistry* **1995**, *99*, 9299.
- [55] B. Weiland, J. Hüttermann, M. E. Malone, P. M. Cullis, *International Journal of Radiation Biology* **1996**, *70*, 327.
- [56] D. Becker, A. Bryant-Friedrich, C. Trzasko, M. D. Sevilla, *Radiation Research* **2003**, *160*, 174.
- [57] P. Toure, F. Villena, G. G. Melikyan, *Organic Letters* **2002**, *4*, 3989.
- [58] J. Hüttermann, W. A. Bernhard, E. Haindl, G. Schmidt, *Journal of Physical Chemistry* **1977**, *81*, 228.

- [59] C. Von Sonntag, Hagen.U., A. Schön-Bopp, D. Schulte-Frohlinde, *Adv. Radical Biol.* **1981**, 9, 109.
- [60] C. Von Sonntag, Hagen.U., A. Schön-Bopp, D. Schulte-Frohlinde, *The Chemical Basis of Radiation Biology*, Taylor & Francis, London, **1987**.
- [61] G. Behrens, G. Klotzenburg, D. Schulte-Frohlinde, *Zeitschrift Fur Naturforschung C-a Journal of Biosciences* **1982**, 37, 1205.

## 6. A NEW MODIFIED THYMIDINE AS PRECURSOR FOR A THYMINE-BASED RADICAL AND AS ELECTRON INJECTOR INTO DNA

In this chapter the EPR study of *in situ* radical formation upon irradiation of the photocleavable thymidine derivative **3** (Fig. 6.1) is presented.

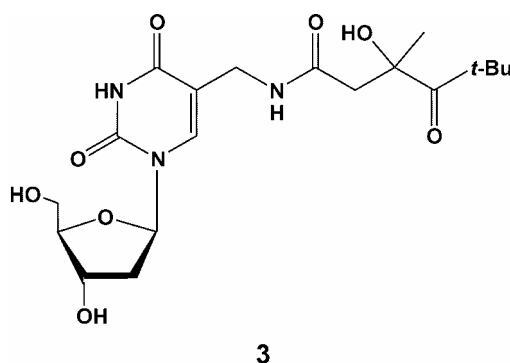


**Figure 6.1.** Structure of the modified thymine **3**.

As described in the introduction of the previous chapter, after UV-vis irradiation of 4'-pivaloyl modified DNA strands a sugar radical  $C3'^{•+}$  is formed (see Scheme 5.1 for the details of the proposed mechanism), leading to the oxidation of the adjacent guanine to  $G^{•+}$ . To avoid the formation of  $C3'^{•+}$ , Giese and co-workers synthesized **3**, which has the photocleavable pivaloyl group at the end of a long side chain attached at the C5 position of the base. This compound should allow to initiate Excess Electron Transfer in DNA, since it is believed that after the homolytic C-C bond cleavage (Norrish type I reaction) at the pivaloyl site, the *in situ* radical formed is injected into the thymine base, due to the lowest reduction potential of that base<sup>[1]</sup> (see also section 1.2.1).

Here for the first time EPR spectroscopy is used to analyze the radicals formed upon irradiation of **3** and to study the mechanism involved in their generation. In particular the aim is to check whether UV-vis irradiation of **3** leads to an electron transfer to the thymine base, which would be necessary to use **3** as electron injector in DNA.<sup>[2]</sup>

## **6.1 MATERIALS AND METHODS**

### **6.1.1 Sample preparation**

The thymidine derivative **3** (Fig 6.1) was prepared by Giese and co-workers as described previously. <sup>[2]</sup>

The solutions of **3** were prepared in the same way as for **1** (see section 5.1), with final concentrations of 7 mM in H<sub>2</sub>O, D<sub>2</sub>O or CH<sub>3</sub>CN.

The thiol “L-Glutathione reduced” (m.f. C<sub>10</sub>H<sub>17</sub>N<sub>3</sub>O<sub>6</sub>S ) was purchased from Fluka and used without further treatment to prepare water solutions with 5 equivalents of thiol per equivalent of nucleoside.

### **6.1.2 Generation of radicals by UV Irradiation**

Samples of **3** were UV-irradiated following the same procedure described in section 5.1.2 for the 4'-pivaloylated nucleoside **1**: they were photolyzed for 10 min at 77 K by using a high-pressure mercury lamp of 500 W in conjunction with a 320 nm cut off filter.

## **6.2 RESULTS**

### **6.2.1 Sample dissolved in H<sub>2</sub>O and D<sub>2</sub>O**

The first EPR measurements were done on **3** dissolved in H<sub>2</sub>O. Water was chosen because a simple spectrum was expected, as already verified in the case of the 4'-pivaloyl substituted thymidine **1** (see chapter 5), where water sensitive radicals like the *tert*-butyl could be suppressed. At 80 K the spectrum depicted in Fig. 6.2 was detected.

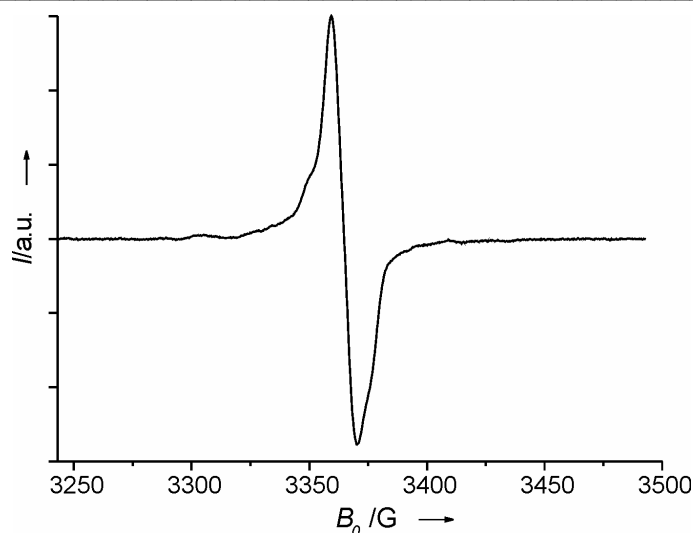


**Figure 6.2.** Continuous wave X-band EPR spectrum of **3** in  $H_2O$ , irradiated and measured at 77 K. 256 scans were accumulated. All the EPR spectra presented in this chapter were acquired at a microwave power of 0.1 mW, modulation amplitude of 2.5 G, a receiver gain of  $1 \times 10^5$ , a conversion time and a time constant of 40.96 ms.

The single asymmetric central line of Fig. 6.2 is characterized by a  $g$ -factor at zero crossing of  $2.0023 \pm 0.0005$  and a peak-to-peak linewidth of 11.0 G, which is probably due to  $g$  anisotropy or to unresolved hyperfine lines. The absence of an evident hyperfine pattern does not allow a clear assignment. Nevertheless, the absence of both a center doublet with a splitting of 15 G typical for a  $T^{\bullet-}$ <sup>[3]</sup> and the “octet fingerprint” of  $TH^{\bullet}$ <sup>[4, 5]</sup>, suggested to exclude the presence of radicals centered on the thymine base. The outer lines of Fig. 6.2 are too small and too far from the center field for a thymine-based radical.

Several attempts have been made to verify if the spectrum of Fig. 6.2 (this pattern from now it will be simply called “central singlet”) converts to another pattern or gives a clear indication of superposition of different patterns. Changing the solvent to  $D_2O$  did not change the EPR pattern of the spectrum in Fig. 6.2. Applying EPR power saturation measurements the intensity of the “central singlet” varied as depicted in Fig. 6.3, leaving the pattern unaltered.

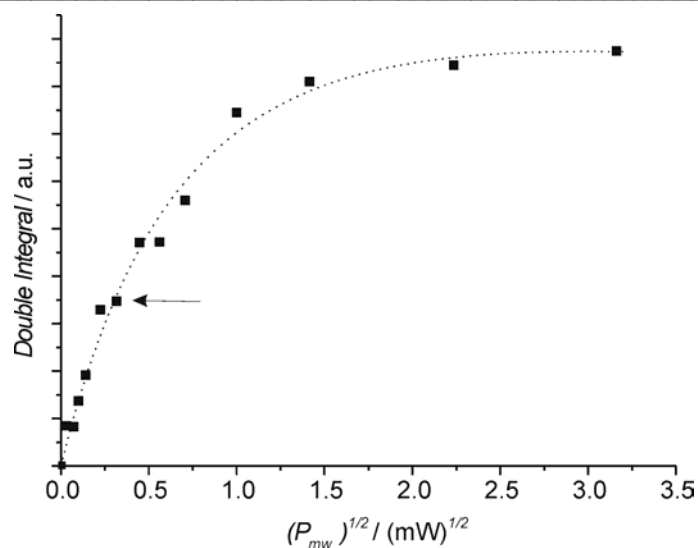


**Figure 6.3** Plot of double integrals from EPR spectra of UV-irradiated **3** in  $\text{H}_2\text{O}$  at 77 K as function of  $(\text{microwave power})^{1/2}$ . The arrow indicates the data point corresponding to a mw power of 0.1 mW, which is the power used to acquire the spectra presented in this chapter. The fitting function depicted has been performed with the function described in eq. (2.31), giving  $b=1$  and  $P_{1/2}= 0.4 \text{ mW}$ .

Different irradiation periods on sample **3** did not produce any changes on the EPR features with respect to the spectrum in Fig. 6.2. The maximum of intensity was reached after 20 min of irradiation (see Fig. 6.4).



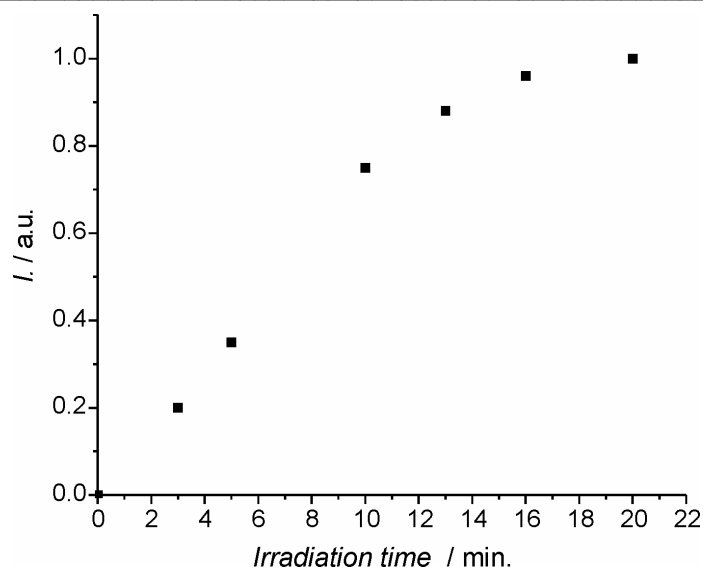


**Figure 6.4** Plot of EPR double integrals of UV-irradiated **3** in  $H_2O$  at 77 K as function of irradiation time. The intensities are normalized to the spectrum obtained after 20 min of irradiation.

Temperature annealing up to 180 K did not change the “central singlet”. EPR spectra recorded at 77 K after such an annealing procedure showed that the spectral intensity diminished with respect to the one in Fig. 6.2, indicating that the radical/s had decayed (see Appendix A, Fig. A.3).

HPLC analysis (all the HPLC analysis were done in the group of Prof. Giese, University of Basel, Switzerland) was performed on the sample that gave the spectrum of Fig. 6.2, and showed that ketone **7** (see Scheme 6.1) was formed as a product (see Appendix B, Fig. B.2). Similarly, when a sample of **3** dissolved in  $H_2O$  was irradiated at RT, ketone **7** was formed as the main product (90%).

Glutathione compounds were often used by Giese and co-workers as H-donors in order to influence the efficiency of reactions in which the intermediates can be H-trapped.<sup>[2, 6, 7]</sup> Therefore when mixtures of **3** and glutathione (1:5) in  $H_2O/CH_3OH$  (4:1) were irradiated at RT, the products (see Scheme 6.1) alcohol **6** and ketone **7** were detected by HPLC (co-injection and MS), the former up to 30 % in yield. In systems in which the thymine **3** was replaced with adenine or benzene, only the corresponding alcohols were formed. Then EPR measurements on irradiated samples of **3** plus the glutathione (1:5) compound were done in our laboratories to verify if the radical/s that give Fig. 6.2 are affected by the presence of an H-donor: no changes from the spectrum in Fig. 6.2 were visible.

## 6.2.2 Sample dissolved in CH<sub>3</sub>CN

EPR measurements were also performed at 77 K on **3** dissolved in acetonitrile after irradiation at 77 K with UV light above 320 nm. Interestingly, the spectrum detected is more complicated than the one in H<sub>2</sub>O and is depicted in Fig. 6.5.

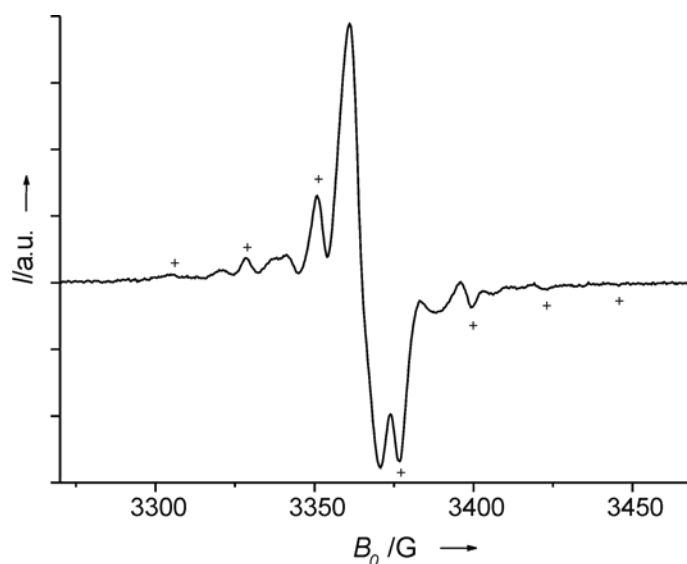


**Figure 6.5** Continuous wave X-band EPR spectrum of **3** in CH<sub>3</sub>CN irradiated and measured at 77 K. 128 scans were accumulated. The lines marked + belong to the *tert*-butyl radical (typically represented by ten lines if the intensity is strong enough, see also section 2.5.2).

It was possible to estimate a *g*-factor for the central line of  $2.0027 \pm 0.0005$ , similar to the value given for the “central singlet” presented in Fig. 6.2.

The following control measurements have been carried out: i) no signal was obtained with thymine or thymidine photolyzed under the same conditions; ii) negligible signal was detected from unmodified thymidine in the presence of di-*tert*-butylketone (see Appendix A, Fig. A.4). These measurements reveal that the spectrum above arises from radicals that are not the result of direct UV damage on the sample or on the solvent, but are the consequence of the homolytic C,C-bond cleavage at the site of the pivaloyl substituent, like in the case of the 4'-pivaloyl substituted thymidine **1** (see also sections 5.1.3 and 5.2.1).

Based on findings on **1** (see chapter 5) it was supposed that the spectrum of Fig. 6.5 could be a superposition of several components: a first component could be immediately

attributed to the *tert*-butyl radical (lines marked +); a second one was supposed to give the central line of the spectrum; finally a third component was thought to be present due to the side lines detected near the *tert*-butyl radical lines.

A confirmation of a multicomponent spectrum came from the addition of a drop of water to the solution of **3** in acetonitrile: in this case the outer lines of the *tert*-butyl, but probably also the nearby small lines are lowered in intensity (Fig. 6.6).

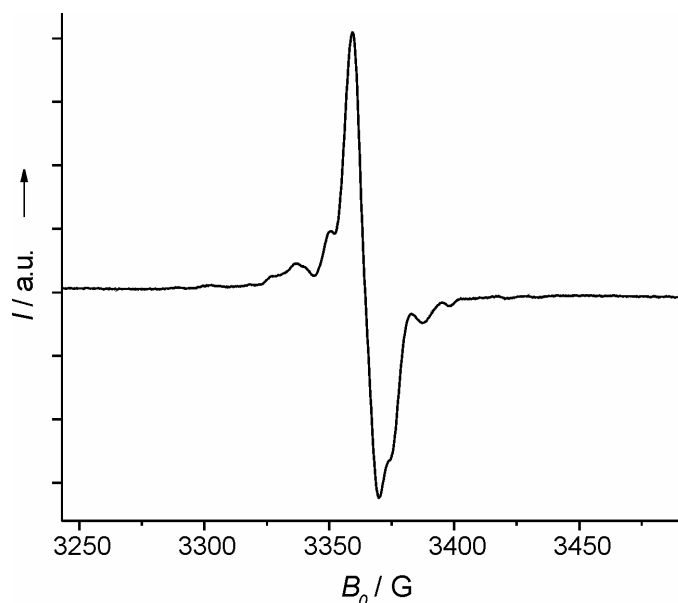


**Figure 6.6** Continuous wave X-band EPR spectrum of **3** in  $\text{CH}_3\text{CN}$  (plus a drop of water) irradiated and measured at 77 K. 128 scans were accumulated.

Since more than one component is influenced by the water, subtraction of Fig. 6.6 from Fig. 6.5 did not give a clear pattern (see Appendix A, Fig. A.5).

Surprisingly, storing for one week at 77 K the sample that gave the spectrum in Fig. 6.5, leads to a drastic change in its spectral features, as it can be seen from the spectrum in Fig. 6.7. This spectrum has a double integrated area that is  $\approx 15\%$  of the area of spectrum in Fig. 6.5 and is clearly simplified: the *tert*-butyl radical and the central component had decayed and only a symmetric pattern remained. The central line is characterized by a  $g$ -factor of the center line at zero crossing of  $2.0035 \pm 0.0005$  which is similar to the one attributed to the thymyl radical<sup>[8]</sup> (see also Table 5.1 in chapter 5).

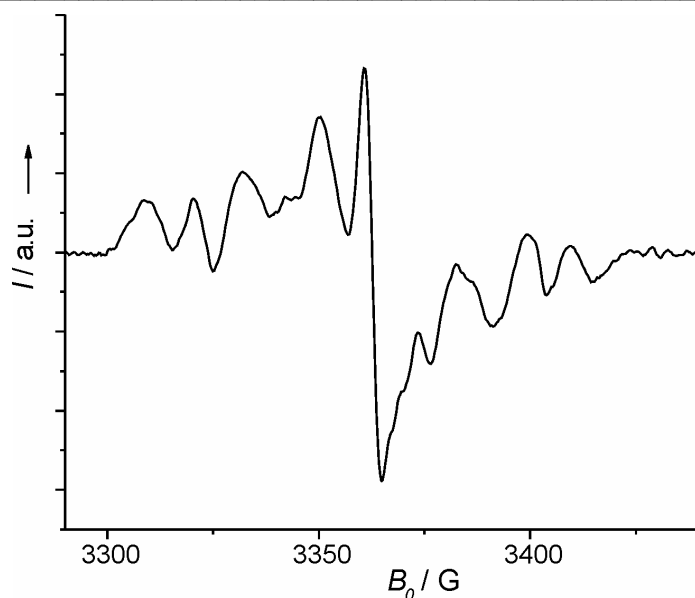


**Figure 6.7** Continuous wave X-band EPR spectrum at 77 K of the same sample the spectrum of Fig. 6.5, but measured after storage for one week at 77K. 256 scans were accumulated.

### 6.2.3 Simulations and computer reconstruction of experimental spectra

Assuming that the spectrum in Fig. 6.7 is constituted of only one paramagnetic species, a simulation was performed with hyperfine coupling constants of 39.2 G and 10.5 G attributed to two groups of two equivalent protons (details are given in Table 6.1). The simulation is superimposed onto the experimental spectrum in Fig. 6.8. The  $g$ -factor and the hf coupling constants of the remaining radical after storage at 77 K are similar to those observed for the unsubstituted thymine radical (the thymil radical) in frozen solution<sup>[8]</sup> (see also Table 5.1 in chapter 5) and are consistent with the assignment to the radical **5a** of Scheme 6.1.

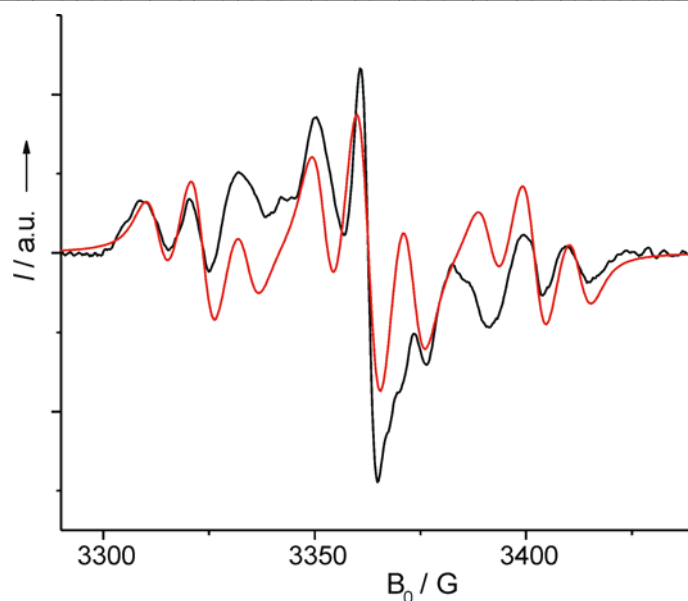


**Figure 6.8** Simulation (red curve) of the spectrum of the thymine-based radical **3** using hyperfine coupling constants  $a_{\text{iso}}(^1\text{H}) = 10.5 \text{ G}$  for the two hydrogen atoms at the  $\text{CH}_2$  group in position C(5) and  $a_{\text{iso}}(^1\text{H}) = 39.2 \text{ G}$  for the two methylene hydrogens at C(6). The line width is chosen to be 6 G. The experimental spectrum is overlaid in black.

The fact that the  $g$ -factor and the shape of the central line in Fig. 6.2 and Fig. 6.5 are similar led to the assumption that the “central singlet” is one of the components of the spectrum in Fig. 6.5, the other two being the *tert*-butyl radical and the thymine-based radical of Fig. 6.7. The spectra of Fig. 6.2 and of Fig. 6.7 were subtracted from the one in Fig. 6.5 yielding the pattern in Fig. 6.9, which clearly resembles the ten lines of the *tert*-butyl radical, although the spectrum still presents a central line and it is less “clean” than the one in Fig. 5.7, due to the double subtraction. The simulation of such a spectrum, done with the values given in Table 6.1, is visible in Fig. 6.9.

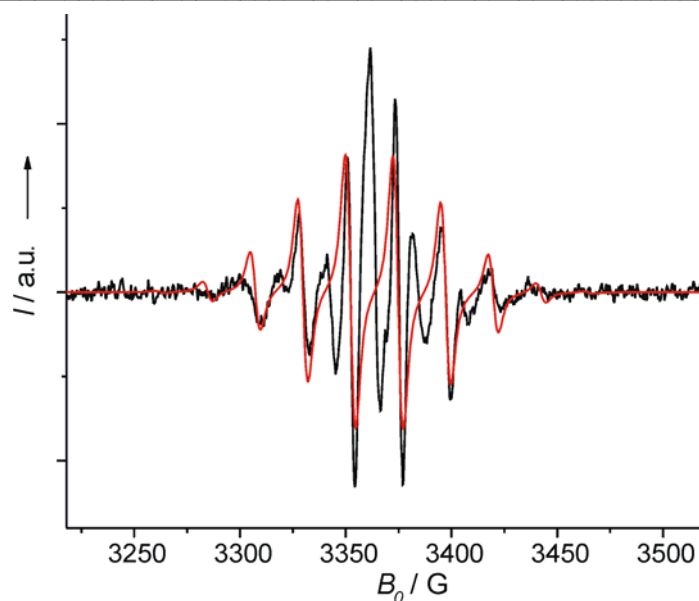


**Figure 6.9** Simulation of the *tert*-butyl spectrum (red curve) using a hyperfine coupling constant of  $a_{\text{iso}}(^1\text{H}) = 22.7 \text{ G}$  for the nine equivalent methyl hydrogens and a line width of 4.5 G. The experimental spectrum is overlaid in black.

**Table 6.1** Simulation data for the spectra assigned.

Radical	Position	$a_{\text{iso}} \text{ [G]}$		$g\text{-factor}$	
		Literature	This work	Literature	This work
<b><i>tert</i>-butyl</b>	9H (3 Me)	22.74 <sup>[9, 10]</sup>	$22.7 \pm 0.5$	2.0026 <sup>[9]</sup>	$2.0030^{\text{b}} \pm 0.0008$
	$Lw^{\text{a}}[\text{G}]$		$4.5 \pm 2.0$		
<b>Thymine based<sup>c</sup></b>	2H (C5)	20.5 <sup>[11]</sup> , 20.2 <sup>[12]</sup>	$10.5 \pm 1.0$	2.0035 <sup>[13]</sup>	$2.0035 \pm 0.0005$
	2H (C6)	40.5 <sup>[11]</sup> , 37.6 <sup>[12]</sup>	$39.2 \pm 2.0$		
	$Lw^{\text{a}}[\text{G}]$		$6.0 \pm 1.0$		

<sup>a</sup> The line components were assumed to be Gaussian and the peak-to-peak linewidth is presented. <sup>b</sup>The  $B_0$  necessary for the calculation of the  $g$ -factor (eq. 2.36) was calculated as average value from the zero crossing  $B_i$  values of the 3<sup>rd</sup> and 8<sup>th</sup> lines of the *tert*-butyl spectrum (Fig. 6.9). <sup>c</sup> Literature data for the thymyl radical (see chapter 5, Table 5.1).

On the other hand, adding both the normalized experimental spectra of Fig. 6.2 and of Fig. 6.7 to the normalized *tert*-butyl simulated spectrum of Fig. 6.9 with a ratio of 1:0.22:0.1 respectively, gave the total spectrum of Fig. 6.10, which is superimposed to the one of Fig. 6.5 and looks very similar to it.

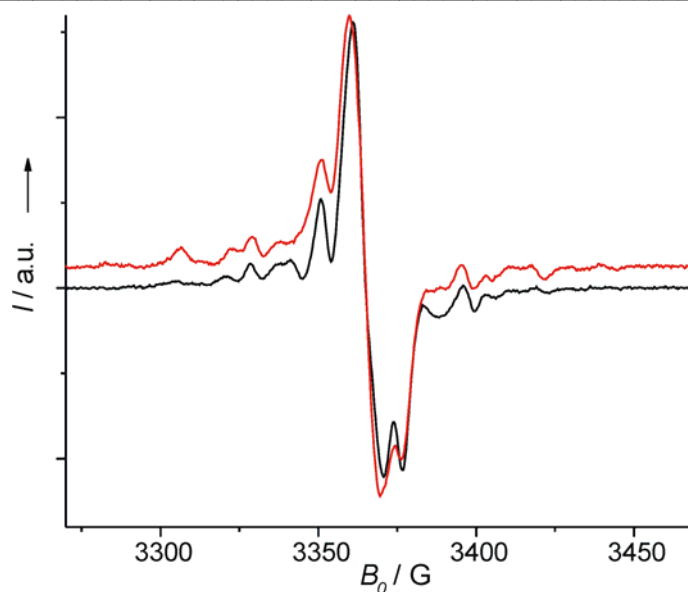


**Figure 6.10** Sum (red curve) of the three normalized spectral components from Fig. 6.2, Fig. 6.7 and Fig. 6.9 (simulated spectrum) in a ratio 1:0.22:0.1 respectively, overlaid with the spectrum of **3** in acetonitrile (black curve).

### 6.3 DISCUSSION AND CONCLUSIONS

For the first time it was possible to detect an EPR signal from thymidine derivative **3** after UV irradiation. Similarly to the case of the 4'-Pivaloyl Substituted-Thymidine **1** (see chapter 5), sample **3** showed a multicomponent spectrum in acetonitrile. On the contrary only a broad “central singlet” could be detected in water.

It can be concluded from the experiments in acetonitrile that at least three different radicals are generated upon irradiation of the thymidine derivative **3**, giving rise to a 10-line, a “central singlet” and a 9-line spectra. The 10-lines in Fig. 6.5 (marked lines +) with peak-to-peak splittings of 22.7 G can be unambiguously assigned to the *tert*-butyl radical: the pattern could be isolated and simulated with parameters matching the ones from the literature (see Table 6.1). The sensitivity to water is also characteristic for the *tert*-butyl radical.<sup>[14]</sup> Its formation can be explained as the result of the Norrish I type cleavage of **3** at the pivaloyl group: a similar behavior has been detected for the 4'-Pivaloyl Substituted-Thymidine **1** (see section 5.3) and analogous systems (see section 5.1.3).

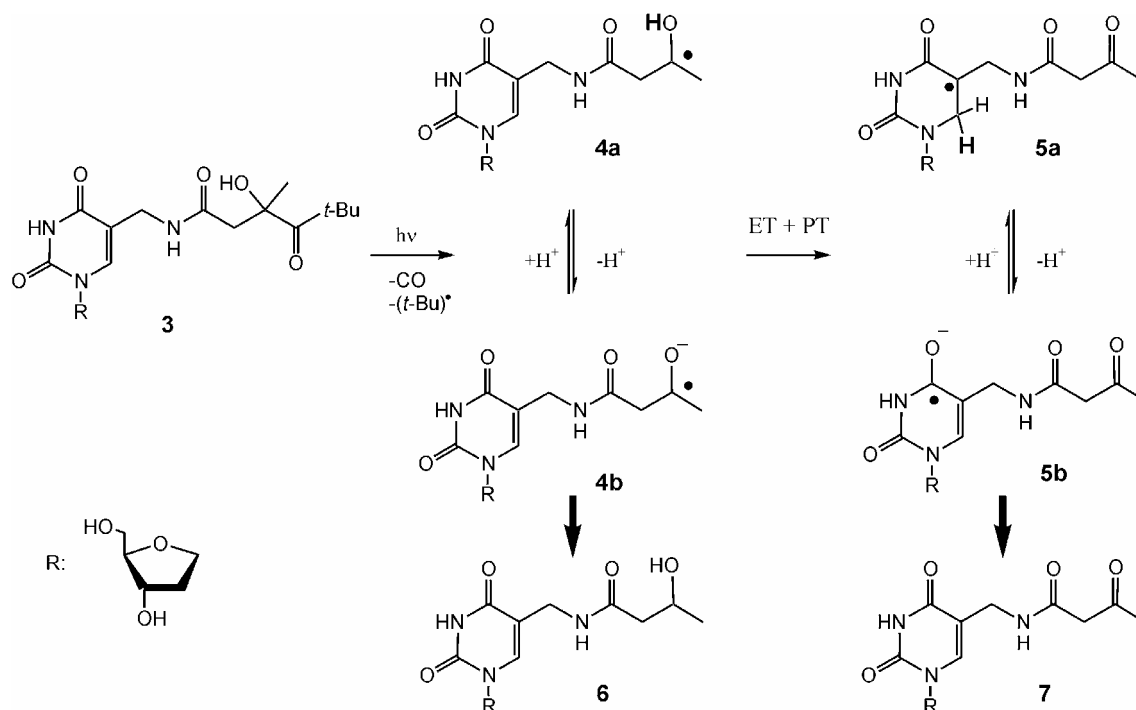
The spectrum in Fig. 6.7 does not show the typical “octet-pattern” of a thymyl radical as observed in the case of the 4'-pivaloylated thymidine. However the “octet-pattern” is due to

hyperfine couplings of the hydrogen atoms at the C(6) position and at the methyl group attached at C(5) while in the case of **3** one of the hydrogen atoms at the methyl group is substituted by one nitrogen. As a consequence the EPR spectrum should possess a different pattern. It was in fact possible to simulate the spectrum in Fig. 6.7 taking into account two pairs of equivalent hydrogen nuclei. The simulated spectrum resembles the experimental one and the hyperfine couplings of 39.2 G for the two equivalent hydrogens at C(6) and 10.5 G for the two equivalent  $\beta$  hydrogens at C(5) are similar to the values of the unsubstituted thymyl radical in frozen solution (see Table 5.1, chapter 5). Assuming that the atoms in  $\beta$  position with respect to C(5) occupy symmetrically equivalent positions in the molecule, due to the fast rotation of the attached group, a hf coupling  $a_{iso} = 0.8$  G can be calculated for the  $\beta$  nitrogen atom, according to eq. 2.19. Such a small coupling would indeed disappear under the linewidth of Fig. 6.7. Nevertheless it can also be that anisotropic hf interactions are present, since at 77 K the long chain attached at C(5) may be not tumble as fast as a methyl group (see also the “Summary and Outlook” chapter).

The species that gives rise to the “central singlet” in almost all the spectra is the only one that is detectable in both water and acetonitrile. This assumption can be validated by the following EPR observations: the  $g$ -factor in the two spectra in Fig. 6.2 and Fig. 6.5 has similar values; the central line of Fig. 6.5 is similar to the one in the “central singlet” spectrum; finally it is possible to use the “central singlet” line from Fig. 6.2 (**3** in water solution) to reconstruct the spectrum in acetonitrile.

On the basis of the EPR and HPLC results, the reaction Scheme 6.1 can be finally proposed for the radical generation after UV irradiation of **3**.





**Scheme 6.1** Reaction of the modified thymine **3**. Both electron transfer (ET) and proton transfer (PT) reactions occur from **4** to **5**.

Similar to the results obtained from **1** and from other analogous systems, after irradiation the Norrish type I reaction occurs, leading to a pivaloyl radical (that immediately decarbonylates to a *tert*-butyl radical) and to the hydroxyl radical **4a** on the modified molecule are generated.

The HPLC detection of **7** as a final product and the presence of alcohol **6** as additional final product when the H-donor glutathione was added confirms that a homolytic cleavage has to occur at the pivaloyl site and shows that two intermediate radicals should be present, **4a** and **4b** (hydroxyl and ketyl radical respectively). To account for **5a**, detected by EPR in acetonitrile at 77 K, an electron transfer from the intermediate radicals to the thymine base has to happen. Deprotonation of the hydroxyl radical **4a** has to occur for efficient electron transfer from the electron-injecting radical to the thymine.<sup>[2]</sup> In DNA experiments, the surrounding water or phosphate ions might accept the proton. Even the neighboring carbonyl group could assist the deprotonation of the hydroxyl radical. Thus, electron transfer is presumably coupled with proton transfer as it was also found in

the case of the 4'-pivaloylated thymidine,<sup>[8]</sup> and it is proposed that the proton originates from the -OH group of the hydroxyl radical intermediate **4a**.

Intermolecular reaction pathways leading to the formation of the thymyl radical **5a** can be excluded, since a reaction between thymine and the *tert*-butyl or solvent radicals do not yield the spectrum in Fig. 6.7 and no free electrons are generated with this low energy setup. Furthermore, a direct formation of **5a** due to UV damage of the thymine base can also be excluded, because no signal was observed by using thymine or thymidine instead of **3**. The assumption that the electron transfer is coupled with proton transfer that originates from the molecule itself is confirmed by the fact that the thymine-based radical was observed in acetonitrile, which does not release protons. Additionally, the proton transfer has to be fast, because a doublet spectrum<sup>[5]</sup> of the thymine radical anion was not observed, which may imply that it is coupled with the electron transfer, or the reaction occurs directly by hydrogen atom transfer.

To date, a definitive assignment of the “central singlet” to a paramagnetic species cannot be done. In principle both the intermediates **4a** and **4b** could account for the “central singlet” spectrum. The paramagnetic species that gives the “central singlet” is trapped at 77 K both in water and acetonitrile, and decays with time. But, while in acetonitrile the subsequent formation of the electron transfer product **5a** is detectable by cw-EPR, this is not possible in water. A reason for that might be due to its follow-up reactions with water molecules, which have to happen faster than the EPR time scale. As a confirmation, adding a drop of water to the acetonitrile solution instantaneously leads to the disappearance of the thymyl **5a** pattern (see Fig. 6.6 and Appendix A, Fig. A.5). In DNA the thymyl radical would be protected from water thus possessing a longer lifetime.

It is worth noting that the nucleotide derivative of **3** has been recently used with success as excess electron injector in DNA moieties modified with a thymine dimer as electron detection system.<sup>[2]</sup>

---

## 6.4 REFERENCES

- [1] C. A. M. Seidel, A. Schulz, S. Sauer, *Journal of Physical Chemistry* **1996**, *100*, 5541.
- [2] B. Giese, B. Carl, T. Carl, T. Carell, C. Behrens, U. Hennecke, O. Schiemann, E. Feresin, *Angewandte Chemie* **2004**, *116*, 1884.
- [3] M. D. Sevilla, Vanpaeme.C, C. Nichols, *Journal of Physical Chemistry* **1972**, *76*, 3571.
- [4] B. Weiland, J. Hüttermann, *International Journal of Radiation Biology* **1998**, *74*, 341.
- [5] P. M. Cullis, J. D. McClymont, M. E. Malone, A. N. Mather, I. D. Podmore, M. C. Sweeney, M. C. R. Symons, *Journal of the Chemical Society-Perkin Transactions 2* **1992**, 1695.
- [6] B. Giese, A. Dussy, E. Meggers, M. Petretta, U. Schwitter, *Journal of the American Chemical Society* **1997**, *119*, 11130.
- [7] A. Dussy, E. Meggers, B. Giese, *Journal of the American Chemical Society* **1998**, *120*, 7399.
- [8] O. Schiemann, E. Feresin, T. Carl, B. Giese, *Chemphyschem* **2004**, *5*, 270.
- [9] H. Paul, H. Fischer, *Helvetica Chimica Acta* **1973**, *56*, 1575.
- [10] R. W. Fessenden, R. H. Schuler, *Journal of Chemical Physics* **1963**, *39*, 2147.
- [11] B. Pruden, W. Snipes, W. Gordy, *Proceedings of the National Academy of Sciences of the United States of America* **1965**, *53*, 917.
- [12] M. D. Sevilla, Vanpaeme.C, G. Zorman, *Journal of Physical Chemistry* **1972**, *76*, 3577.
- [13] P. S. Pershan, R. G. Shulman, B. J. Wyluda, J. Eisinger, *Science* **1965**, *148*, 378.
- [14] H. Schuh, E. J. Hamilton, H. Paul, H. Fischer, *Helvetica Chimica Acta* **1974**, *57*, 2011.



---

## SUMMARY AND OUTLOOK

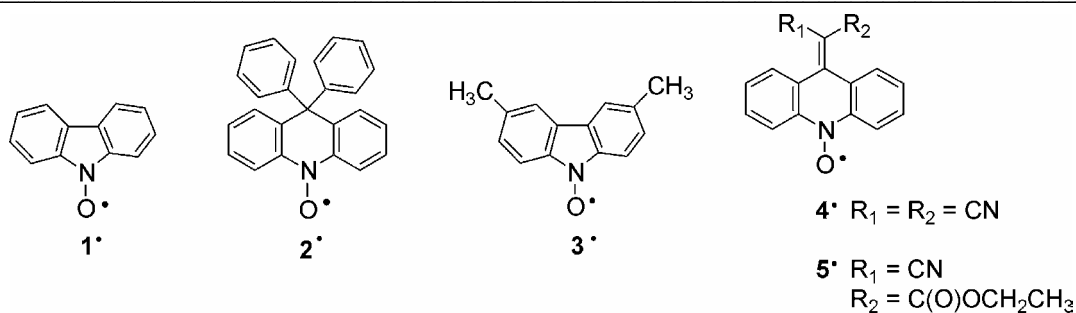
In this thesis Electron Paramagnetic Resonance spectroscopy (EPR) is used to probe whether and how four different methods can be used to introduce radicals in DNA. In particular the first method analysed here involves the use of stable nitroxides as intercalators between DNA base pairs. The other methods involve the generation of transient radicals within DNA using cw-UV light: in particular transient guanine radicals selectively generated in DNA by the flash quench technique, and thymine base radicals generated upon irradiation of two different chemically modified thymidine nucleosides are here studied.

These investigations on the applicability of such methods to selectively introduce radicals in DNA are necessary in order to understand if and how it can be possible to generate biradicals in DNA in specific positions. These studies are the essential starting point within a project having as long term goal to measure the exchange coupling constant  $J$  in biradical DNA and to correlate it with the charge transfer rate constant  $k_{CT}$ .

Moreover, the understanding of the photoinduced processes that occur upon UV-vis irradiation of the two specifically modified thymidines is important, since these systems are currently used as charge injectors into DNA.

In the following, a summary of the results obtained is given for each of the four methods studied, together with a short outlook.

**Stable Aromatic Nitroxides.** To investigate  $J$  coupling in biradical DNA generated with stable intercalated aromatic nitroxides it is necessary that the interacting spins are well inside the DNA base stack. For that reason intercalation ought to happen with the N-O group between the bases or, if this does not occur, the spin density has to be delocalised into the intercalating part of the nitroxide. Therefore the spin density distribution on the following potential intercalators aromatic nitroxides has been analyzed.



Simulations of the room temperature cw X-band EPR spectra of the above compounds were done. These aromatic nitroxides show resolved hyperfine couplings for all the ring protons and, in the case of  $3^*$ ,  $4^*$  and  $5^*$ , even to the methyl and nitril substituents, respectively. DFT studies (made by Jörg Fritscher) on the hyperfine coupling constants of the same compounds are in good agreement with the simulated EPR data and allow a specific assignment of the couplings. These investigations show that the spin density is delocalised into the  $\pi$ -system. Thus such stable aromatic nitroxides could be in principle used to investigate J coupling in DNA when intercalated into the double helix.

*Outlook.* Intercalation studies, i.e. by means of crystallographic techniques, should be made in order to prove the effective ability of these compounds to be inserted between two base pairs. After the intercalation properties of the aromatic nitroxides within a DNA duplex have been proved, it would be interesting to generate biradical DNA tethering two of them to the double helix. Then the interaction between two radicals in DNA could be inquired by means of PELDOR or by cw X-band EPR, via the half-field signal. With these methods it should be possible to get new insights on the spin-spin exchange interaction (measuring J), and eventually correlate it with the  $k_{\text{CT}}$ .

**Transient Guanine Radicals.** Transient guanine radicals are generated in DNA by means of the flash quench technique, which makes use of photoexcitable ruthenium intercalators. The selectivity involved in the guanine radical formation is essential for future studies on the exchange coupling constant J.

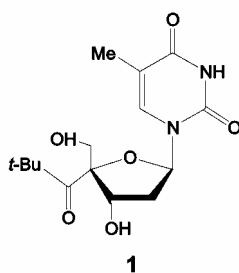
In previous applications of this method, the EPR spectra were recorded during irradiation at room temperature. Herein the irradiation procedure is tested in a different way: the contemporary irradiation and freezing of the sample makes it possible to trap the guanine radical at 80 K and to detect it with EPR spectroscopy. The single line obtained is more intense than the guanine radical singlet at room temperature, but is still a weak signal.

These studies show that it is possible to generate highly selective guanine radicals in DNA duplexes.

*Outlook.* The first step towards further characterization of the guanine radical would be to increase the signal to noise of the spectrum obtained. This is possible if the mechanism of radical trapping can be further improved. For that purpose it would be challenging to use or to build a freeze quench apparatus that allows controlled freezing of the sample and contemporary irradiation. Then, to characterize the guanine radical via its *g*- and hyperfine-tensor it would be interesting to perform high-field EPR measurements and different multifrequency (S-, X-) ESEEM methods. In order to attempt an analysis of the J coupling using the transient guanine radicals generated in DNA by means of the flash quench technique, two ruthenium intercalators can be tethered to the 5'-ends of a duplex containing only two guanine bases. In this way two guanine radicals within one duplex and with a fixed distance between them should be generated.

#### **Transient thymyl radicals from the UV irradiated 4'-Pivaloyl Substituted Thymidine.**

For the first time, it was possible to detect an EPR signal at 77 K from a thymidine nucleoside **1** modified with the photocleavable pivaloyl group in the 4' sugar position, after UV irradiation. The modified nucleoside is depicted below:



Different experimental approaches were used to simplify the composite spectrum initially obtained in acetonitrile, and finally three spectral components were identified as the *tert*-butyl radical, the thymyl radical and a sugar radical, which has been proposed to be the C5' sugar radical. The experimental data also allowed proposing a mechanism for the radical formation involving an electron/proton transfer step from the 4'-sugar radical (generated after Norrish type I cleavage of **1** at the pivaloyl site) to the thymine base. With these results it has been demonstrated that the pivaloyl group attached at the 4' sugar position can be used to selectively reduce a thymine base.

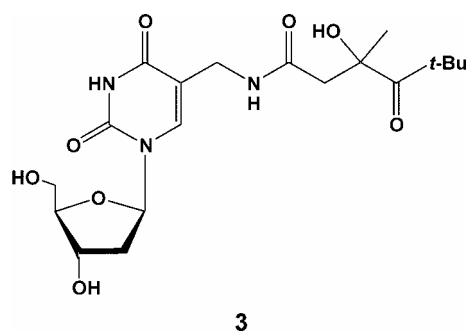
Therefore a duplex DNA modified with the nucleotide derivative of such a compound and with no guanine bases in the vicinity has been tested to verify if with this system is possible to selectively inject excess electrons into DNA. In this case a composite spectrum was detected, which has been attributed to a superposition of different radical species, but no radical on the thymine base was identified.

*Outlook.* The assignment of one component spectral component to the C5' sugar radical still needs to be proved. In particular is not clear if the pattern isolated at X-band is due to  $g$  tensor anisotropy or to hyperfine interaction. In order to separate the two contributions two different approaches can be used. First high-field measurements should be performed, which should allow for the assignment of the  $g$  tensor parameters. Second, low-field EPR measurements can be done in order to minimize the  $g$  tensor contribution on the pattern and to detect only the hyperfine interactions, which are not field dependent. From the computational side, DFT calculations of hyperfine coupling constants performed on different sugar radicals can be done.

It would be interesting to further investigate the DNA modified with the nucleotide derivative of **1**. From the mechanism findings on the single nucleoside and from the first measurement on the modified DNA, it can be deduced that in order to site specifically generate thymyl radicals in DNA, the modified nucleotide has to be attached to the DNA at the 3'-end or by ether linkage.

### **Transient thymil radicals from a new modified thymine after UV irradiation.**

For the first time, it was possible to detect an EPR signal at 77 K after UV irradiation of a thymidine nucleoside **3** modified with the photocleavable pivaloyl group in a different position. The modified nucleoside is depicted below:





Similar to the preceding case, it was possible to deconvolute the initial composite spectrum and to assign the single spectral components to a *tert*-butyl radical, an intermediate radical (ketyl or hydroxyl) and a thymil radical. To account for the presence of the thymine based radical, a mechanism is proposed where a hydrogen or proton coupled electron transfer step from the first formed (via Norrish type I cleavage of **3** at the pivaloyl group) intermediate radical to the thymine base takes place. These results are a direct confirmation that an excess electron can be transferred selectively onto the thymine base.

*Outlook.* The spectrum of the isolated thymine base radical can be further analyzed in order to verify if there is a hyperfine anisotropy. This can be investigated experimentally by means of ENDOR and theoretically using DFT calculations. Finally it would be very interesting to analyze with EPR a DNA duplex modified with the nucleotide derivative of **3**.



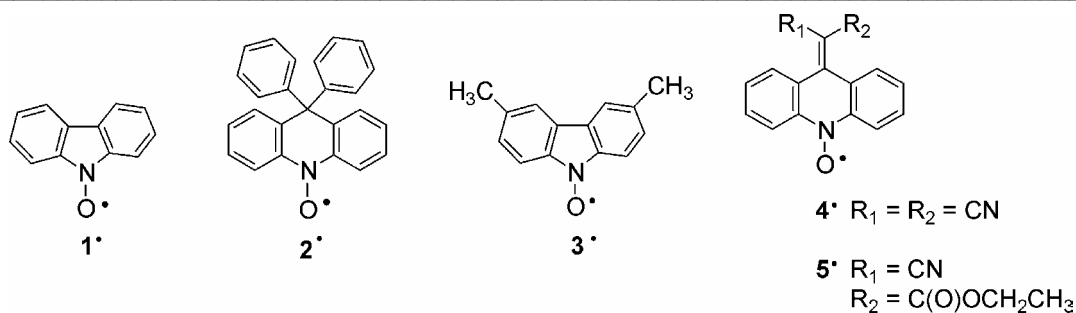
## ZUSAMMENFASSUNG UND AUSBLICK

In der vorliegenden Arbeit wurde mittels Elektronen Paramagnetischer Resonanzspektroskopie (EPR) die Frage untersucht, ob und auf welche Weise Radikale in DNA erzeugt werden können. Zur Erzeugung radikalischer DNA wurden vier verschiedene Methoden analysiert. Zunächst wurde die Erzeugung stabiler Nitroxide als Interkalatoren zwischen DNA-Basenpaaren untersucht. Die weiteren Methoden beruhen auf der Generierung kurzlebiger Radikale in DNA durch UV-Licht. Die selektive Erzeugung kurzlebiger Guanin-Radikale in DNA durch flash-quench-Techniken sowie die Generierung von Thymin-Radikalen durch UV-Bestrahlung zweier chemisch unterschiedlich modifizierter Thymidin-Nukleoside. Die Untersuchung der Anwendbarkeit solcher Methoden zur selektiven Erzeugung von Radikalen in DNA ist vor dem Hintergrund der Frage notwendig, ob und auf welche Weise die Erzeugung von Biradikalen in spezifischen Positionen in DNA möglich ist. Vor dem Fernziel der Bestimmung der Austauschkopplungskonstanten  $J$  in biradikalischer DNA und deren Korrelation mit der charge-transfer-Geschwindigkeitskonstanten  $k_{CT}$  stellen diese Untersuchungen einen wichtigen Ausgangspunkt dar.

Zudem ist das Verstehen photoinduzierter Prozesse, welche bei der UV-Vis Bestrahlung der beiden spezifisch modifizierten Thymidine stattfinden, wichtig, da diese Systeme derzeit zur Injektion von Ladungen in DNA dienen.

Im folgenden werden die Ergebnisse der Untersuchung der oben genannten vier Methoden zusammengefasst und ein kurzer Ausblick gegeben.

**Stabile aromatische Nitroxide.** Um die Austauschkopplung  $J$  in biradikalischer DNA, welche durch die Interkalation stabiler aromatischer Nitroxide erzeugt wurde, zu untersuchen, ist es notwendig, die wechselwirkenden Spins innerhalb der Basenstapel zu positionieren. Daher sollten sich entweder die NO-Gruppen zwischen den Basenstapeln befinden oder, falls dies nicht möglich ist, Spindichte sollte durch Delokalisierung auf den interkalierenden Teil der Nitroxide übertragen werden. Aus diesem Grund wurden die Spindichteverteilungen der folgenden potentiell interkalierenden aromatischen Nitroxide analysiert.



An den bei Raumtemperatur aufgenommenen cw-X-Band EPR-Spektren wurden Simulationen durchgeführt. Die Spektren der aromatischen Nitroxide zeigen aufgelöste Hyperfeinkopplungen für alle Ringprotonen und in den Fällen  $3^*$ ,  $4^*$  und  $5^*$  auch die Hyperfeinkopplungen der Methyl- und Nitrilsubstituenten. DFT-Studien (durchgeführt von Jörg Fritscher) bezüglich der Hyperfeinkopplungskonstanten stimmen gut mit den Ergebnissen der Simulation überein und erlauben eine exakte Zuordnung der Kopplungen. Die Untersuchungen belegen die Delokalisierung der Spindichte auf das aromatische  $\pi$ -System, wodurch diese Nitroxide prinzipiell für eine Untersuchung der Austauschkopplung  $J$  in DNA geeignet erscheinen, wenn eine Interkalation in die Doppelhelix gelingt.

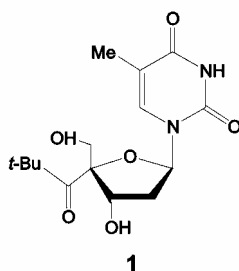
Ausblick: Um die Möglichkeit zur Interkalation dieser Verbindungen zu prüfen, sollten weitere Untersuchungen durchgeführt werden, beispielsweise durch röntgenographische Methoden. Nach Prüfung der Interkalations-Eigenschaften erscheint die Erzeugung von biradikalischer DNA durch Verknüpfung von zwei aromatischen Nitroxiden mit den DNA-Doppelhelix besonders interessant. Die Wechselwirkung zwischen den beiden Radikalen kann durch PELDOR- oder cw-X-Band EPR untersucht werden. Hierdurch können Informationen über die Spin-Austauschwechselwirkung  $J$  erhalten und diese schließlich mit der charge-transfer-Geschwindigkeitskonstanten  $k_{\text{CT}}$  korreliert werden.

**Kurzlebige Guanin-Radikale.** Durch die Verwendung photochemisch anregbarer Ruthenium-Interkalatoren wurden kurzlebige Guanin-Radikale in DNA mittels flash-quench-Technik generiert. Dabei ist die Selektivität, mit der die Guanin-Radikale gebildet werden, von besonderer Bedeutung für zukünftige Untersuchungen in bezug auf die Austauschwechselwirkung  $J$ . Bei vorangegangenen Anwendungen dieser Methode wurden die EPR-Spektren bei Raumtemperatur während der Bestrahlung aufgenommen; hier wurde eine andere Bestrahlungsprozedur getestet: Das gleichzeitige Bestrahlen und Einfrieren der Probe ermöglicht Abfangen und EPR-spektroskopischen Nachweis des

Guanin-Radikals bei 80 K. Das dabei erhaltene EPR-Spektrum besteht aus einer einzelnen, im Vergleich zum Raumtemperaturspektrum des Guanin-Radikals intensiveren Linie. Gleichwohl ist das Signal schwach. Insgesamt zeigt das Experiment, daß eine selektive Erzeugung eines Guanin-Radikals in DNA möglich ist.

Ausblick: Für eine weitere Charakterisierung des Guanin-Radikals sollte in einem ersten Schritt das Signal-zu-Rauschen Verhältnis der aufzunehmenden Spektren erhöht werden. die Methode der freeze-quench-Technik zum Abfangen der Radikale sollte durch eine Apparatur verbessert werden, die ein kontrolliertes Einfrieren der Probe bei gleichzeitiger Bestrahlung ermöglicht. Zur Charakterisierung des Guanin-Radikals durch seine g- und Hyperfein-Tensoren sollten Hochfeld-EPR-Messungen und verschiedene ESEEM-Methoden bei verschiedenen Frequenzen (S-Band, X-Band) durchgeführt werden. Für eine Untersuchung der Austauschwechselwirkung in biradikalischer DNA mittels flash-quench-Technik könnten zwei Ruthenium-Interkalatoren mit den 5'-Enden eines DNA-Doppelstranges, welcher nur zwei Guanin-Basen enthält, verknüpft werden. Auf diese Weise könnten zwei Guanin-Radikale innerhalb eines Doppelstranges in einem bestimmten Abstand zueinander erzeugt werden.

**Kurzlebige Thymyl-Radikale aus UV-bestrahlten 4'-Pivaloyl substituiertem Thymidin.** Erstmals war es möglich, ein EPR-Signal bei 77 K zu detektieren, nachdem ein mit der photochemisch abtrennbaren Pivaloyl-Gruppe in 4'-Position substituiertes Thymidin-Nukleosid mit UV-Licht bestrahlt wurde. Die folgende Formel gibt das modifizierte Nukleosid wieder:



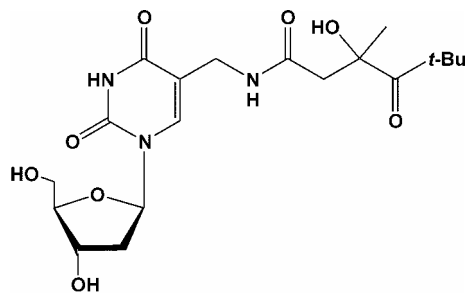
Um das ursprünglich in Acetonitril erhaltene überlagerte Spektrum zu vereinfachen, wurden verschiedene experimentelle Anläufe unternommen, und schließlich konnten drei spektrale Komponenten identifiziert werden: Ein tert.-Butyl-Radikal, ein Thymyl-Radikal und ein Zucker-Radikal mit dem ungepaarten Elektron an C5'-Position. Die

experimentellen Daten lassen auch Rückschlüsse auf den Mechanismus der Radikalentstehung zu, wobei ein Elektron/Proton-Transfer von einem 4'-Zucker-Radikal (entstanden nach der Norrish- Type-I Teilung von **1** an der Pivaloyl-Gruppe) zur Thymin-Base angenommen wird. Hierdurch konnte gezeigt werden, daß die an der 4'-Position mit dem Zucker-Rest verknüpfte Pivaloyl-Gruppe zur Reduktion einer Thymin-Base genutzt werden kann. Daher konnte ein mit einem entsprechenden Nukleotid-Derivat modifizierter DNA-Doppelstrang ohne benachbarte Guanin-Basen untersucht werden, um zu überprüfen, ob mit diesem System eine selektive Injektion überschüssiger Elektronen in DNA möglich ist. Hier wurde ein überlagertes Spektrum verschiedener Radikale erhalten; jedoch konnte keine radikalische Thymin-Base identifiziert werden.

Ausblick: Die Zuordnung einer der spektralen Komponente zum C5'-Zucker-Radikal bedarf noch der Überprüfung. Insbesondere ist nicht geklärt, ob das bei X-Band Frequenz erhaltene Aufspaltungsmuster seine Ursache in einer g-Anisotropie oder einer Hyperfeinwechselwirkung hat. Um die beiden Beiträge zu separieren, können zwei unterschiedliche Wege beschritten werden. Zunächst sollten Hochfeld-EPR-Messungen durchgeführt werden, um die g-Tensor-Parameter zu ermitteln. Ferner könnten durch Tieffeld-EPR-Messungen die feldunabhängigen Hyperfeinwechselwirkungen detektiert und der Beitrag des g-Tensors zum Aufspaltungsmuster minimiert werden. Schließlich könnten DFT-Berechnungen bezüglich der Hyperfeinkopplungskonstanten an unterschiedlichen Zucker-Radikalen durchgeführt werden. Ferner erscheinen weitere Untersuchungen an DNA, welche mit dem Nukleotid-Derivat **1** modifiziert wurde, interessant. Anhand der mechanistischen Befunde am einzelnen Nukleotid und aus der ersten Messung an der modifizierten DNA kann abgeleitet werden, daß das modifizierte Nukleotid am 3'-Ende der DNA oder über eine Ether-Gruppe angeknüpft werden sollte, um seitenspezifisch Thymyl-Radikale in DNA zu erzeugen.

#### **Kurzlebige Thymyl-Radikale aus neu modifizierten Thymin nach UV-Bestrahlung.**

Erstmals war es möglich, ein EPR-Signal bei 77 K zu detektieren, nachdem ein mit der photochemisch abtrennbaren Pivaloyl-Gruppe an einer anderen Position substituiertes Thymidin-Nukleosid **3** mit UV-Licht bestrahlt wurde. Nachfolgend ist das modifizierte Nukleosid wiedergegeben:



3

Ähnlich wie im vorhergehenden Fall war es möglich, das ursprünglich überlagerte Spektrum zu dekonvolvieren und einzelne spektrale Komponenten zuzuordnen: Ein tert.-Butyl-Radikal, ein radikalisches Intermediat (Ketyl- oder Hydroxyl-Radikal) und ein Thymyl-Radikal. Um das Auftreten des Thymyl-Radikals zu erklären, wird ein Mechanismus vorgeschlagen, bei dem ein Wasserstoff- oder Proton-vermittelter Elektron-Transfer-Schritt vom zunächst (durch Norrish-Type-I Teilung von **3** an der Pivaloyl-Gruppe) gebildeten radikalischen Intermediat zur Thymin-Base stattfindet. Diese Ergebnisse bestätigen, daß ein überschüssiges Elektron selektiv auf die Thymin-Base übertragen werden kann.

Ausblick: Das Spektrum der isolierten radikalischen Thymin-Base sollte weiter analysiert werden, um eine eventuelle Hyperfein-Anisotropie zu überprüfen. Experimentell kann dies durch ENDOR-Spektroskopie und theoretisch durch DFT-Rechnungen geschehen. Schließlich ist eine Untersuchung einer mit dem Nukleotid-Derivat **3** modifizierten DNA mittels EPR-Spektroskopie von Interesse.





---

## APPENDIX A. CONTROL MEASUREMENTS AND ADDITIONAL SIMULATION SPECTRA

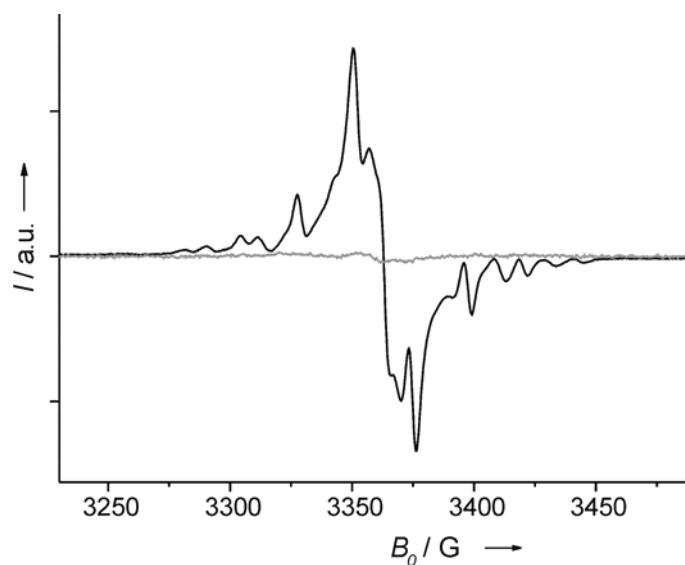


**Figure A.1** Comparison between the EPR spectrum of the 4'-pivaloyl substituted thymidine (black curve) in  $\text{CH}_3\text{CN}$ , and the spectrum of a solution of unmodified thymidine and di-tert-butylketone in a 1:1 molar ratio (gray curve). Both samples were irradiated and measured at 77 K. The experimental conditions used for both samples are the same as in Fig. 5.5.

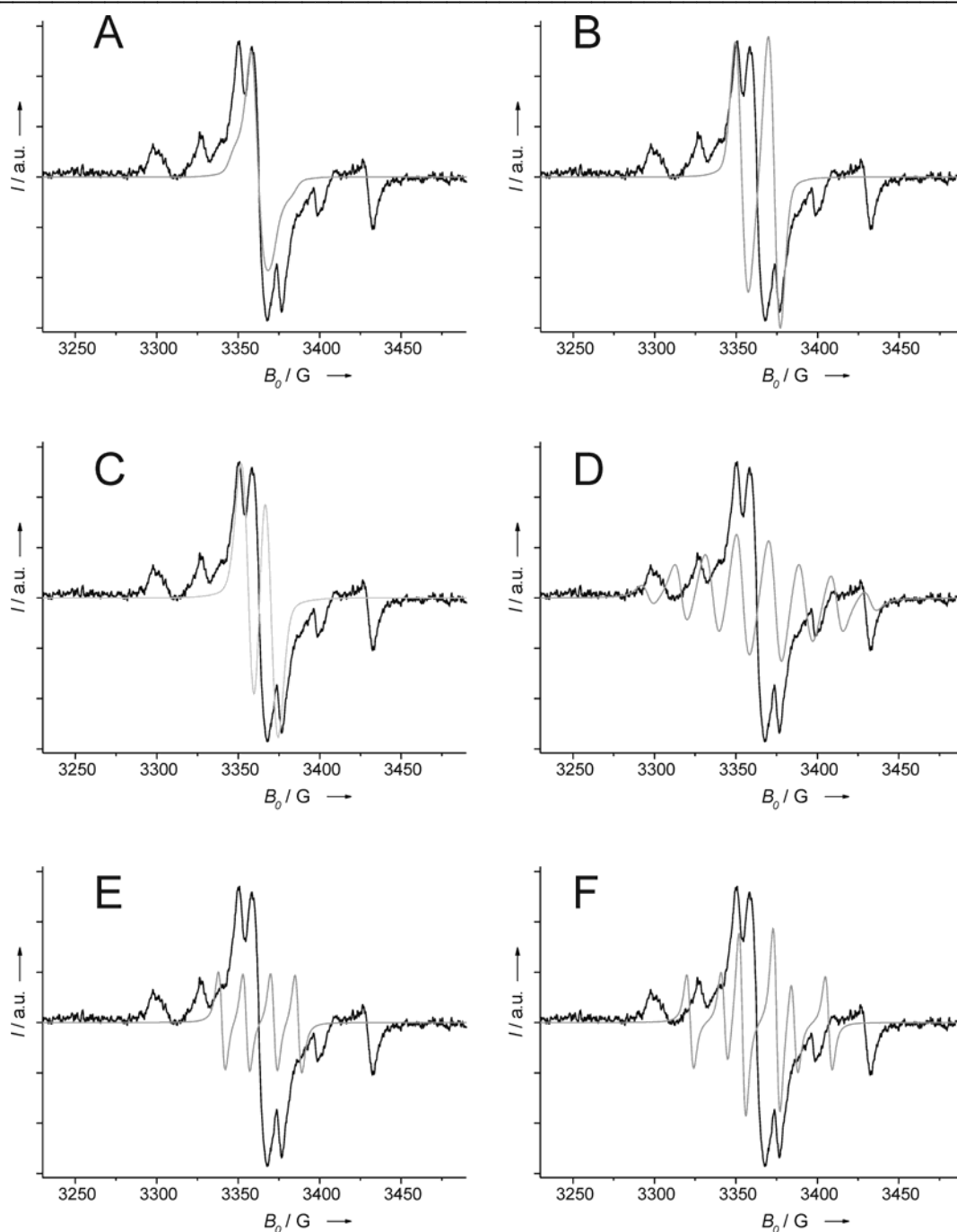


**Figure A.2** In each figure the EPR spectrum of Fig. 5.7 is superimposed (black line) on the following simulations (gray line). A) Simulated spectrum of guanine radical cation  $G^{\bullet+}$  ( $Lw=6$  G). B) simulated spectrum of cytosine radical anion  $C^{\bullet-}$  ( $Lw=7$  G). C) Simulated spectrum of thymine radical anion  $T^{\bullet-}$  ( $Lw=7.5$  G). The parameters for A, B, C were taken from [Weiland, B., Hüttermann, J., van Tol, J., *Acta Chemica Scandinavica* **1997**, 51, 585]. D) Simulated spectrum of thymine radical (same as in Fig. 5.14b). E) Simulated spectrum of a  $C1^{\bullet}$  sugar radical with two  $\beta$  couplings of  $a_{iso}(^1H) = 15$  G,  $a_{iso}(^1H) = 32$  G ( $Lw=6$  G). F) Simulated spectrum of a  $C3^{\bullet}$  sugar radical with couplings  $a_{iso}(2x(^1H)) = 32$  G and  $a_{iso}(^1H) = 21$  ( $Lw=7.5$  G).

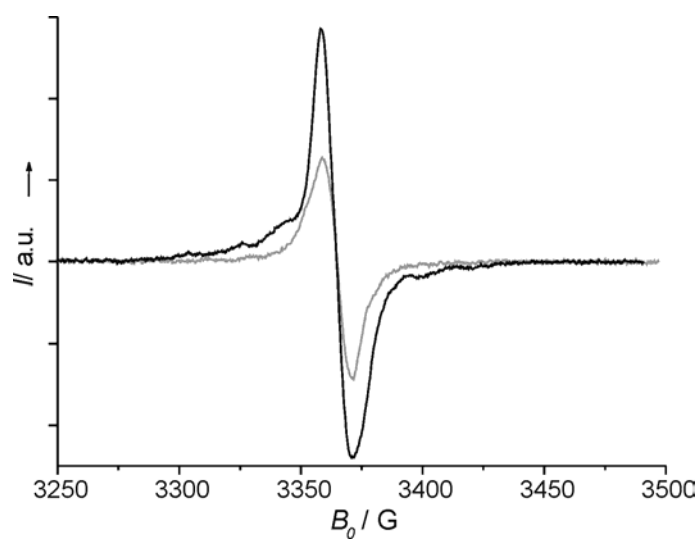


**Figure A.3** Comparison between the EPR spectrum of **3** in H<sub>2</sub>O irradiated and measured at 77 K (black curve), and the same spectrum measured at 77 K after annealing at 180 K (grey curve). The EPR parameters are the same.

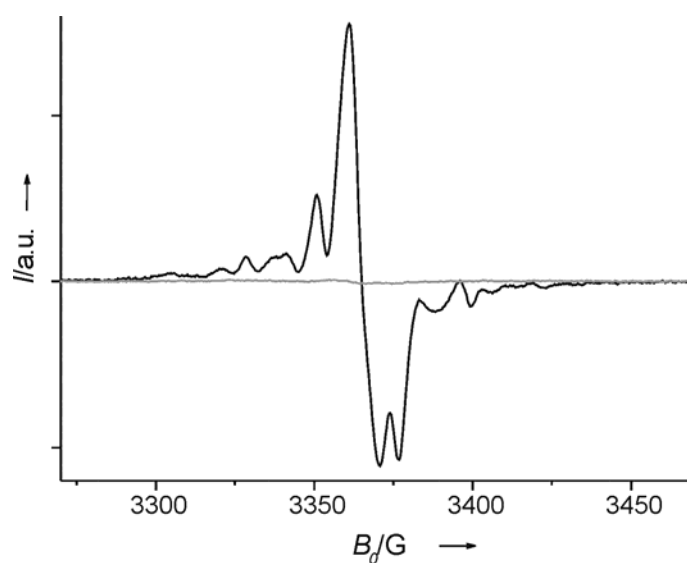


**Figure A.4** Comparison between the EPR spectrum of irradiated **3** (black curve) in CH<sub>3</sub>CN and the spectrum of a solution of unmodified thymidine and di-tert-butylketone in a 1:1 molar ratio (grey curve). Both samples were irradiated and measured at 77 K. The experimental conditions used for both samples are the same as in Fig. 6.5.

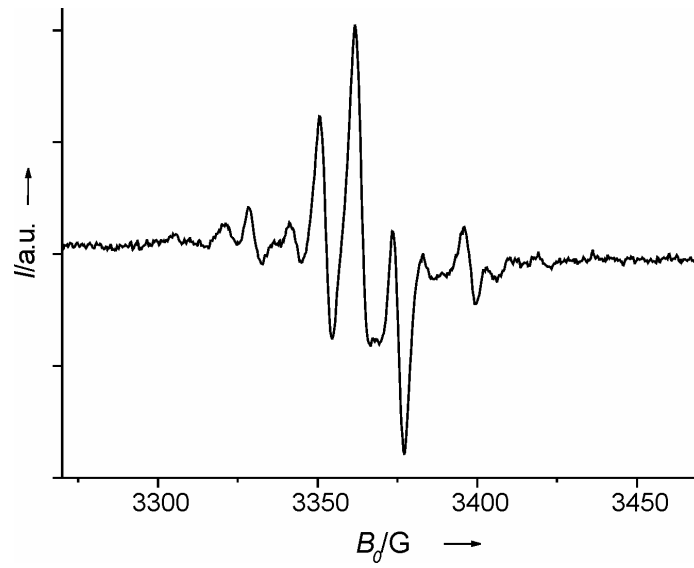


**Figure A.5** Spectrum generated by subtraction of the spectrum in Fig. 6.6 from the spectrum in Fig. 6.5.

## APPENDIX B. HPLC CHROMATOGRAMS

The following HPLC analyses were done by Dr. T. Carl in Prof. B. Giese's group, University of Basel, Switzerland.

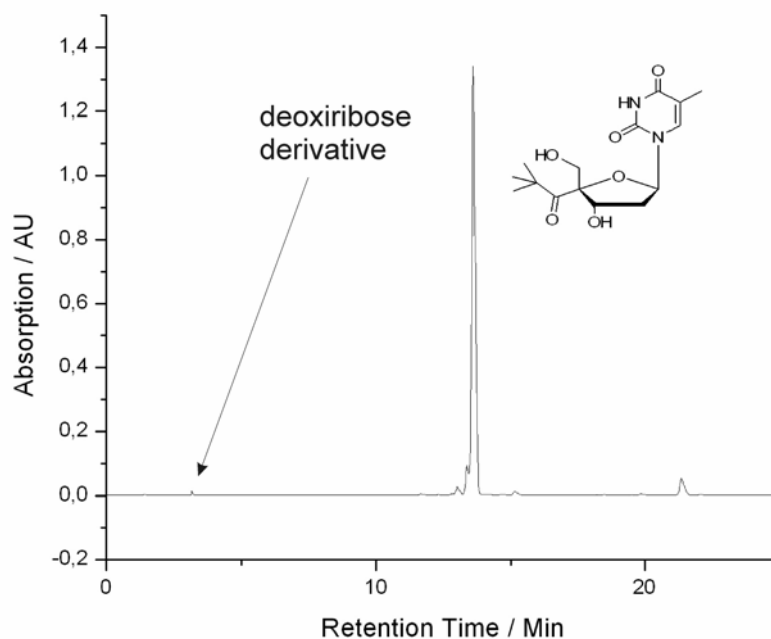


**Figure B.1** HPLC chromatogram of **1** after irradiation. A deoxiribose derivative is detected as a product at short retention time.



**Figure B.2** HPLC chromatogram of **3** after irradiation. Ketone **7** is detected as a product at short retention time.

## LEBENS LAUF

### Persönliche Daten:

Name: Emiliano Feresin  
Geburtsdatum: 3.März,1974  
Geburtsort: Palmanova (Udine, Italy)  
Eltern: Roberto Feresin  
Rosa Maria Feresin, geb. Andrian  
Familienstand: ledig

### Schulbildung:

1985 – 1988 Mittelschule in Aiello del Friuli (Udine, Italy)  
1988 – 1993 “G. Marinelli”, Udine naturwissenschaftliches Gymnasium  
in Udine (Italy)  
Juli 1993 Abitur

### Studium:

1993 – 2000 Studium der Chemie an der Universität Padova (Italy)  
November 2000 Diplom in Chemie  
seit May 2001 Promotionsstudium am  
Institut für Physikalische und Theoretische Chemie,  
Fachbereich Chemische und Pharmazeutische Wissenschaften,  
Johann Wolfgang Goethe-Universität in Frankfurt am Main





## Acknowledgements

*I would like to thank the people involved in the realization of this work:*

*Prof. Thomas F. Prisner, for giving me the opportunity to work in his group, having access to such a stimulating amount of EPR facilities and for his kind support during these years.*

*P. D. Dr. Olav Schiemann, for introducing me in the world of Electron Transfer in DNA, providing expertise, contributing to the achievements of new results*

*Dr. Marina Bennati, for fruitful discussions and for her excellent introduction to the high field EPR during my training period at the Transmission Mode*

*Dr. Fraser MacMillan, for stimulating discussion concerning science and life*

*Mario Beyer and Dr. Jörg Fritscher, for the preparation of the nitroxides and the DFT calculations*

*Moreover I thank All the group members, for the nice working atmosphere. Thanks in particular to Dr. Jörn Plackmeyer for the German translation of the Summary, and to Melanie Hertel for fruitful discussion*

*This work would not have been possible without the samples and excellent expertise of Prof. B. Giese (University of Basel, Switzerland )*

*Dr. T. Carl and Dr. B. Carl (University of Basel, Switzerland )*

*This work benefited from the financial support of the DFG. The University of Padova is thanked for financial Aid.*

*Finally I would like to thank Mauro, Tomaso, Gianni, Matteo, Emanuela, Susanna, Ralf... Federico and Alessandro, for their help and friendship and my family for the support during these years.*

*TO Enrica, because you know...*